
[All ETDs from UAB](#)

[UAB Theses & Dissertations](#)

1998

Analysis and characterization of the metabolic and morphologic responses to uniaxial deformation of osteoblasts cultured on Ti-6Al-4V.

Deborah F. Rigsby
University of Alabama at Birmingham

Follow this and additional works at: <https://digitalcommons.library.uab.edu/etd-collection>

Recommended Citation

Rigsby, Deborah F., "Analysis and characterization of the metabolic and morphologic responses to uniaxial deformation of osteoblasts cultured on Ti-6Al-4V." (1998). *All ETDs from UAB*. 6228.
<https://digitalcommons.library.uab.edu/etd-collection/6228>

This content has been accepted for inclusion by an authorized administrator of the UAB Digital Commons, and is provided as a free open access item. All inquiries regarding this item or the UAB Digital Commons should be directed to the [UAB Libraries Office of Scholarly Communication](#).

INFORMATION TO USERS

This manuscript has been reproduced from the microfilm master. UMI films the text directly from the original or copy submitted. Thus, some thesis and dissertation copies are in typewriter face, while others may be from any type of computer printer.

The quality of this reproduction is dependent upon the quality of the copy submitted. Broken or indistinct print, colored or poor quality illustrations and photographs, print bleedthrough, substandard margins, and improper alignment can adversely affect reproduction.

In the unlikely event that the author did not send UMI a complete manuscript and there are missing pages, these will be noted. Also, if unauthorized copyright material had to be removed, a note will indicate the deletion.

Oversize materials (e.g., maps, drawings, charts) are reproduced by sectioning the original, beginning at the upper left-hand corner and continuing from left to right in equal sections with small overlaps. Each original is also photographed in one exposure and is included in reduced form at the back of the book.

Photographs included in the original manuscript have been reproduced xerographically in this copy. Higher quality 6" x 9" black and white photographic prints are available for any photographs or illustrations appearing in this copy for an additional charge. Contact UMI directly to order.

UMI

A Bell & Howell Information Company
300 North Zeeb Road, Ann Arbor MI 48106-1346 USA
313/761-4700 800/521-0600

ANALYSIS AND CHARACTERIZATION OF THE METABOLIC AND
MORPHOLOGIC RESPONSES TO UNIAXIAL DEFORMATION OF
OSTEOBLASTS CULTURED ON TI-6AL-4V

by

DEBORAH F. RIGSBY

A DISSERTATION

Submitted to the graduate faculty of The University of Alabama at Birmingham,
in partial fulfillment of the requirements for the degree of Doctor of Philosophy

BIRMINGHAM, ALABAMA

1998

UMI Number: 9839856

**Copyright 1998 by
Rigsby, Deborah F.**

All rights reserved.

**UMI Microform 9839856
Copyright 1998, by UMI Company. All rights reserved.**

**This microform edition is protected against unauthorized
copying under Title 17, United States Code.**

UMI
300 North Zeeb Road
Ann Arbor, MI 48103

**Copyright by
Deborah F. Rigsby
1998**

ABSTRACT OF DISSERTATION
GRADUATE SCHOOL, UNIVERSITY OF ALABAMA AT BIRMINGHAM

Degree PhD Program Biomedical Engineering
Name of Candidate Deborah F. Rigsby
Committee Chair Linda C. Lucas
Title Analysis and Characterization of the Metabolic and Morphologic
Responses to Uniaxial Deformation of Osteoblasts Cultured on Ti-6AL-4V

The primary objective of this research was the development and testing of a system for evaluating effects of quantified, uniform, dynamic mechanical load on osteoblasts growing on an actual dental/orthopedic implant material. MC3T3-E1 cells were plated onto titanium alloy (Ti-6Al-4V) coupons and subjected to uniform, uniaxial stress via a custom 4-point bend apparatus and a model MTS Model 8581 mini-Bionix™, servo-hydraulic testing machine. Peak loads of 3000 microstrain ($\mu\epsilon$) or 6000 $\mu\epsilon$ were established in a cyclic pattern (1 hertz [Hz] for 30 minutes [min]) and quantified using 90° rosette strain gages attached to a DATAQ data acquisition system. At various time points after loading (1 hour [hr]-48 hr), cells were evaluated for changes in morphology or alignment by digital imaging using 5-chloromethylfluorescein diacetate (CMFDA) and rhodamine-phalloidin and for changes in expression of the genes for hypoxanthine phosphoribosyltransferase (HPRT), collagen, osteopontin, and β -1 integrin using quantitative reverse transcriptase polymerase chain reaction (RT-PCR). No significant, reproducible alterations in morphology or alignment were observed using the current

loading parameters. Data from quantitative RT-PCR experiments were compared by 2-way ANOVA of values for messenger ribonucleic acid (mRNA) copy number of each target gene normalized to 100,000 copies of the housekeeping gene, HPRT. Main effects examined were load and time; post-hoc analysis was by Student-Newman-Keuls pairwise multiple means comparison test. Interactions of load and time were only examined when ANOVA indicated a significant interaction effect, and then only pre-planned comparisons were made. Copy number for collagen was elevated with 3000 μE of load and at 24 and 48 hr after loading; for β -1 integrin, copy number was increased at 24 and 48 hr and significant interactions of time with load were also present; for osteopontin, a significant increase in copy number was observed at the 48 hr timepoint, but no changes due to load were observed. This study demonstrated the usefulness of this novel strain application system for evaluating effects of mechanical loading on bone cells in contact with dental/orthopedic implant materials. By virtue of the ability to apply quantified, uniform, dynamic deformation, this system will also allow exploration of signaling pathways used in mechanosensory force transduction.

DEDICATION

It is with great honor and appreciation that I dedicate this dissertation research to Theela Laura Roberts. This body of work is a direct result of her constant encouragement and support throughout the lengthy journey of my education. She was known to her family and to most of the people in her community as a great lady of wit and wisdom. She was known to me as "Grandma." Thank you for everything Grandma--We did it.

ACKNOWLEDGMENTS

I would like to initially thank my graduate committee, Drs. Linda Lucas, Charles Prince, Martha Bidez, Jack Lemons, and Leonard Meuninghoff, for all of their guidance, patience, and support. An investigation this size could not be possible without the assistance of numerous talented and supportive colleagues. I would like to thank the following people from the laboratory of Dr. Charles Prince; Patricia Hicks, Dr. Pi Ling Chen, and Sharon Matlock. As I wandered through the world of molecular biology, I received enormous help from the personnel in the laboratories of Dr. Rick Hockett, including Rebecca Gilleland, Cindy James, Scott Chiz, Angel Rivera, Karen Janowski, and Robin Dzialo. During the development and fabrication of the strain application system, invaluable contributions were made by Jerry Sewel, Fred Molz, Paul George, Winston Greer, Todd Strong, Jeannie Haman-Plummer, Dan Heur, and Regina Messer. A very special thanks goes to my colleague and friend, Jason Plummer, for his tremendous support from beginning to end. I would also like to thank Dr. Ashley Ford and the staff of Calera Dental Center for their patience while I finished and defended this work. It goes without saying that I thank my wonderful parents, McArthur and Laura Rigsby, and sister, Kaylyn George, for their constant encouragement. They will always have my love and admiration.

TABLE OF CONTENTS

	<u>Page</u>
ABSTRACT	iii
DEDICATION	v
ACKNOWLEDGMENTS	vi
LIST OF TABLES	ix
LIST OF FIGURES	x
LIST OF ABBREVIATIONS	xii
INTRODUCTION	1
HYPOTHESES	10
SPECIFIC AIMS	11
SELECTION OF AN OSTEOBLAST MODEL	12
DEVELOPMENT OF THE MECHANICAL LOADING SYSTEM	16
Design of the Strain Application Device	17
Titanium Alloy Sample Design and Preparation	20
Gage Application and Strain Monitoring System	23
Plating of MC3T3-E1 Cells	25
Strain Application Protocol	27
DEVELOPMENT OF THE CELL IMAGING METHODOLOGY	30
Cellular Staining Protocol	31
Microscopic Imaging Technique	33

TABLE OF CONTENTS (Continued)

	<u>Page</u>
DEVELOPMENT OF THE QUANTITATIVE RT-PCR METHODOLOGY	35
Construction of Template BNC-1	38
Preparation of the DNA Competitor From BNC-1	41
Preparation of the RNA Competitor From BNC-1	41
Cell Harvesting Techniques	42
Reverse Transcription	43
Polymerase Chain Reaction	44
Agarose Gel Analysis.....	44
Plate-Based EIA	45
Labeling of Detection Oligos	46
Optimization of Primer Pairs	47
Comparison of Densitometry and EIA	47
RESULTS	48
Production of Quantified Dynamic Strain	48
Morphological Response to Uniaxial Deformation.....	51
Metabolic Response to Uniaxial Deformation	52
Agarose gel analysis	52
Comparison of gel densitometry and EIA	53
Data from quantitative RT-PCR	66
DISCUSSION	75
SUMMARY	85
CONCLUSIONS	87
LIST OF REFERENCES	88
APPENDIX	97

LIST OF TABLES

<u>Table</u>	<u>Page</u>
1 Strain protocol for morphological and metabolic analyses	29
2 Statistical analysis of recorded strain.....	51
3 Quantitative RT-PCR data	67
4 Two-Way balanced design analysis of variance for collagen.....	69
5 Two-Way balanced design analysis of variance for osteopontin.....	71
6 Two-Way balanced design analysis of variance for β -1 integrin.....	73

LIST OF FIGURES

<u>Figure</u>	<u>Page</u>
1 MC3T3-E1 cells.....	14
2 ROS 17/2.8 cells.....	14
3 Photoelastic coating showing uniform stress in 4-point bending.....	17
4 4-Point bend fixtures can produce compression or tension	18
5 Schematic of four point bend fixture	20
6 Titanium alloy sample dimensions	21
7 BNC-1 template map	39
8 Strain profile graph	49
9 Agarose gel of collagen competition	52
10 MC3T3-E1 cells imaged 24 hr following strain application	54
11 8-Hr control MC3T3-E1 cells	56
12 MC3T3-E1 cells imaged 8 hr following strain application	58
13 MC3T3-E1 cells imaged 4 hr following strain application	60
14 Control vs. strained cells at the 24-hr timepoint	62
15 Comparison of densitometry and EIA methodology.....	64
16 Graph of collagen expression for 4 timepoints and 3 loads.....	70
17 Graph of osteopontin expression for 4 timepoints and 3 loads.....	72

LIST OF FIGURES (Continued)

<u>Figure</u>	<u>Page</u>
18 Graph of β -1 integrin expression for 4 timepoints and 3 loads.....	74

LIST OF ABBREVIATIONS

Al	Aluminum
α -MEM	Alpha modification of Eagle's Minimum Essential Medium
cAMP	Cyclic Adenosine Monophosphate
cGMP	Cyclic Guanosine Monophosphate
CMFDA	5-chloromethylfluorescein diacetate
CP	Commercially Pure
DMSO	Dimethyl Sulfoxide
EtBr	Ethidium Bromide
GITC	Guanidine Isothiocyanate
HBSS	Hank's Balanced Salt Solution
HMDS	Hexamethyldisilazane
HPRT	Hypoxanthine phosphoribosyltransferase
hr	Hour
Hz	Hertz
$\mu\epsilon$	Microstrain
min	Minutes
mRNA	Messenger Ribonucleic Acid
MTS	Mechanical Testing Systems

LIST OF ABBREVIATIONS (Continued)

PBS	Dulbecco's Phosphate Buffered Saline Solution
PCR	Polymerase Chain Reaction
PGE ₂	Prostaglandin E ₂
PNP	P-Nitrophenyl Phosphate
RBM	Rat Bone Marrow
RT	Reverse Transcriptase
s	Second
SEM	Scanning Electron Microscope
S-T-C	Self Temperature Compensating
Ti	Titanium
Ti-6Al-4V	Titanium Alloy
UAB	University of Alabama at Birmingham
UV	Ultra Violet
V	Vanadium

INTRODUCTION

Periodontal disease, irreversible pulpitis, and trauma are just a few of the conditions that may necessitate the extraction of one or more teeth from the human maxilla or mandible. Over 20 million people in the United States alone are completely edentulous in one or both arches. Partial edentulism is even more widespread (1). Edentulism, whether partial or complete, can lead to varying degrees of speech impediments, decreased masticatory efficiency, and poor esthetics. This alteration in function and/or appearance often creates the need for prosthodontic intervention. Dental implants have become a life-enriching treatment option that offers both improved health and a better outlook for patients facing edentulism and its sequelae.

Attempts to replace missing teeth with endosteal implants made of stone and ivory have been traced back to the ancient Egyptian and South American civilizations (2). Metal implants of lead, gold, tantalum, iridium, stainless steel, and cobalt alloy were developed in the early 20th century (3). Cobalt-chromium-molybdenum subperiosteal and titanium (Ti) blade implants introduced in the 1940s and 1960s, respectively, became the most successful implant devices used from 1950 through 1980. Nonmetal biomaterials, such as carbon (4), aluminum (Al) oxide (5), and hydroxyapatite (6) were introduced in the 1970s and have experienced limited success.

One of the most significant events in the history of implant dentistry occurred in 1978 at a conference in Toronto, Canada. Professor Per-Ingvar Branemark presented the first two-stage threaded titanium root-form implant (7). While conducting animal studies in Göteborg, Sweden, Professor Branemark discovered that Ti implants placed in the femurs of rabbits could not be removed from the bone after a period of healing. He termed this interaction between bone and the titanium implants “osseointegration” and defined it as the: “direct structural and functional connection between ordered, living bone and the surface of a load-carrying implant (8).” In the time since Branemark’s introduction of osseointegrated implants, long-term prospective studies have offered evidence of prolonged survival, freestanding function, bone maintenance, and an improved benefit-to-risk ratio over all previous dental implants (9). With osseointegration a clinical reality, root-form implants have become implantology’s most dominant design.

In an effort to optimize the interaction between bone and dental or skeletal implants, many researchers have focused their attention on the implant-to-tissue interface (10-28). The importance of the events that take place at the interfacial zone between an implant and the host tissue can not be overstated. This complex interaction involves not only biomaterial and biocompatibility issues but also the alteration of the mechanical environment that occurs when placement of an implant disturbs the normal physiological distribution of forces, fluids, and cell communication.

The term interface is defined as a plane forming the common boundary between two parts of matter or space (29). The interface may represent a discrete boundary between the two materials or it may consist of a region or zone of interaction between the

two materials. The interface that exists between a dental implant and bone is an example of the latter (14, 28, 30).

The implant-to-tissue interface is an extremely dynamic region of interaction. This interface completely changes character as it goes from its genesis (placement of the implant into the prepared bony site) to its maturity (healed condition). The biomechanical environment plays an immediate role in the quality and compositional outcome of the new interface. For example, extensive research shows that if the implant is stable in the bone at the time of placement, the interface is more likely to result in osseointegration (24, 31). Relative movement (or micromotion) between the implant and the bone at the time of placement is more likely to favor the development of a fibro-osseous interface (27, 32). The healing stage of the interface, however, is only the beginning of its dynamic nature. Functional loading of the implant brings additional biomechanical influences which greatly affect the composition of this junction.

A current topic of intense research is the transduction of loading-induced strain at the interface into a signal that can direct the interfacial tissues to respond or remodel. It has been proven that bone responds to both hormonal and biomechanical (functional loading) regulation. These two regulating mechanisms are often in opposition to each other. Research has shown that even in instances where there is a large demand for calcium (the primary objective for hormonal regulation), functional loading can compete and maintain bone mass (33). It has been theorized that the actual strain that is perceived by the bone tissue initiates a chain reaction of events that results in a biological response. For tissue strain to influence bone adaptation at the bone/implant interface, it must elicit

some sort of a chemical or biological response in a strain-sensitive population. The current hypothesis is that bone cells in conjunction with the extracellular matrix comprise the strain-sensitive population and each plays a vital role in the mediation of the interface. Based on this rationale, it would seem that the objective of a good implant design would be to ensure a strain environment within the host bone tissue and at the interface that favors osseointegration of the implant.

The desire to optimize the effects of strain at the bone-to-implant interface to encourage osseointegration was largely fostered by biomechanically-based bone remodeling theories. Frost proposed the theory of the "mechanostat" (34). He postulated that bone mass is a direct result of the mechanical usage of the skeleton. This agrees with Wolff's law (35), which, in summary, states that "form follows function." Frost established a mechanical adaptation chart relating trivial loading, physiologic loading, overloading, and pathologic loading zones to ranges of microstrain. His studies showed that strains in the range of 1,500 to 25,000 stimulated increases in cortical bone mass until the strains were reduced to the threshold range or minimum effective strain. This process of the mechanostat would effectively switch the bone modeling "on" and "off". This phenomenon led him to the "flexure drift" hypothesis in which he proposed that long bones were geometrically curved in order to minimize the strain distribution down the long axis of the bone. He suggested that the curvature of the long bones canceled the bending moment caused by the eccentric pull of the muscles.

Experimental testing of these ideas led to controlled loading of avian ulnae (36). Strain gages were used to determine physiological peak strains. The bones were loaded in

a controlled manner based on these peak strains. Loads were constant (static) and dynamic, and some of the bones were isolated from loading. The short periods of dynamic loading showed an increase in the bone area (cross-section) of 24%, whereas the static loading and the lack of loading resulted in a 13% decrease in bone area. Loading was done via external fixators and Steinmann pins which were connected to an Instron™ machine that applied the cyclic load. It was concluded from these studies that an optimum strain environment exists for each specific anatomical area and that the peak strains innate for that area should be maintained to optimize the bone's response.

Cowin (37) proposed potential mechanisms by which bone cells sense mechanical load. Tissue-level strains were regarded as macroscopic strains averaged over a significant volume of bone tissue, whereas cell-level strains were defined as highly localized strains at the cell lacunae level. Cowin suggested that cell-level strains were almost 10-fold greater than tissue-level strains based on the confines and geometry of the lacunar shape. The proposed mechanisms included membrane deformation (action potential), intracellular action (passage of secondary messengers), and extracellular action (streaming potentials).

Though the exact mechanism for the initial detection and conversion of mechanical stress into a biochemical signal has yet to be determined, several theories have been proposed. One possible transduction pathway is the extracellular matrix-integrin-cytoskeletal network (38). Cells attach to the extracellular matrix via membrane spanning glycoproteins called integrins. The integrins attach to the actin cytoskeleton through several actin-associated proteins such as vinculin, talin, tensin, and α -actinin (39). The

cytoskeleton has been shown to connect the extracellular matrix with the cytoplasmic constituents of the cell (40), allowing physical stimuli to be rapidly transmitted to the nucleus, possibly altering gene expression. Experimental evidence does, in fact, suggest that cellular attachment to the extracellular matrix plays an important role in the regulation of cellular proliferation, differentiation, morphogenesis, and gene expression (41-43).

To date, there has been great diversity in the methodology used to apply deformation to various populations of cultured cells. Of the many methods used to deform the substrate on which cells are grown, several attempts have been made to deform circular diaphragms by the use of hydraulic or uniform pressure loading. Hasegawa (44) placed a Petriperm dish with a thin flexible Teflon base on a convex template which increased the surface area of the base of the dish by 4%. Banes (45) developed a device called the Flexcell, which applies strain via a vacuum on circular culture wells with a thick silastic plate as a substrate. Gorfien & Winston (46) described a device for stressing endothelial cells biaxially on thin circular Mitrathane membranes inflated at 1 Hz. Yeh & Rodan (47) subjected osteoblast-like cells grown on collagen ribbons to cyclic uniaxial tension.

The characterization of the biological responses resulting from cellular deformation is equally as diverse as the deformation methodologies themselves. Fluctuation in the concentrations of intracellular second messenger molecules has been reported by numerous investigators (47-52). In general, cell surface receptors relay information by activating a chain of events that alters the concentration of one or more small intracellular signaling molecules often referred to as second messengers or intracellular mediators. In

turn, these messenger molecules pass the signal on by altering the behavior of selected cellular proteins. Some of the most widely used intracellular mediators are cyclic adenosine monophosphate (cAMP), Ca^{2+} , and cyclic guanosine monophosphate (cGMP) (53).

Prostaglandin E_2 (PGE_2) and prostacyclin are paracrine agents that are released by osteoblasts in response to mechanical strain (47, 54-56). Both of these prostaglandins are released by bone in organ culture after a mechanical loading stimulus (57, 58), and when prostaglandin production is blocked by indomethacin, the anabolic effect of mechanical load *in vivo* is greatly depressed (59).

Harrell (48) observed that isolated osteoblasts grown on a polystyrene plate that had an orthodontic jack screw glued to its bottom responded to continuous strain by increasing PGE_2 concentrations followed in minutes by an increase in cAMP release. Rodan et al. (49) agreed that the second messenger cAMP was affected by mechanical strain and also reported changes in cGMP and calcium ions. Yeh & Rodan (47) suggested that prostaglandins might be involved in the transduction of mechanical strain but did not apply physiological levels of strain to their samples. Fluid shear experiments performed by Reich et al. (50) demonstrated that osteoblasts respond with an increase in cellular levels of inositol triphosphate.

Osteoblasts form bone by secreting many extracellular matrix proteins, including type I collagen, osteopontin, osteocalcin, osteonectin, biglycan, and decorin. Many of these proteins are currently being investigated with regard to their role in the transduction of mechanical strain. Osteopontin was first purified from rat bone matrix and is

considered to play an important role in the cascade of events required for the formation of bone matrix (60). Expression of osteopontin messenger ribonucleic acid (mRNA) has been shown to be elevated as a sequelae of mechanical stress (61). Osteocalcin, also known as bone Gla protein, is widely used as a marker for bone metabolism. Studies have shown that the expression of osteocalcin can be stimulated or depressed by mechanical stress both *in vivo* (62) and *in vitro* (63-65).

Though these cell culture studies generate promise for the quantitative delineation of the mechanically induced cellular response of bone, the enthusiasm for all of these studies must be tempered in light of the experimental models that have been used. Virtually all of these models employ some form of polyurethane membrane, collagen ribbon, or silastic plate as the substrate upon which the cells are grown and mechanically stimulated. Given the complex host-biomaterial interactions within the human body, the cellular response of isolated bone cells on polyurethane membranes or collagen ribbons is likely to be significantly different than bone cells in intimate contact with a contemporary implant biomaterial such as titanium alloy. In order to more appropriately explore the effects of mechanical strain on the cells of the bone-to-implant interface, an experimental system that allows growth of osteoblastic-like cells on the surface of an actual implant material is needed.

The goal of this investigation involved the development of an *in vitro* system in which osteoblasts can adhere to and proliferate on a titanium alloy (Ti-6Al-4V) substrate and subsequently be subjected to a controlled, quantified, uniform mechanical strain. Following completion and optimization of the *in vitro* system, an in-depth analysis of

some of the resultant biological responses of the osteoblasts was conducted. Observation of morphological alterations, and measurement of changes of the mRNA levels for osteopontin, β -1 integrin and type I collagen were the focus of this analysis.

HYPOTHESES

1. Living osteoblasts that are attached to a Ti-6Al-4V substrate are physiologically or pathologically affected by an alteration in the magnitude of strain present on the surface of the substrate. An increase in the environmental $\mu\epsilon$ will induce attached osteoblasts to realign the long axis of their cytoskeleton from an orientation that is random to one that is essentially perpendicular to the axial line of strain.
2. Reorganization of the cytoskeleton caused by changes in the strain environment may be mediated by altered expression and/or reorganization of osteoblast integrins.
3. Metabolic changes which result from cytoskeletal alterations are expected to include modification in the expression of genes related to the osteoblast phenotype. These strain induced changes in gene expression are expected to increase the production of proteins such as type I collagen, and osteopontin.

SPECIFIC AIMS

The specific aims are

1. To determine an appropriate osteoblast model to serve as an *in vitro* system in which osteoblasts adhere to and proliferate on implant materials and are subsequently subjected to a controlled mechanical strain.
2. To design an experimental testing system that will allow the application of dynamic, quantifiable, uniform, uniaxial deformation to viable osteoblasts attached to a Ti-6Al-4V substrate.
3. To use the experimental testing system developed in specific aim 2 to apply known magnitudes of strain to viable osteoblasts followed by observation and documentation of any morphological and/or organizational changes.
4. To measure mRNA levels of β -1 integrin in controlled and strained osteoblasts at varying timepoints.
5. To measure osteopontin mRNA levels in controlled and strained osteoblasts at varying timepoints.
6. To measure type I collagen mRNA levels in controlled and strained osteoblasts at varying timepoints.

SELECTION OF AN OSTEOBLAST MODEL

The determination of an appropriate osteoblast model was necessary as a first step toward the development of an *in vitro* system in which osteoblasts adhere to and proliferate on implant materials and are subsequently subjected to a controlled mechanical strain.

A preliminary study was conducted to compare the proliferation and morphological features of primary rat bone marrow cells (RBM) and three widely used osteoblastic cell lines (MC3T3-E1, MG-63, and ROS 17/2.8) (Courtesy of Dr. Charles Prince, Department of Nutrition Sciences, University of Alabama at Birmingham (UAB), Birmingham, Alabama) grown on both tissue culture plastic and polished commercially pure (CP)-Ti.

These cells, which are widely used as models of osteoblasts (66), were chosen because they display a range of osteoblast phenotypic markers and include primary cells (RBM) as well as clonal cell lines of normal (MC3T3-E1) and osteosarcoma origin (ROS 17/2.8 and MG-63). All of these cell populations produce type I collagen, the major protein of bone, and contain receptors for the osteotropic hormone, calcitriol, the hormonal form of vitamin D. All cell populations except the MG-63 cells express the bone matrix protein, osteopontin; however, only the RBM and MC3T3-E1 cells are capable of mineralized bone formation *in vitro*.

Cells (10,000/50 μ l of medium) were seeded onto 1.5 cm discs of Ti or onto tissue culture plastic on Day 0 and allowed to attach for 4 hr before removal of non-adherent cells. After growth for 2, 4, 6, and 8 days, triplicate samples were harvested and cells were counted with a Coulter counter. Mean values of cell numbers at each timepoint were determined and analyzed by ANOVA. As expected, each cell population proliferated to a different extent ($p < 0.0001$) with ROS 17/2.8 > RBM and MG-63 > MC3T3-E1; however, no difference in proliferation was noted for cells grown on CP-Ti versus plastic.

Cells that were grown on tissue culture plastic were observed at each time point using a Nikon™ Diaphot Phase Contrast microscope. Photographs were taken at 4 hr and 2, 4, 6, and 8 days after seeding. To observe the cells grown on CP-Ti, one extra disc was plated for each of the cell lines for scanning electron microscope (SEM) observation at the 4-hr and 2-day timepoints. The hexamethyldisilazane (HMDS) technique (67) was used to fix and dry the samples for SEM evaluation. This technique involved a series of dehydration steps using ethanol followed by submersion in HMDS for 30 min. After complete air drying, the SEM samples were sputter-coated with gold using a Denton™ Vacuum Desk-1 Cold Sputter-Etch unit and were viewed with a Philips™ 515 SEM. Micrographs were taken of the 4-hr and 2-day SEM samples.

Desirable characteristics of an osteoblastic cell model used to study the bone cell response to mechanical strain include both rapid attachment of the cells to Ti as well as early spreading tendencies. Increased area of contact between the cell and the strained environment develops as the cell spreads on the substrate. All of the cells in this

experiment attached well to the Ti, but the MC3T3-E1 cells showed the most spreading. The MC3T3-E1 cells also spread sooner than the other cell populations, which could be an advantage for detection of early cellular response to strain. Fig. 1 shows a SEM micrograph of MC3T3-E1 cells attached and spread on CP-Ti. Experiments conducted in the laboratory of Dr. Charles Prince have shown that no significant difference exists between the attachment characteristics of MC3T3-E1 cells grown on CP-Ti or Ti-6Al-4V.

The rounded morphology maintained by the ROS 17/2.8 (Fig. 2), and MG-63 cell populations and the inherent heterogeneity of the RBM cells make them less desirable as models for strain studies.

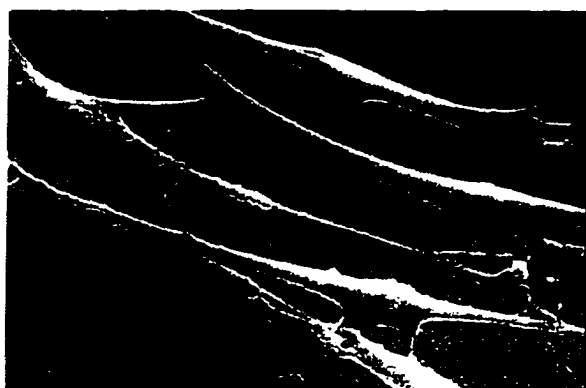


Fig. 1. MC3T3-E1 cells.

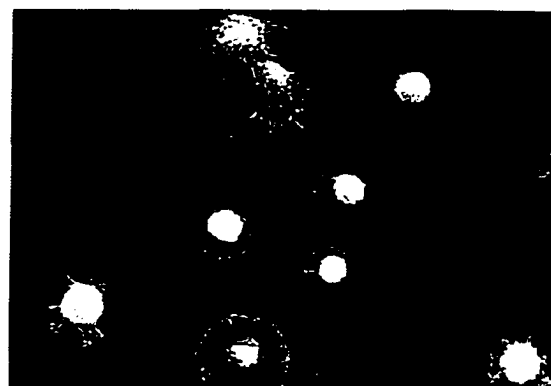


Fig. 2. ROS 17/2.8 cells.

Based on these data, the MC3T3-E1 cells exhibit attachment and proliferative characteristics which make them an appropriate osteoblastic cell model for *in vitro* studies

of osseointegration to orthopedic and dental implant materials and are thus the cells that were used in this work.

DEVELOPMENT OF THE MECHANICAL LOADING SYSTEM

Multiple *in vitro* techniques have been used to stimulate mechanical loading at the cellular level. Each of the different methods of strain application produces different types of cellular deformation, including hypotonic swelling, hydrostatic pressure, uniaxial stretch, biaxial stretch, and fluid shear stress (68).

Numerous investigators have demonstrated the responses of a wide variety of cell types in culture to these varied mechanical perturbations. The mechanical parameters employed (strain distribution, magnitude, frequency, and duration), however, have been diverse and, at times, incompletely defined, making it difficult to formulate a generalized relationship between particular features of mechanical deformation and cellular activity (69). In many of the experiments where the strain magnitude has been defined, the reported cellular responses are the result of strains that likely exceed the physiological range. Additionally, many of the substrates on which the cells are observed are not representative of an interface that would be present *in vivo*.

Of the most common loading methods discussed above, uniaxial stretch and fluid shear most closely simulate the types of deformation bone cells undergo *in vivo* (38). Hypotonic swelling never occurs in bone under physiological conditions and biaxial stretch does not accurately simulate the Poisson's effect that occurs in mineralized tissue

in vivo (38). Hydrostatic pressure almost never occurs in mineralized bone but can occur in bone marrow in the epiphyseal regions (70).

Design of the Strain Application Device

Uniaxial deformation was chosen as the appropriate loading scheme for this study. In order to create a uniformly strained environment along the surface of the titanium substrate, a strain application system which placed the substrate in pure bending was developed. A member subjected to equal and opposite couples acting in the same longitudinal plane is said to be in a state of pure bending (71).

The most practical method for placing a material in pure bending is to utilize the 4-point bend method. Theoretical and experimental evidence shows that although a homogeneous bar placed in 4-point bend results in stress concentrations in the local area of load application, a uniform, uniaxial stress distribution is established in the area between the contact points. A photoelastic study (72) seen in Fig. 3 depicts a homogeneous material placed in 4-point bending. The parallel dark fringes indicate that in the portion of the strip medial to the points of load application, the stress distribution is the same in all vertical cross sections.



Fig. 3. Photoelastic coating showing uniform stress in 4-point bending (Taken from S. Timoshenko, *Strength of Materials*, 2nd Ed., Lancaster Press, p 349, 1941.)

Jones et al. (51) used a 4-point bending device to apply a defined cyclical load to toughened glass plates. Strain gages mounted in several areas on the culture surface of 10 different plates showed that identical loads resulted in identical strains over the entire area of the culture surface.

In addition to the creation of a uniformly strained region, the use of the 4-point bend method allows the titanium substrate to be placed in tension or compression by manipulating points of load application (Fig. 4). This may provide valuable information when cellular response to these two loading regimes are compared. A review of the literature has shown that dynamic or cyclic loading is necessary to cause a significant metabolic change to occur in the bone cell population both *in vivo* and *in vitro* (36, 38, 44, 46, 52, 69, 73-81).

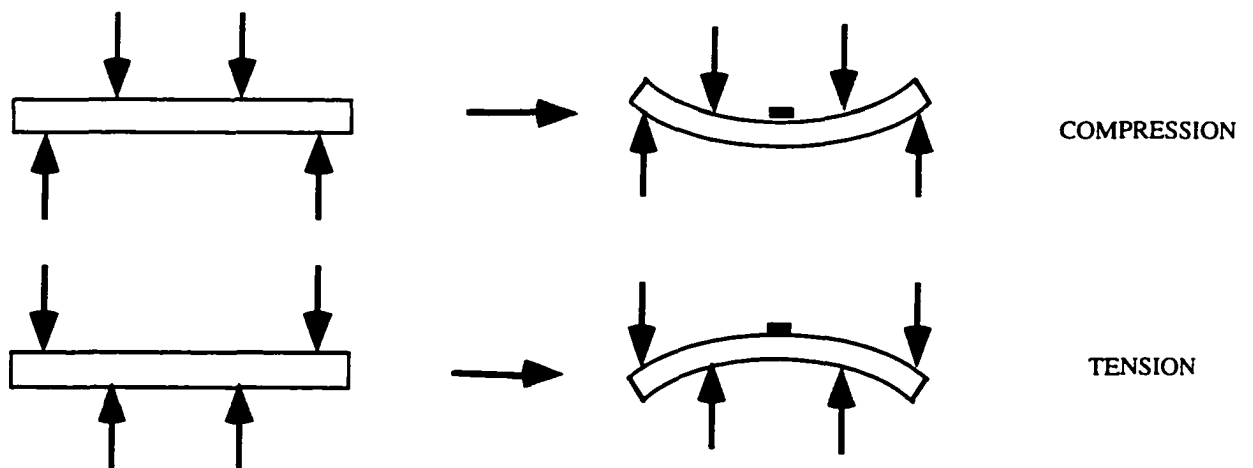


Fig. 4. 4-point bend fixture can produce compression or tension.

The greater the rate of change of applied strain in bone, the more bone formation is increased (82). This important observation has been replicated several times and demonstrates that static stretch of cells *in situ* is not sufficient to activate a bone-modeling response (38). The effect of applied strains on bone is dictated not only by the rate of the applied loads, but also by the magnitude and duration (38). Lower magnitude loads applied for many cycles can cause the same anabolic effects as larger loads applied for a limited number of cycles. For instance, Rubin & Lanyon (81) demonstrated that the application of 2050 $\mu\epsilon$ at a frequency of .5 Hz for four consecutive cycles per day produced the same maintaining effect on bone mass in immobilized limbs as 100 consecutive cycles of 1000 $\mu\epsilon$ applied at the same frequency (.5 Hz).

In order to carefully control the magnitude, duration, and rate of applied loads to the Ti-6Al-4V substrate, the Mechanical Testing Systems (MTS) Model 8581 mini-Bionix™, servo-hydraulic testing machine was chosen. The MTS is currently located in the Biomechanics Laboratory of the UAB Department of Biomedical Engineering, Birmingham, AL. The MTS, in conjunction with the 458A1 Microprofiler, allows the production of quantifiable, cyclical strain profiles in the Ti-6Al-4V substrate. The Microprofiler™ serves as a wave generator that is used to design a specific load or displacement profile.

The standard 4-point bend fixtures designed by the company do not allow enough vertical space between the points of contact and the cross bar for cells and media. A design for fixtures which do allow space and are interchangeable within the MTS load

frame to allow either compression or tension of the substrate has been adapted from 4-point bend fixtures described in the 1995 ASTM volume 15.01. Fig. 5 represents a drawing of the 4-point bend fixture that was designed and used in this study.

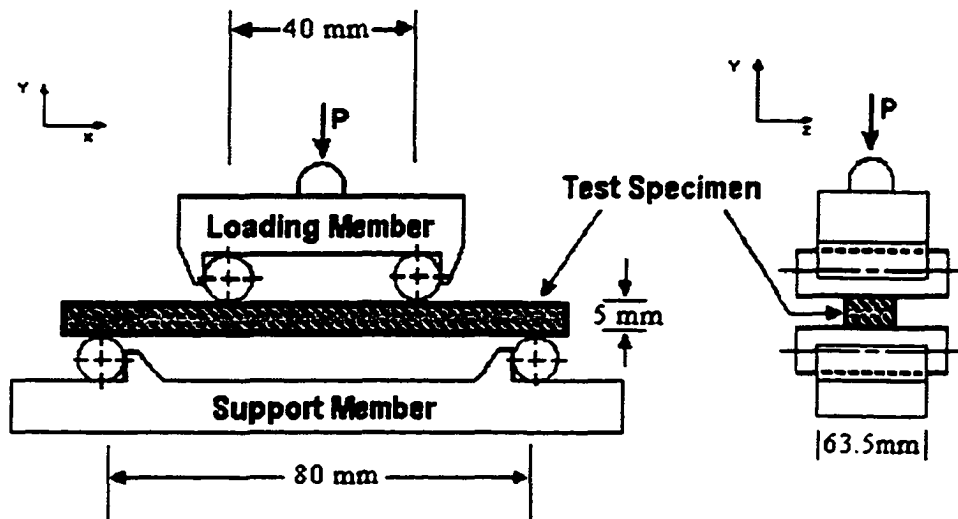


Fig. 5. Schematic of four point bend fixture.

Ti-6Al-4V Sample Design and Preparation

As mentioned earlier, Ti-6Al-4V is commonly used as the material of choice for both surgical and dental implants; therefore, Ti-6Al-4V was chosen as the substrate on which to culture the MC3T3-E1 cells. Ten rectangular coupons of Ti-6AL-4V, measuring 100 mm x 30 mm x 5 mm, (Fig. 6) were obtained from Innovations, a company located in Drummons, TN. All samples were measured, and each requested dimension fell within the specified tolerance range. One side of each coupon was scored, both horizontally and vertically, to create a visual guide for ideal placement of the strain gages. A fine blade and

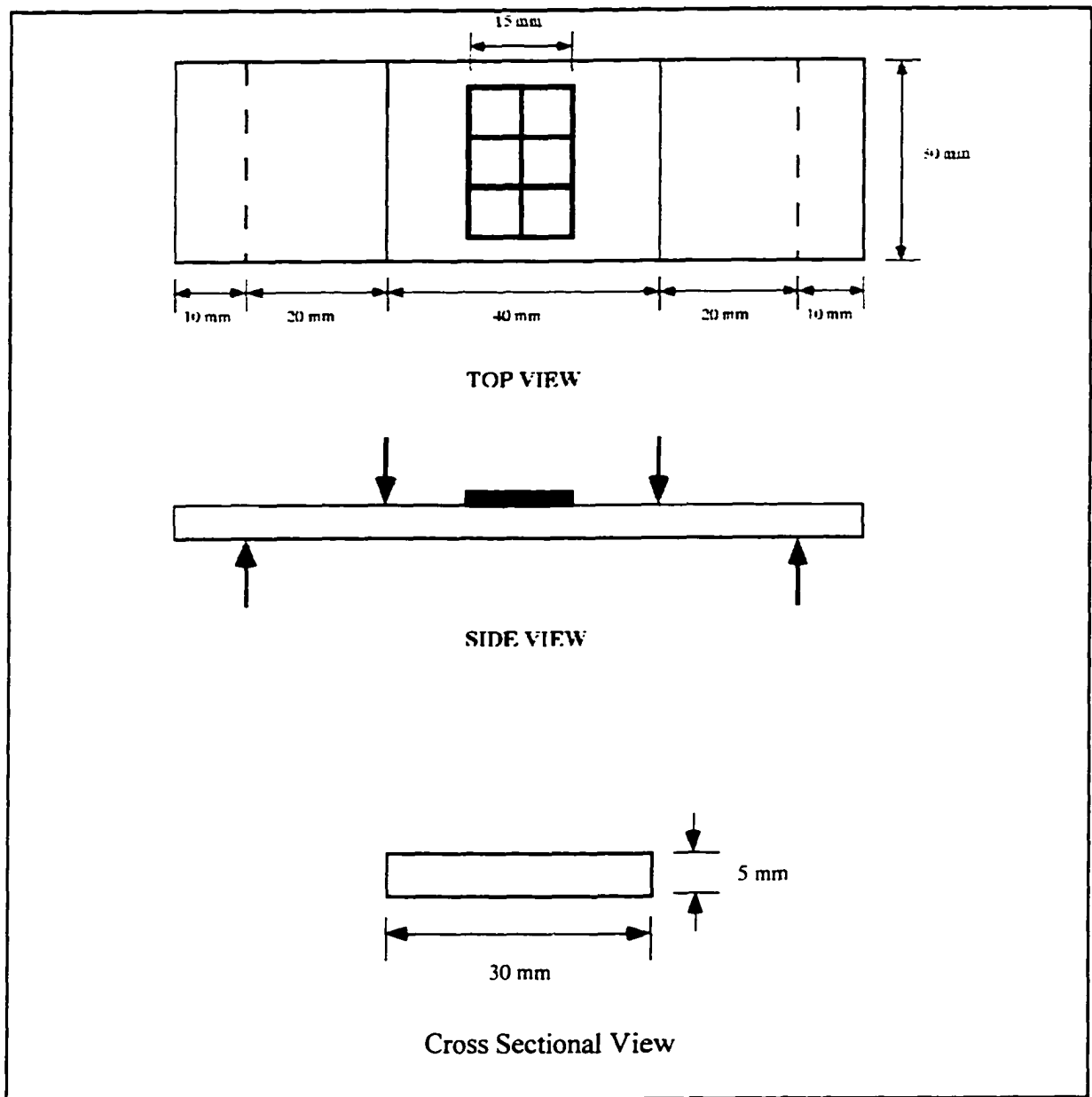


Fig. 6. Ti-6Al-4V sample dimensions.

a level graphite table was used to ensure accurate markings on all of the coupons. The surface of the Ti-6AL-4V coupons opposite the score marks was polished to a mirror finish using grit paper and alumina on a Beuhler Polishing Machine™. The final polish was achieved using 0.3 micron alumina .

The next step in sample preparation involved cleaning and passivation of the coupons. All samples were covered in benzene and placed in the ultrasonic cleaner for 10 min. The samples were then rinsed with distilled water and placed in acetone in the ultrasonic cleaner for another 10 min. After rinsing again with distilled water, the samples were placed in the ultrasonic cleaner covered in 95% ethanol. Following a third distilled water rinse, the samples were placed in a container of 40% volume nitric acid for 30 min and allowed to passivate. The samples were then rinsed with distilled water and allowed to air dry before application of the custom wells.

The next step in sample design involved developing a method to divide each coupon into six discrete sections so that multiple cellular samples could be evaluated from one test. In addition to the divisions themselves, retention of cell media for each compartment was another design criteria. In order to meet both of these design specifications, 16-well chamber slides were purchased from Fisher Scientific, Springfield, NJ. The polystyrene elevations were removed and modified to create 6-well sections that fit transversely on the Ti-6Al-4V coupons. The gasket that secured the wells to the original glass slides was destroyed when the wells were removed. Pure silicone (Dow Corning, Midland, MI) was used to affix the modified 6-well section to the Ti-6Al-4V

coupons. Silicone was chosen as the luting agent because it has a much lower elastic modulus ($E < 8,280 \text{ MPa}$) (83) than that of the Ti-6Al-4V ($E = 110 \text{ GPa}$) (84) and should not create any stiffening or bracing effects which might alter the strain distribution during cyclic loading. This assumption was verified by measuring strain on the surface of the Ti-6Al-4V samples with and without the silicone wells following application of the same load. The polystyrene covers used as the ceiling on the 6-well section were modified from the original cover plates that came on the 16-well slides.

As soon as the wells were successfully attached to the clean, passivated, Ti-6Al-4V samples, they were placed in a ultra violet (UV) hood for 24 hr. The cover plates were turned up so that the surface that would be facing the cell media was exposed to the UV light. After the UV treatment, the covers were secured on the wells and the samples were transported to the biomechanics laboratory for placement of the strain gages.

Gage Application and Strain Monitoring System

In order to accurately record the dynamic strain perceived by the attached cells on the surface of the Ti-6Al-4V samples, self-temperature-compensating (S-T-C) strain gages (WK06125TM 350) (Measurements Group, INC, Raleigh, NC) were used. These gages were chosen because they have a fatigue life of 10,000 cycles at $\pm 3,000 \mu\epsilon$. The fatigue life of the gage is an important consideration when dynamic testing is being done. A fatigue life of 10,000 cycles was sufficient for this work because it exceeded the 1,800 cycle strain regimen that was used.

Another reason for the selection of the WK06125TM 350 gage was that it was arranged in a 90° T-rosette fashion. This allowed one leg of the gage to read strain along the normal axis of the sample, while the other leg read the transverse strain.

In order to accurately measure the axial and transverse strain, precise positioning of the gages was necessary. A dissecting microscope was used to ensure that the gages were aligned along the score marks previously placed on the Ti-6Al-4V samples. This method of gage placement resulted in the gages being positioned directly beneath the cell wells on the opposite side of the coupon. Since any strain induced on the surface of the homogeneous, symmetrical, coupon directly opposite the cell wells is equal to the strain on the surface to which the cells are attached, measurement of this strain allows determination of the exact strain perceived by the attached cells. Other than the use of score marks instead of graphite positioning lines, the gages were applied according to the manufacturer's specifications.

Following proper application of the strain gages, lead wires were soldered to the terminals to allow connection to the Model D1-510-32 DATAQ PC-based data acquisition system (MTS Systems Corporation, Eden Prairie, MN). After soldering these lead wires, two coats of M-coat were applied over the gages and terminals to seal and protect them from exposure to the humid environment that would be encountered in the incubator following the plating of the cells. Once the lead wires were attached and coated, they were cut to the appropriate length to allow them to passively extend from the strain fixtures of the MTS to the DATAQ system. The wires were then coiled and

taped to allow easy transportation to the tissue culture hood for plating of the MC3T3-E1 cells.

As mentioned above, the Model D1-510-32 DATAQ PC-based data acquisition system was chosen to monitor and record the strain profiles created in this study. The DATAQ system strain gage excitation modules transfer strain data to an associated PC which uses the software program WINDAQM to record the strain wave profile as the strain in the coupon goes from zero to the peak strain and back to zero again. For each strain test, dynamic data from the axial gage, the transverse gage, and input from the MTS load cell is recorded and saved for subsequent evaluation.

Before each test run of 1,800 cycles, the strain gages and the load cell had to be zeroed out. The gages chosen for this study were 350 Ω gages. The stock connections for the DATQ were designed for 120 Ω gages and as a result, the 350 Ω gages could not initially be zeroed out prior to testing. To avoid having to subtract the initial strain reading from all subsequent readings when using the non-zeroed 350 Ω gages, a custom connection with two 400 Ω resistors and two 1-K potentiometers was fabricated. This new set-up allowed the 350 Ω gages to be zeroed prior to testing and made the subsequent waveform analysis more ideal.

Once the data acquisition system was optimized, the Ti-6Al-4V coupons were loaded using the MTS and the strain fixtures previously discussed. This loading was done both statically and dynamically, with and without wells attached. It was observed that within the strain range of this study, which was within the elastic range of the Ti-6Al-4V,

a distinct load applied by the MTS could be correlated with a distinct strain on the surface of the Ti-6Al-4V coupon. The addition of the 6-well section via the silicone gasket did not alter this correlation in any way.

Plating of MC3T3-E1 Cells

Frozen MC3T3-E1 cells were obtained from the laboratory of Dr. Charles W. Prince. The cells were initially thawed and plated in 75-ml flasks in 10 ml of HEPES α -MEM medium (Fisher Scientific). The cells were allowed to attach and grow until they were almost confluent along the bottom of the flask. In order to count the cells prior to plating them on the Ti-6Al-4V coupons, all of the medium was removed and the cells were rinsed with 5 ml of Hank's balanced salt solution (HBSS) to remove any remnants of serum. Five mls of sterile filtered pronase (0.001% pronase E, 0.02% EDTA in HBSS) was then added to the flask, and it was placed back in the incubator and allowed to incubate for 5 min. This process caused the cells to detach from the flask. After the cells were visibly detached, 5 mls of media was added to the flask and the entire volume was transferred to a 15-ml centrifuge tube. The tube was placed in a table top centrifuge and was allowed to spin on setting 4 for 5 min to pellet the cells. The pellet was resuspended in 5 mls of media, and 40 μ l of the resuspension was added to 20 ml of isotone solution for counting in the Coulter counter. Once cell number was determined by the Coulter counter, the cells were diluted to the appropriate volume to produce 2,000 cells per 25 μ l.

It was determined that the wells on the Ti-6Al-4V samples could retain 195 μl of media with the cover plate in place. In order to obtain an even distribution of the cells in these small wells, the following protocol was followed: 170 μl of HEPES α -MEM (Fisher Scientific) was initially placed in each well. HEPES α -MEM does not require CO_2 buffering and can be used without supplemental CO_2 . This feature prevented the need for special environmental regulation during the strain regimen. Twenty five microliters of the diluted cell suspension was placed very slowly into each well using a manual pipetor. The cover plates were placed on top of the wells and the coupons were placed in the incubator over night to allow the cells to attach and spread on the polished Ti-6Al-4V surface. This plating protocol was used for each round of testing. Following strain testing and the appropriate analysis (morphological or metabolic), the wells were removed from the Ti-6Al-4V surfaces and the coupons were polished, cleaned, passivated, and made ready for the next series of tests.

Strain Application Protocol

The Ti-6Al-4V samples with the MC3T3-E1 cells attached were removed from the incubator after overnight incubation and placed in the 4-point bend fixture in the MTS. The lead wires were uncoiled and attached to the appropriate channels on the custom bread board of the DATAQ. Three channels representing the axial gage, the transverse gage, and the load cell of the MTS were visible when the WINDAQM 200 M

software was initiated. Prior to any loading, the gage channels were zeroed using the potentiometers on the bread board and the load cell was zeroed using the microprofiler™.

Although the 4-point bend fixture was designed to deliver either a compressive or tensile load, a dynamic compressive load was chosen for this investigation.

The MTS was operated in load control following a sinusoidal loading profile that was programmed into the microprofiler. A sinusoidal wave profile was selected for this dynamic strain investigation because it more closely mimics the pattern of masticatory movements (85) than other wave form options. Although a person's individual chewing pattern is largely based upon coordination of condylar guidance, incisal guidance, plane of occlusion, cusp angles, and the curve of Spee, this pattern has been shown to develop in a way similar to that of the characteristic individual gait of walking (85). A value of 1,800 cycles at 1 Hz (cycle per second) was used because it is estimated that people average around 1,800 chewing strokes per day (86).

In order to test the hypothesis that different magnitudes of dynamic strain would cause different morphological and metabolic responses, two strain magnitudes (3,000 $\mu\epsilon$ and 6,000 $\mu\epsilon$) were used throughout the course of this investigation.

For the 3,000 $\mu\epsilon$ experiments, a single loading cycle consisted of a compressive load being applied until the axial strain gage read 3,000 $\mu\epsilon$ and release of that load until the gage read 0 $\mu\epsilon$. As stated above, this sinusoidal wave from 0 $\mu\epsilon$ to 3,000 $\mu\epsilon$ and back to 0 $\mu\epsilon$ took 1 second (s). The same protocol was used with the 6,000 $\mu\epsilon$ tests.

The WINDAQM software recorded the waveforms of the axial gage, the transverse gage, and the load cell during the entire 1,800 cycle test. The program was set up to take 50 strain readings for each cycle from each channel. This resulted in the recording of 150 data points per second for 30 min yielding 270,000 data points per test. This ensured that very detailed waveforms could be subsequently analyzed, and the actual strain perceived by the cells attached to the Ti-6Al-4V substrate could be reported.

Following the strain regimen, the Ti-6Al-4V samples were removed from the 4-point bend fixture and were placed back into the incubator. At the appropriate time-points, the cells were harvested or fixed as determined by the method of analysis (Table 1).

Table 1. Strain protocol for morphological and metabolic analysis.

<u>Morphological Analysis</u>			
<u>Strain Magnitude</u>	<u>Hz</u>	<u>Number of Cycles</u>	<u>Timepoints</u>
3,000 $\mu\epsilon$	1	1,800	1hr, 4hr, 8hr, 12hr, 24hr
Control 0 $\mu\epsilon$	0	0	1hr, 4hr, 8hr, 12hr, 24hr
6,000 $\mu\epsilon$	1	1,800	1hr, 4hr, 8hr, 12hr, 24hr
Control 0 $\mu\epsilon$	0	0	1hr, 4hr, 8hr, 12hr, 24hr
<u>Metabolic Analysis</u>			
<u>Strain Magnitude</u>	<u>Hz</u>	<u>Number of Cycles</u>	<u>Timepoints</u>
3,000 $\mu\epsilon$	1	1,800	1hr, 4hr, 24hr, 48hr
6,000 $\mu\epsilon$	1	1,800	1hr, 4hr, 24hr, 48hr
Control 0 $\mu\epsilon$	0	0	1hr, 4hr, 24hr, 48hr

DEVELOPMENT OF THE CELL IMAGING METHODOLOGY

Endothelial and aortic smooth muscle cells are commonly used for investigating strain-induced alteration of cellular alignment. Ives et al. found that human and bovine endothelial cells responded differently to various types of strain. The cells oriented themselves parallel to the direction of shear strain induced by fluid flow, but perpendicular to the axis of mechanical deformation on a cyclically stretched polyurethane membrane (87). Previous work with osteoblast-like cells stimulated by cyclic mechanical strain also resulted in the alignment of the cells perpendicular to the strain vector. This perpendicular alignment was noted at 4 hr after loading and was significant by 12 hr (88). Buckley et al. suggested that the preferred orientation may have resulted from a mechanical effect on the osteoblast, wherein cell attachments were broken in the maximum strain direction, leaving only those attachments already present in the least strained conformation. A second hypothesis is that the cells may resolve their focal contacts and move in order to minimize the strain to which they are subjected.

Another study involving osteoblast-like cells was reported by Carvalho et al. (89). They investigated cytoskeletal organization in mechanically strained bone cells isolated from the alveolar processes of Sprague-Dawley rats. The earliest change in cytoskeletal organization was noted 30 min after the initiation of the strain protocol. They

observed that the cells oriented themselves perpendicular to the long axis of the applied mechanical strain

Both of the studies cited above (88, 89) used osteoblast-like cells cultured on the Flexcell straining apparatus. As previously mentioned, measurement of the actual strain induced by the flexible membrane is difficult and is often vaguely reported. The use of the strain application device designed for this investigation, in combination with fluorescent staining methodologies, permits the observation of cytoskeletal rearrangement in response to known magnitudes of strain.

Cellular Staining Protocol

Rhodamine phalloidin and 5-chloromethylfluorescein diacetate (CMFDA) were used in conjunction with fluorescence microscopy were the stains used in this study to compare the alignment and morphology of strained and unstrained cells. The CMFDA, also known as Cell Tracker™, and rhodamine phalloidin were obtained from Molecular Probes, Eugene, Oregon. Rhodamine phalloidin allowed visualization of the actin cytoskeleton of the cells, and the Cell Tracker™ stain targeted the entire cytoplasm of the MC3T3-E1 cells and provided a means of assessing cell shape and number.

In order to stain the cells using Cell Tracker™, the cells had to be vital. In general, the Cell Tracker™ stain contains an acetate group which normally makes the compound non-fluorescent. When this lipid soluble compound is taken across the cell membrane, cell esterases clip the acetate moiety resulting in a fluorescent compound. This is how the

cellular cytoplasm can be visualized. In order to prevent any interference of this stain with normal cellular metabolism, the stain was introduced 30 min before the cells were fixed according to the appropriate timepoint following straining.

The 50 μg vials were stored in the freezer until ready for use. In order to hydrate the desiccated stain and create a stock vial, 11 μl of DMSO was added to the vial to yield a 10 mM solution. To obtain the 5 μM solution that was desired to actually add to the cell wells, 2 μl of the stock vial was mixed with 2 ml of media.

Thirty minutes before the appropriate timepoint, the Ti-6Al-4V coupons with the cells attached were removed from the incubator. All media was removed from the wells, and the cells were rinsed one time with PBS. One hundred and ninety microliters of the Cell Tracker™/media dilution was placed in each well, and the samples were put back in the incubator for 30 min. After this incubation period, the cells were fixed using 37% formaldehyde. This fixation process involved removal of the stain/media mixture followed by two rinses with PBS. One hundred and ninety microliters of the 37% formaldehyde was added to each well, and the samples were allowed to sit at room temperature in the tissue culture hood for 6 min. The wells were then rinsed twice with PBS. This completed the fixing process.

The rhodamine phalloidin stain consists of a rhodamine tag conjugated to a phalloidin molecule. Once inside the cell, the phalloidin binds to the polymerized actin filaments. To prepare the stock vial of rhodamine phalloidin, the contents of the original vial were dissolved in 1.5 ml of methanol. This stock vial was stored at -20°C . To

prepare the staining solution that would be added to the cell wells. 15 μ l (for 12 wells) was removed from the stock vial and placed in a Coulter counter vial under the hood to allow evaporation of the methanol. Just prior to use, the rhodamine phalloidin was reconstituted in 600 μ l of PBS. This volume allowed the disbursement of 50 μ l of the stain solution into each of the wells.

Prior to staining with the rhodamine phalloidin stain, the cells, fixed as above, were then permeablized by the addition of 100 μ l of 0.5% Triton X-100 in PBS to each well. Following a 6-min incubation at room temperature, the wells were rinsed twice with 190 μ l of PBS. All PBS was aspirated from the wells, and 50 μ l of the rhodamine phalloidin stain dilution was added to each well. The samples were incubated at room temperature in the dark for 10 min. Following this incubation, the stain solution was removed from each well and they were rinsed three times with PBS. This completed the dual staining process. At this point, the 6-section cell wells were removed from the Ti-6Al-4V coupons and the cells were ready to be imaged.

Microscopic Imaging Technique

The stained cells were viewed and the images captured using an inverted Zeiss Axiovert 35 Microscope (Zeiss, West Germany) in conjunction with a Photometrics Sensys camera (Photometrics, Tucson, Arizona) and IP Lab Spectrum software loaded on a Power Macintosh computer. In order to consistently position the Ti-6Al-4V samples for viewing with the Zeiss microscope, a custom microscope stage was designed. The custom stage is interchangeable with the original standard slide stage that is provided with

the microscope. The custom stage contains a rectangular opening that precisely fits the Ti-6Al-4V samples. The titanium samples were inverted in the custom stage, and the attached, fixed cells were viewed through the objectives below the stage. The cytoskeletal orientation or alignment was visible when rhodamine phalloidin stain was used in conjunction with a Texas Red (570) filter. A FITC (490) filter was used to view the Cell Tracker™ stain. These two filters used different wavelengths to visualize their respective stains. By simply rotating the filter wheel on the microscope, both stains could be visualized in the exact same field of view. This feature allowed two images of the exact same cells to be captured. One image reflects the rhodamine phalloidin stained cytoskeletons, while the other shows the Cell Tracker™ stained cytoplasm of the cells present in that field.

Two stains, 2 conditions (strained vs. control), 6 wells per coupon, 5 timepoints (1 hr, 4 hr, 8 hr, 12 hr, 24 hr), and two strain magnitudes (3,000 $\mu\epsilon$ and 6,000 $\mu\epsilon$) resulted in the capture of 240 images.

DEVELOPMENT OF THE QUANTITATIVE RT-PCR METHODOLOGY

Alterations in gene expression caused by mechanical perturbation of osteoblast-like cells are currently being evaluated by numerous investigators (58, 75, 76, 90, 91). Experimental methods such as *in situ* hybridization, RIA and nuclear run-on assays are often used to quantify the degree of gene expression at both the protein and mRNA levels (90-92). These methods are very useful in certain situations; however, small sample sizes such as those used in this investigation present a problem for these conventional methods. In order to maximize the sensitivity of the analysis of the mRNA obtained from the strained and control cell samples of this investigation, quantitative reverse transcriptase-polymerase chain reaction (RT-PCR) utilizing plate based EIA methodology was used (99).

The first step in conventional RT-PCR involves a process in which mRNA from the cells is reverse transcribed into cDNA. The small amount of target cDNA is then amplified by PCR. The PCR mimics the DNA replication process that occurs naturally within cells. The cDNA is first heated to separate the two template strands. Small 20 - 30 base fragments (primers) of DNA complementary to the region of interest are then annealed to the single-stranded templates. A heat-stable Taq polymerase adds nucleotides to the primer and eventually makes a complementary copy of the template. Since one

PCR cycle can act as the template for the next, the number of new DNA molecules doubles with each PCR cycle. One PCR cycle takes less than 2 min. Thirty PCR cycles can produce around 1 million copies of the original cDNA in less than 3 hr.

Although conventional RT-PCR is an extremely useful tool used to amplify small amounts of DNA, it is difficult to use quantitatively (93-96). Methods have been used that incorporate a radioactive label into the amplified DNA in order to measure the product yield, but this process gives no true measure of initial cDNA concentrations (97).

As a means of solving this problem, researchers developed a process called competitive PCR (94-96, 98). This method involves the addition of known amounts of a synthetic DNA fragment that is slightly larger or slightly smaller than the DNA that is to be amplified (analyte DNA). Both the analyte DNA and the competitor DNA are added to the PCR reaction; due to the similarity of their sequences, both fragments are amplified.

Following PCR, the amplified fragments, which differ slightly in size, can be fractionated on agarose gels, stained with ethidium bromide (EtBr) and quantified using densitometry (99). By plotting the ratio of analyte DNA to the competitor DNA versus the known copy number of the competitor DNA added, the number of copies of the analyte DNA can be determined. The use of competitor DNA controls for the inefficiencies of the PCR. However, when RT-PCR is used, the aforementioned method does not control for the RT reaction (99). In order to provide controls for the entire process, investigators developed methods to generate RNA competitors for the DNA subclones that could be added in known quantities to the initial RT reaction (93-95).

This revised methodology gives reproducible, accurate results, but when it is used with the agarose gel analysis system, the number of samples that can be analyzed at one time is limited. Additionally, in order to analyze several DNA fragments, cDNA of each analyte must be cloned individually and then subcloned in a slightly longer or shorter form to use as competitors during PCR.

A method developed by Hockett et al. uses a general cloning vector, pQPCR1, for building RNA competitors that does not require prior cDNA cloning (99). This general cloning vector was designed to accommodate multiple primer templates that allow simultaneous quantification of several different analytes from a single RT reaction. This vector was constructed in the pBluescript plasmid and contains a 230-base pair 'stuffer' fragment that allows discrimination between amplified endogenous DNA and competitor DNA by sequence specific hybridization. The pQPCR1 vector also contains a 'spacer' segment that ensures that the distance RT must synthesize cDNA remains nearly the same for the analyte cDNA and the competitor.

The spacer segment is flanked by a 15-base pair poly A+ tail which is used to prime cDNA synthesis using oligo dT. Lastly, the pQPCR1 vector contains several restriction endonuclease sites on each side of the stuffer segment that allow the desired PCR primer templates to be cloned in (99).

Due to the small sample sizes used in the current investigation and the desire to measure subtle changes in the mRNA expression of the strained cells, the quantitative RT-PCR methodology as described by Hockett et al. was utilized.

Construction of the Template BNC-1

The competitor construct used in this investigation, designated BNC-1, was designed with the aid of R.D. Hockett (Department of Pathology, UAB, Birmingham, AL). The BNC-1 construct was designed to include PCR primer templates for osteopontin, osteocalcin, type I collagen, and $\beta 1$ integrin. The 5' and 3' template map for the BNC-1 construct is shown in Fig. 7.

The 5' and 3' templates of BNC-1 were created by synthesizing their respective sense and antisense oligonucleotides on a oligonucleotide synthesizer (Midland Certified Reagent Company, Midland, TX). The sense and antisense oligonucleotides of the 5' template were resuspended to 1 $\mu\text{g/ml}$ and stored in a -80°C freezer. The 3' oligonucleotides were resuspended to 10 $\mu\text{g/ml}$ and were also stored at -80°C .

The 5' template of BNC-1 was inserted into the cloning vector by annealing 10 μg of each oligo in 100 μl of 1x annealing buffer (10 mM Tris, pH 7.4, 1 mM EDTA), and ligating the 76 base pair fragment into the KPN-1 and the EcoRI sites of pQPCR1. Sequence analysis of the miniprep DNA confirmed the desired 5' template was inserted. The 3' template was also annealed in 1x annealing buffer and then ligated into the BamHI and XbaI sites of pQPCR1 vector that now contained the 5' template of BNC-1. The insertion of the 3' template was also confirmed by sequence analysis of miniprep DNA.

Fig. 7. BNC-1 template map. This figure shows the sequences of the 5' and 3' template for BNC-1. Restriction sites are represented in italics.

BNC-1 TEMPLATE MAPS

5'-TEMPLATE

	OSTEOCALCIN	COLLAGEN	H3
5'- C	T G C G C T C T G T C T C T C T G	C T A A C C A A G G C T G C A A C	A A G C T T
C A T G G	A C G C G A G A C A G A G A G A C	G A T T G G T T C C G A C G T T G	T T C G A A
KPN-I			
	B-1 INTEGRIN	OSTEOPONTIN	
	A C T G C T A G T G C C A A T G C	C A G G A G A G T G C C G A T C A	G
	T G A C G A T C A C G G T T A C G	G T C C T C T C A C G G C T A G T	C T T A A 5'
			EcoRI

3'-TEMPLATE

BamIII	COLLAGEN	OSTEOPONTIN	Sal-I
G A T C C	C A C G A G T C A C A C C G G A A	A A C G G C C A C T G C A T T T T	G T C G A C
	G T G C T C A G T G T G G C C T T	T T G C C G G T G A C G T A A A A	C A G C T G
	B-1 INTEGRIN	OSTEOCALCIN	
	G T A G C A T T G C T G A G T G G	T T A G G A C C T G T G C T G C C	T
	C A T C G T A A C G A C T C A C C	A A T C C T G G A C A C G A C G G	A G A T C 5'
			Xba

Preparation of the DNA Competitor From BNC-1

Twenty-five micrograms of the BNC-1 plasmid template was linearized with XhoI, gel purified on a 1% agarose gel, and the linearized DNA was extracted from the gel by electrolution. The DNA was cleaned by two phenol/chloroform extractions and was then resuspended in 50 μ l of TE (10 mM Tris, pH 7.4, 1 mM EDTA). Twenty-five microliters of this solution were used to calculate the mass by OD₂₆₀. Dilutions of the BNC-1 competitor DNA ranging from 1 molecule/ μ l to 1×10^7 molecules/ μ l were made in H₂O with 10 μ g/ml of MS-2 phage RNA (Boehringer Mannheim, Indianapolis, IN). Three 50 μ l aliquots of each dilution were made, and all were stored in the -20° C freezer in a box labeled BNC-1.A3 #715.

Preparation of the RNA Competitor From BNC-1

Ten micrograms of linearized BNC-1 DNA was transcribed with T3 polymerase in the following reaction mixture (total volume 100 μ l): 10 μ l XhoI linearized BNC-1, 10 μ l 10 x T3 Ampliscribe Reaction buffer (Boehringer Mannheim, Indianapolis, IN), 1 μ l 1 M DTT, 2 μ l RNase inhibitor (RNasin), 1 μ l 100 mM ATP, 1 μ l 100 mM GTP, 1 μ l 100 mM UTP, 1 μ l 100 mM CTP, 3 μ l ³H-UTP, 3 μ l T3 RNA Polymerase, and 67 μ l RNase free H₂O. One μ l aliquots were taken for total radioactivity counts. After incubation at 37°C for 1 hr, the RNA was purified over oligo dT/latex beads (Oligotex beads, Qiagen, Chatsworth, CA). The mass of competitor was calculated according to the methods described by Hockett et al. (99).

Dilutions of the RNA competitor ranging from 50 copies/ μ l to 1×10^7 copies/ μ l were made into guanidine isothiocyanate (GITC) solution with 10 μ g/ml MS-2 phage RNA and stored at -80°C .

Cell Harvesting Techniques

The primers for osteopontin, osteocalcin, type I collagen, and β -1 integrin were evaluated and optimized prior to use with the strained and controlled cellular RNA. For this optimization process, MC3T3-E1 cells were grown on tissue culture plastic until almost confluent and, using pronase, were then removed from the flask. The cells were pelleted and were then resuspended in α -MEM/Hepes media for counting with the Coulter counter. One million cells were pelleted and then lysed with 1 ml of prepared GITC containing 10 μ g/ml MS-2 phage RNA (GITC, Amresco, Solon, OH) and 0.1 M 2-ME (Sigma, St. Louis, MO) and were stored at -80°C . This cellular extract was used to test the oligonucleotide primers.

MC3T3-E1 cells that were actually grown on the Ti-6Al-4V coupons and were subsequently strained or used as control samples were harvested in a different manner than described above. At the appropriate time-point, 100 μ l of prepared GITC was added to one of the six wells on the Ti-6Al-4V bar. The same 100 μ l was pipeted up and down and was transferred to an adjacent well. This was repeated one more time, and then the cellular extract was placed in an eppendorf tube, labeled, and was stored at -80°C until

RNA extraction could be done. This process produced two samples from each Ti-6Al-4V coupon.

Reverse Transcription

Total RNA was isolated from cells by a modification of the acid/phenol extraction procedure of Chomczynski & Sacchi (100). Two microliters of the cellular extract (1,000 cells/ μ l) was added to 198 μ l of prepared GITC. One hundred and ten microliters of this cell mix was placed into a .5 ml eppendorf tube along with 11 μ l of 2 M sodium acetate pH 4.0. One hundred ten μ l of water saturated phenol (pH 4.3, Amresco, Solon, OH) and 50 μ l of chloroform were added and the tubes were vortexed and then spun in a microcentrifuge at high speed for 4 min. The supernatant was transferred to a new tube, and this process was repeated. After transferring the supernatant for the second time, 100 μ l of chloroform was added, and the extraction process was again performed. The aqueous phase was then transferred to another 0.5 ml eppendorf tube and isopropanol precipitated on dry ice for approximately 15 min. After microcentrifugation, the pelleted sample was washed in 100 μ l of 80% EtOH and air dried. The invisible pellet was resuspended in 10 μ l of water and 1 μ l of 20 ng/ μ l oligo dT (Promega, Madison, WI). The solution was heated at 70°C for 10 min and was then placed on ice for 5 min. Nine microliters of reverse transcription mixture (12 μ l 5 x RT buffer [250 mM Tris pH 8.3, 375 mM KCl, 15 mM MgCl₂], 6 μ l 0.1 M DTT, 6 μ l 2.5 mM dNTPs, 1 μ l Superscript I [Gibco-BRL, Gaithersburg, MD], and 2.25 μ l water) was added, and the tube was placed

at 37°C for 1 hr. This process resulted in the production of cDNA. The cDNA was diluted 1:1 with 1 x RT buffer and was stored at -20°C.

Polymerase Chain Reaction

In a 0.5 ml reaction tube (Bio-Rad, Richmond, CA), 4 µl of the cDNA was combined with 16 µl of the PCR master mix (32 µl 1.25 mM dNTPs, 20 µl 10 x reaction buffer [100 mM Tris pH 8.3 at 20°C, 25 mM MgCl₂, 500 mM KCl], 5 µl of the desired 5' primer, 5 µl of the desired 3' primer, 1 µl of Taq polymerase [Boehringer Mannheim, Indianapolis, IN], and 97 µl of water). The total volume for each reaction tube was 20 µl. This volume allowed 10 µl to be used for gel analysis and left 10 µl for use with the EIA. One drop of molecular biology grade oil (Sigma, St. Louis, MO) was also added to the reaction tube to prevent evaporation during the thermocycling process. The tubes were cycled in a Perkin-Elmer/Cetus model 480 thermocycler at 94°C for 30 s, 55°C for 1 min, and 72°C for 30 s for the 35 cycles.

Agarose Gel Analysis

A 3% agarose gel (3 grams Sea Kem Agarose/100 ml TE buffer) containing 2 µl of ethidium bromide was poured and allowed to set. Ten microliters of the PCR reaction was withdrawn from beneath the mineral oil in the reaction tubes and placed into another tube with 2 µl of loading buffer. TE buffer was added to the gel apparatus, and 12 µl of ØX standard ladder (ØX 174 HAE III), and 12 µl of each PCR reaction was loaded into the gel. The gel was electrophoresed at 100 volts until the size of the resulting bands

could be determined. The gels were then removed from the apparatus, illuminated by UV light and photographed.

Plate-Based EIA

Half-well (200 μ l) EIA plates (Costar, Cambridge, MA) were coated 1 week prior to use with 150 μ l of 5 μ g/ml Avidin-DX (Vector Labs, Burlingame, CA) in plating buffer (0.1 M NaHCO₃, pH 9.7) and were placed at 37°C for 1 hr. The plates were then washed twice with PBS/Tween (PBS was 0.14 M NaCl, 2.5 mM KCl, 10 mM Na₂HPO₄, 2 mM KH₂PO₄, pH 7.8 with 0.2% Tween), and were then blocked with 180 μ l of PBS/BSA (PBS pH 7.8 with 1% BSA and 0.1% azide). The plates were stored at 4°C for up to 1 week in the blocking solution. Just prior to using, the plates were washed twice in PBS/Tween.

Following the PCR procedure, 320 μ l of Tartrazine/PBS/Tween solution was added to each reaction tube, and they were vortexed well. One hundred and thirty microliters of PBS/Tween was added to each well of the EIA plate. Thirty microliters of the each diluted PCR product was added to 4 separate avidin coated wells, two wells to be hybridized with digoxigenin-labeled analyte oligonucleotide, and two wells to be hybridized with digoxigenin-labeled stuffer oligonucleotide. The plates were then placed at 42°C for at least 2 hr. Following this incubation period, the plates were washed twice with an automatic plate washer using PBS/Tween. One hundred and sixty microliters of denaturation solution (50 mM NaOH, 2 mM EDTA pH 8.0) was added, and the plates were allowed to sit at room temperature for 2 min. This denaturation process removed

the strands that were not labeled with biotin. After washing twice with PBS/Tween, 160 μ l of digoxigenin-labeled detection oligo was added to the appropriate wells. The plates were placed at 42°C for at least 1 hr. Following hybridization, the plates were washed 3 times in the plate washer and 160 μ l of anti-digoxigenin Fab fragments alkaline phosphatase conjugated antibody (Boehringer Mannheim, Indianapolis, IN) diluted 1:5000 in PBS/ BSA was added. The plates were then incubated at 37°C for at least 1 hr. The plates were then washed 4 times in the plate washer. Lastly, 180 μ l of p-nitrophenyl phosphate developer solution (PNP), 1 μ g/ml in diethanolamine buffer (1 M diethanolamine, 0.5 mM MgCl_2 , pH 9.8) was added to each well. This cleavage reaction resulted in the development of a yellow color that could be read at OD₄₀₅. Care was taken to avoid air bubbles. The plates were incubated at 37°C, and the OD₄₀₅ was read every 10 min until the readings maxed out at 4.0. The OD₄₀₅ readings were recorded using a Macintosh computer linked to the plate reader. The data was transferred to an IBM computer and analyzed in Microsoft Excel using a template developed by Hockett (99).

Labeling of Detection Oligos

Before labeling with digoxigenin, the detection oligos (synthesized by Midland Certified Reagent Company, Midland, TX) were resuspended to 0.5 mg/ml. Ten μ l of each detection oligo was combined with 4 μ l TdT buffer, 4 μ l CoCl_2 , 1 μ l of ddUTP, and 1 μ l of TdT (Dig Labeling Kit, Boehringer Mannheim, Indianapolis, IN) for a total reaction volume of 20 μ l. This reaction tube was placed in a 37°C water bath for 30 min. At this point, 80 μ l of 20% Formamide buffer was added to make a total volume of

100 μ l. The labeled detection oligos were then stored for up to 4 weeks at 4°C. Detection oligos were labeled for osteopontin, osteocalcin, collagen, β -1 integrin, hypoxanthine phosphoribosyltransferase (HPRT), and stuffer A.

Optimization of Primer Pairs

Cellular extract from the MC3T3-E1 cells grown on tissue culture plastic was used to evaluate and optimize the primer sets. The cellular RNA was extracted and converted to cDNA, and PCR was performed using the 5' and 3' primer pairs of osteopontin, type-I collagen, osteocalcin, and β -1 integrin. The resulting PCR products were run on a 3% agarose gel at 100 volts. The gels were illuminated with UV light and photographed for analysis.

Comparison of Densitometry and EIA

To ensure that the plate-based EIA methodology accurately quantified the analyte and competitor PCR products, simultaneous measurements from a single PCR titration were compared by EIA and EtBr-stained agarose gel electrophoresis. The agarose gel was photographed, and the bands were isolated and analyzed by densitometry. The EIA was evaluated using the plate reader as previously mentioned. The copy number of osteopontin, type-I collagen, and β -1 integrin was determined by each method, and the two were compared.

RESULTS

Production of Quantified Dynamic Strain

Axial and transverse strain gage data as well as load cell data were simultaneously recorded as the Ti-6Al-4V samples underwent 4-point bending. The graph in Fig. 8 shows a 7 s interval from one of the 3,000 $\mu\epsilon$ tests. As the rectangular bar was bent along its long axis, the axial gage was placed in tension and therefore recorded positive strain. At the same time, the transverse gage was placed in compression and recorded negative strain. The load cell also recorded data in the negative direction because it was recording compressive load.

The graph is composed of 1,050 data points out of the total 270,000 datapoints that were recorded for each 30-min test. This large sample rate was chosen to ensure the capture of enough data points to generate a graph that depicted the smooth sinusoidal strain profile that was generated by the Mini Bionix/MTS system.

Since the elastic modulus of the Ti-6Al-4V samples was never exceeded during the 3,000 $\mu\epsilon$ tests or the 6,000 $\mu\epsilon$ tests, thereby preventing permanent deformation or yielding, the strain profiles were nearly identical for each respective peak strain magnitude. Table 2 shows means, standard deviations, and the resultant coefficients of variation of peak strains and maximum loads isolated from two random 5-min samples of the 3,000 $\mu\epsilon$ and the 6,000 $\mu\epsilon$ profiles.

Fig. 8. Strain profile graph. This graph represents a 7-s segment of a 30-min, 1,800 cycle strain test. The repetitive, cyclic nature of the axial strain, transverse strain, and load cell readings are depicted.

Strain Profile

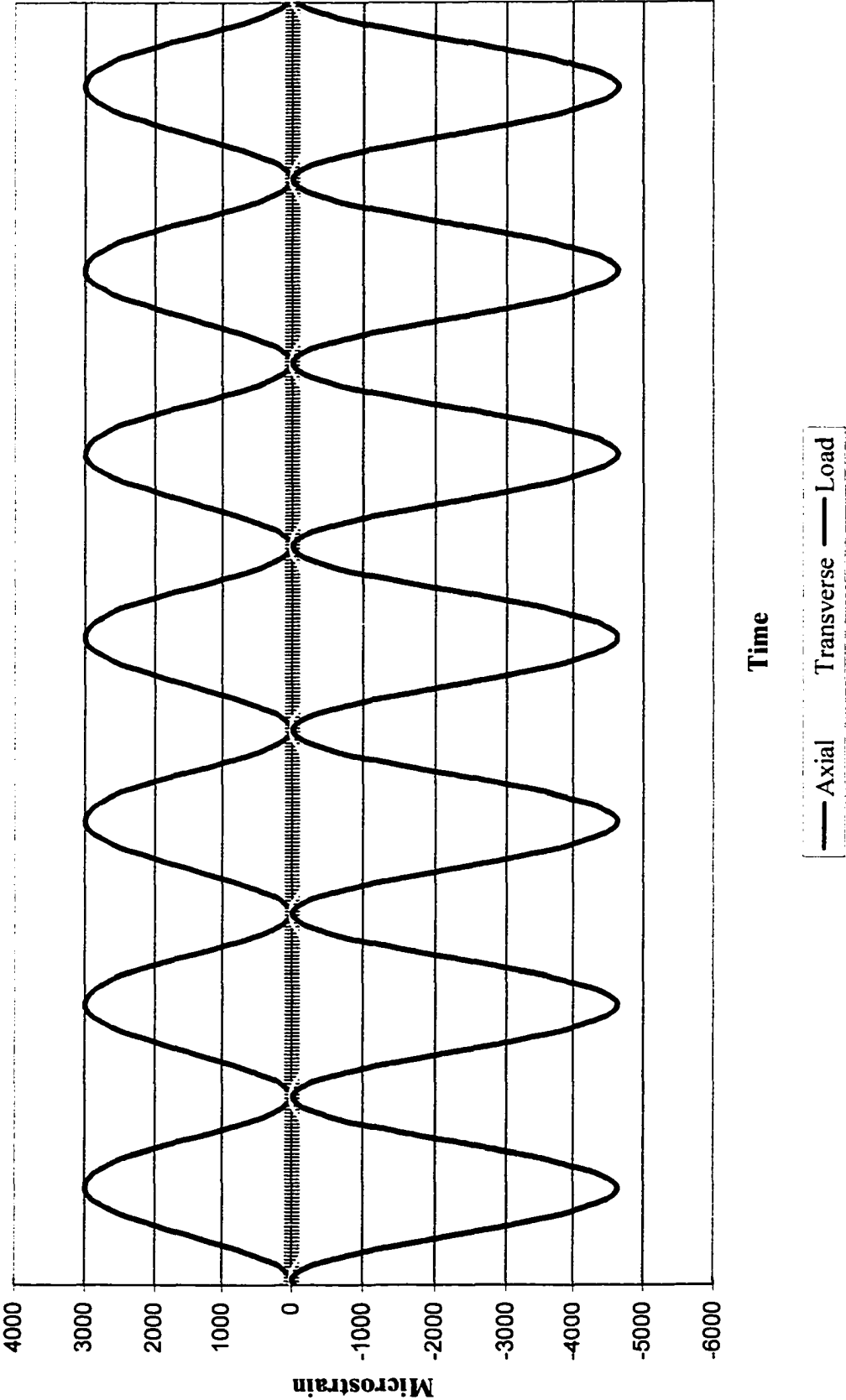


Table 2. Statistical analysis of recorded strain.

<u>Strain / Direction</u>	<u>Data Points</u>	<u>Mean</u>	<u>Std Dev</u>	<u>Range</u>	<u>%CV</u>
3,000 $\mu\epsilon$ Axial	302	3089 $\mu\epsilon$	20.46	117.7	0.66
3,000 $\mu\epsilon$ Transverse	302	-801 $\mu\epsilon$	9.22	44.7	1.15
3,000 $\mu\epsilon$ Load Cell	302	-4791 N	33.93	184.9	7.08
3,000 $\mu\epsilon$ Axial	302	3054 $\mu\epsilon$	13.25	54.5	0.43
3,000 $\mu\epsilon$ Transverse	302	-795 $\mu\epsilon$	4.11	18.0	0.51
3,000 $\mu\epsilon$ Load Cell	302	-4797 N	2.56	12.3	0.05
6,000 $\mu\epsilon$ Axial	300	6136 $\mu\epsilon$	71.68	285.0	1.17
6,000 $\mu\epsilon$ Transverse	300	-1547 $\mu\epsilon$	18.62	73.8	1.20
6,000 $\mu\epsilon$ Load Cell	300	-9566 N	125.72	376.0	1.31
6,000 $\mu\epsilon$ Axial	301	5991 $\mu\epsilon$	177.97	499.3	2.97
6,000 $\mu\epsilon$ Transverse	301	-1507 $\mu\epsilon$	43.08	121.7	2.85
6,000 $\mu\epsilon$ Load Cell	301	-9414 N	283.16	719.9	3.00

Morphological Response to Uniaxial Deformation

At various timepoints after loading (1 hr, 4 hr, 8 hr, 12 hr and 24 hr), control and strained cells were evaluated for changes in morphology and alignment. Two hundred and forty images were captured of the MC3T3-E1 cells attached to the Ti-6Al-4V coupons.

Half of them imaged the CMFDA stained cytoplasm of the attached cells, and the other half showed the rhodamine phalloidin stained actin cytoskeletons. Figs. 10-14 show representative samples of the imaged cells. The methodology developed to observe the osteoblasts attached to the opaque implant material worked extremely well; however, no significant, reproducible alterations in morphology or alignment were observed using the current loading parameters.

Metabolic Response to Uniaxial Deformation

Agarose gel analysis. In order to evaluate the success of the quantitative RT-PCR amplification of the messenger RNA for HPRT, collagen, osteopontin, and β -1 integrin, agarose gel electrophoresis of the PCR products was performed. Fig. 9 shows an example of an agarose gel in which collagen PCR product was analyzed.

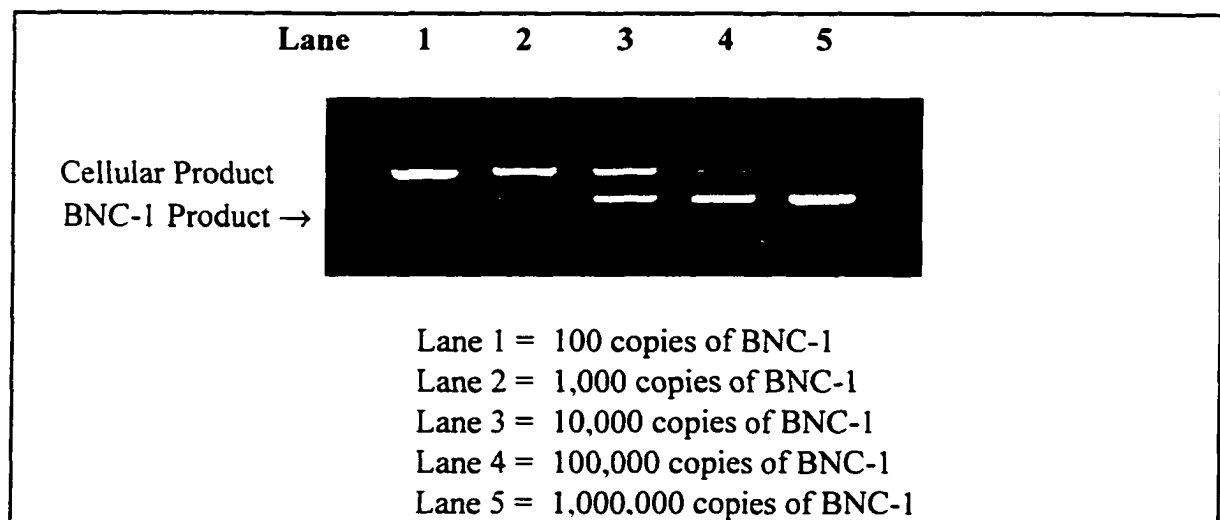


Fig. 9. Agarose gel of collagen competition.

The same procedure was used for each gene product. Note the inverse relationship of the intensity of the upper and lower bands. The lane of the gel in which both bands are relatively the same intensity marks the equilibration point. The number of copies of the competitor can be determined because starting copy number is known and amplified copy number can be calculated using densitometry of the gel or EIA. Once the competitor concentration is determined, the number of copies of endogenous collagen can be determined by comparing endogenous intensity with competitor intensity at the equilibration point.

Comparison of gel densitometry and EIA. In order to ensure that the results of the EIAs matched the results from the agarose gels, a direct comparison was made by evaluating the same PCR product with both densitometry and EIA. The copy numbers of osteopontin, collagen, and β -1 integrin were first obtained from densitometric analysis of the agarose gel. These values were then analyzed by the same Microsoft Excel template that is used by the plate reader/EIA method (see appendix for calculations and graphs of individual EIAs). HPRT had previously been optimized and confirmed by the technicians of Dr. Hockett's laboratory. Fig. 15 demonstrates the titration by EIA and gel densitometry of osteopontin, collagen, and β -1 integrin. The calculated endpoints from each analysis methodology are essentially identical.

Fig. 10. MC3T3-E1 cells imaged 24 hr following strain application. The cells in these images experienced peak strains of 6,000 $\mu\epsilon$ for 1,800 cycles. They were stained, fixed, and imaged 24 hr after the cessation of the strain protocol. Both of these images represent the same cells viewed at 20 x magnification. The only difference is the filter that was used to view the specific stain. A. CMFDA-stained osteoblasts seen through a FITC filter. B. Rhodamine phalloidin-stained osteoblasts seen through a Texas Red Filter.

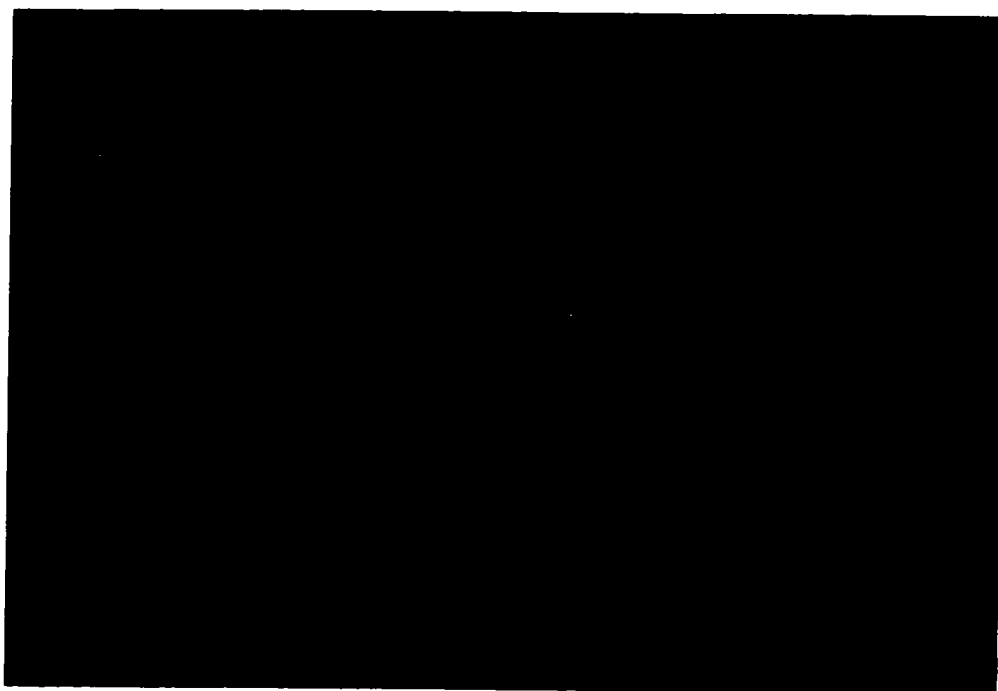
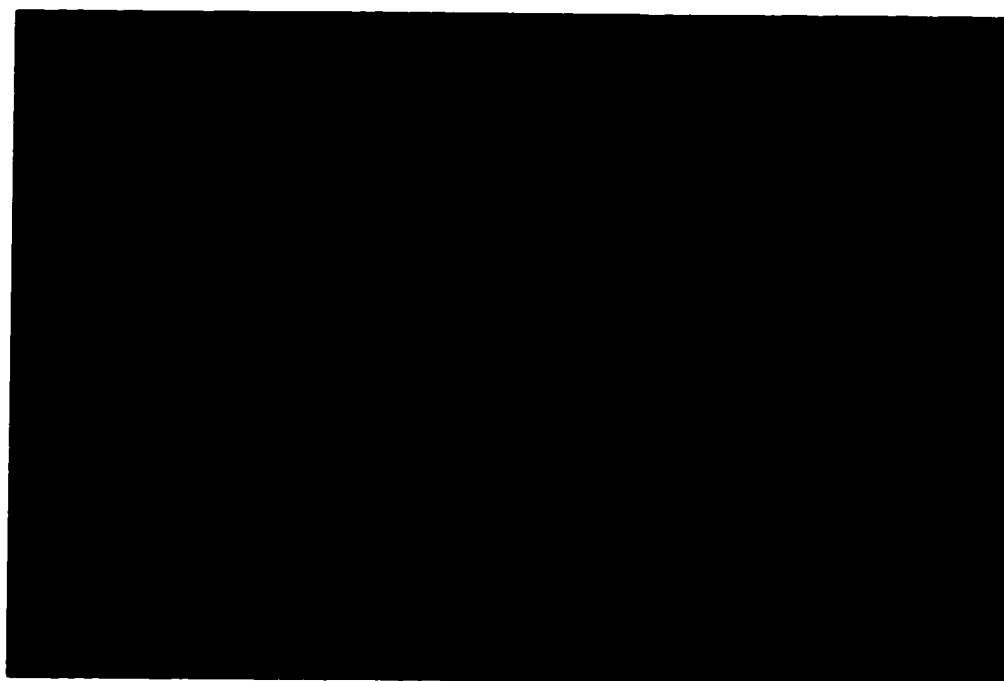
A**B**

Fig. 11. 8-hr control MC3T3-E1 cells. The cells in these images served as controls for the 8-hr timepoint. They were stained, fixed, and imaged 8 hr after the cessation of the 6,000 μE protocol encountered by their strained counterparts. Both of these images represent the same cells viewed at 10 x magnification. The only difference is the filter that was used to view the specific stain. A. CMFDA-stained osteoblasts seen through a FITC filter. B. Rhodamine phalloidin-stained osteoblasts seen through a Texas Red Filter.

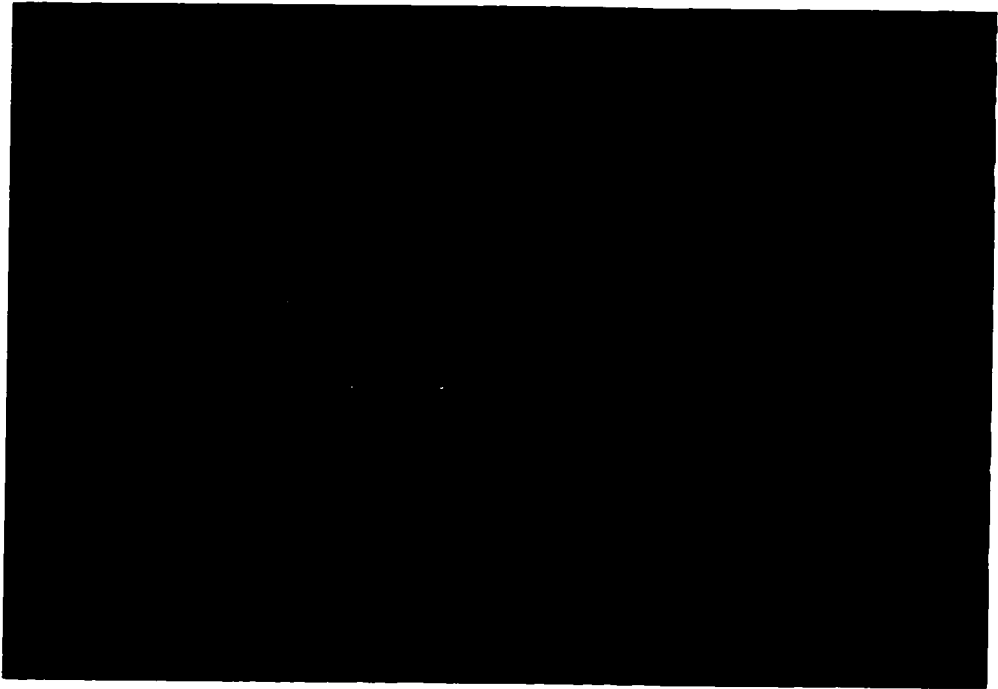
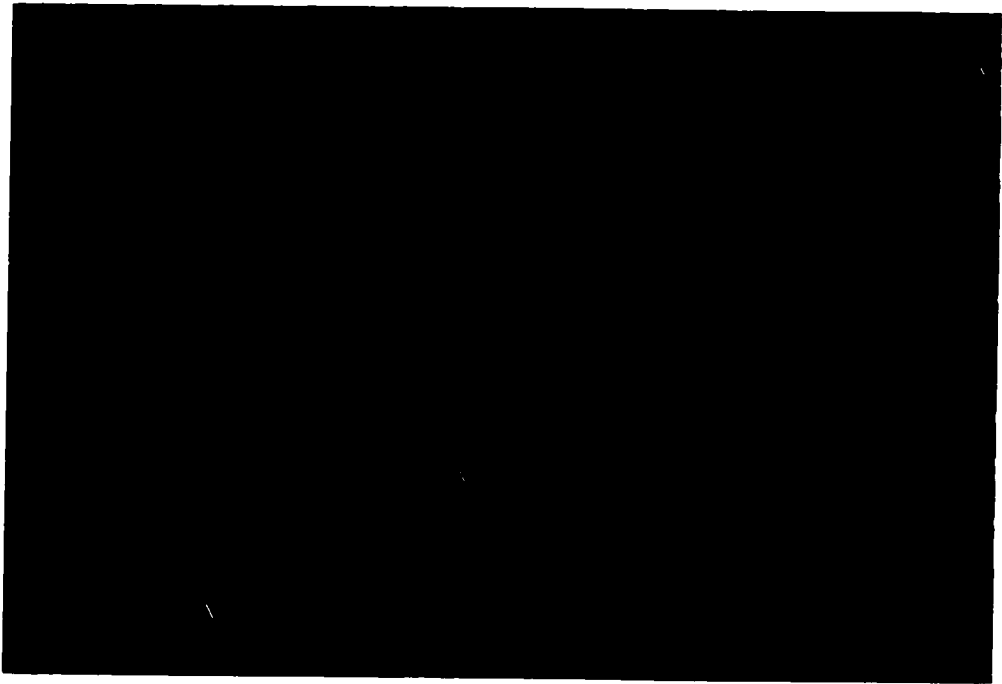
A**B**

Fig. 12. MC3T3-E1 cells imaged 8 hr following strain application. The cells in these images experienced peak strains of 6,000 $\mu\epsilon$ for 1,800 cycles. They were stained, fixed, and imaged 8 hr after the cessation of the strain protocol. Both of these images represent the same cells viewed at 10 x magnification. The only difference is the filter that was used to view the specific stain. A. CMFDA-stained osteoblasts seen through a FITC filter. B. Rhodamine phalloidin-stained osteoblasts seen through a Texas Red Filter.

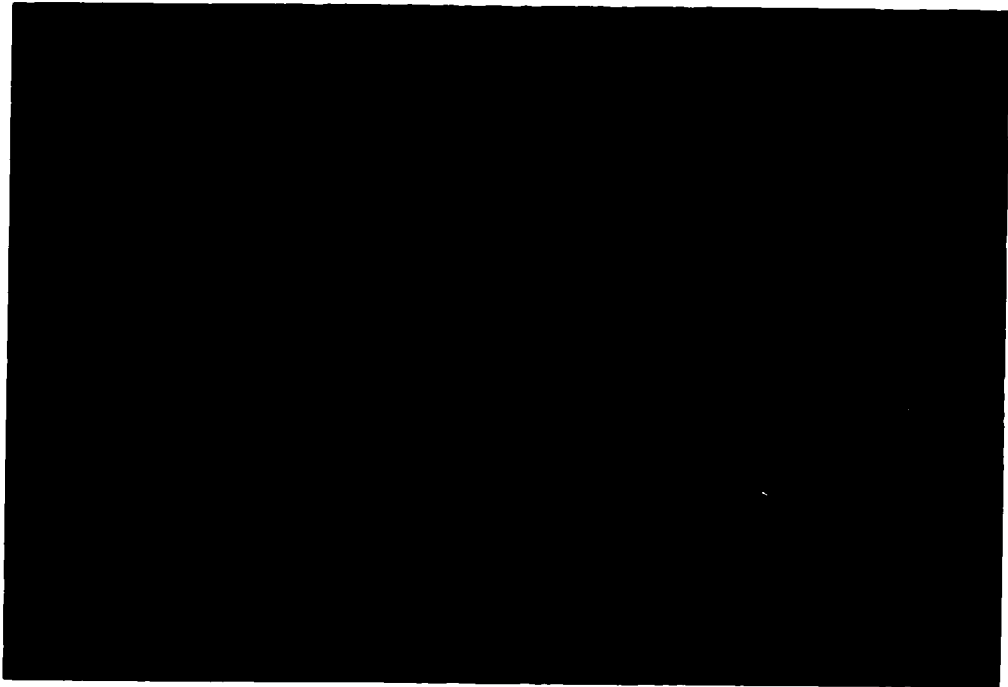
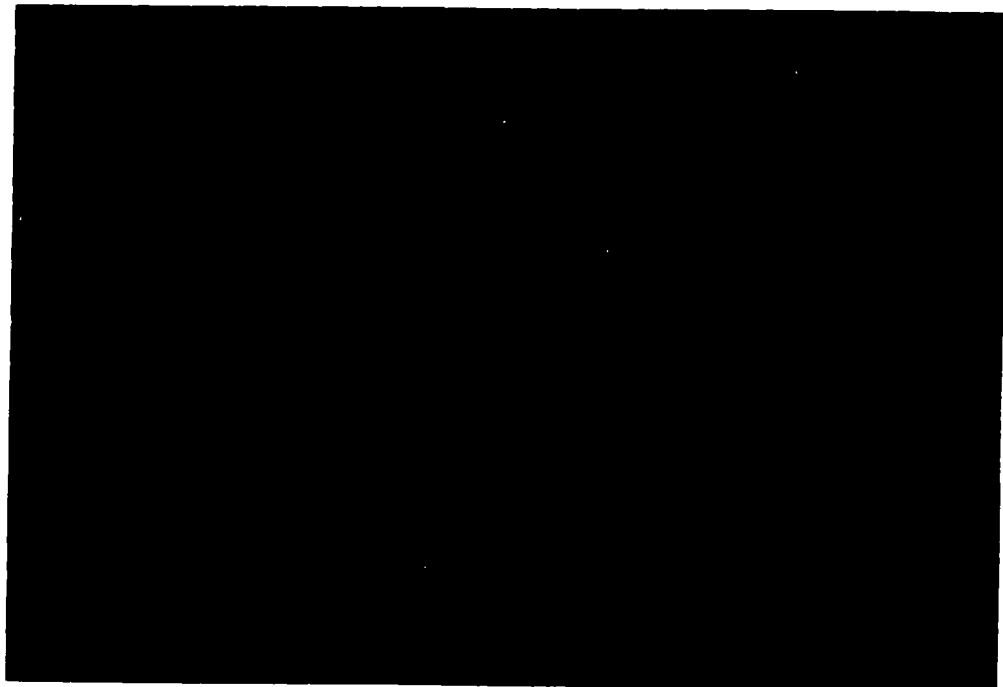
A**B**

Fig. 13. MC3T3-E1 cells imaged 4 hr following strain application. The cells in these images experienced peak strains of $3,000\ \mu\epsilon$ for 1,800 cycles. They were stained, fixed, and imaged 4 hr after the cessation of the strain protocol. Both of these images represent the same cells viewed at 20 x magnification. The only difference is the filter that was used to view the specific stain. A. CMFDA-stained osteoblasts seen through a FITC filter. B. Rhodamine phalloidin-stained osteoblasts seen through a Texas Red Filter.

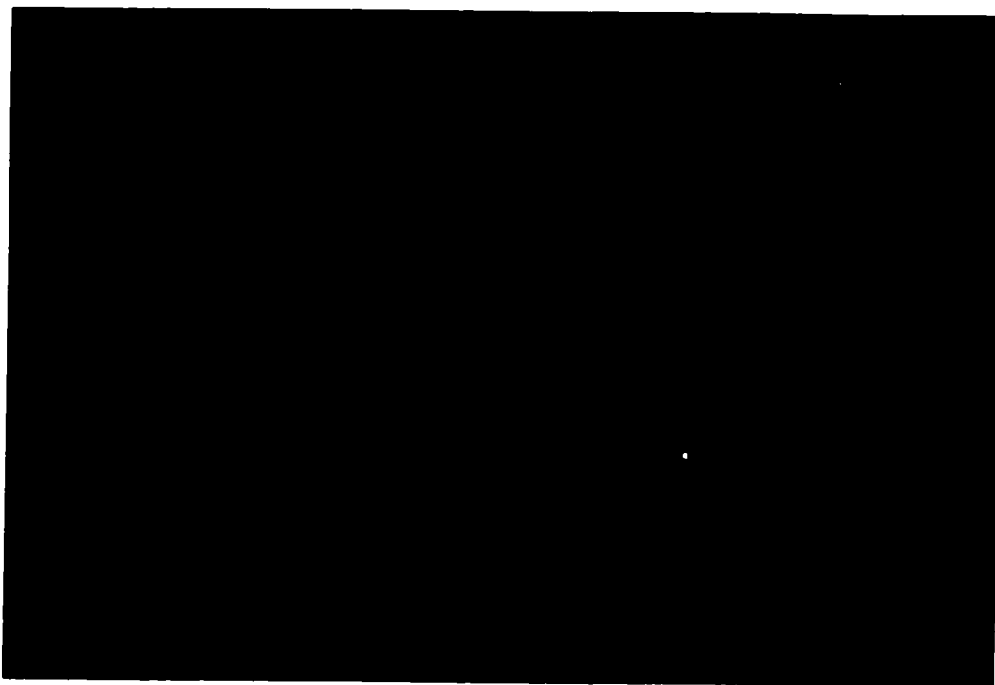
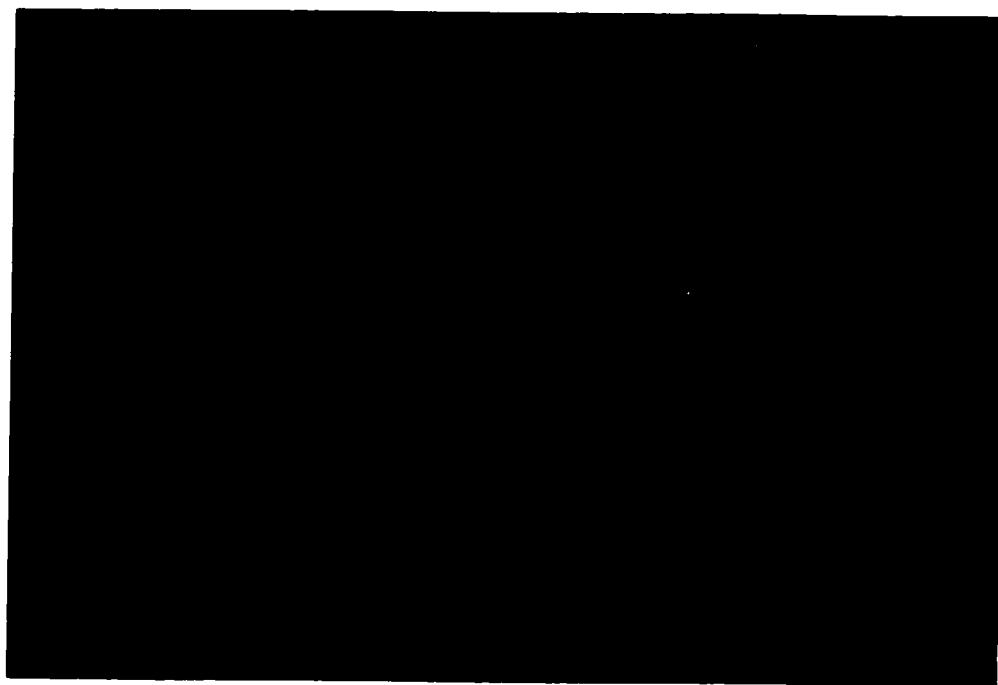
A**B**

Fig. 14. Control vs. strained cells at the 24-hr timepoint. A. The cells in this image served as controls for the 24-hr timepoint. They were stained, fixed, and imaged 24 hr after the cessation of the 6,000 $\mu\epsilon$ protocol encountered by their strained counterparts. This image shows CMFDA-stained osteoblasts seen through a FITC filter. B. The cells in this image experienced peak strains of 6,000 $\mu\epsilon$ for 1,800 cycles. They were stained, fixed, and imaged 24 hr after the cessation of the strain protocol. These cells were also stained with CMFDA and were viewed with a FITC filter.

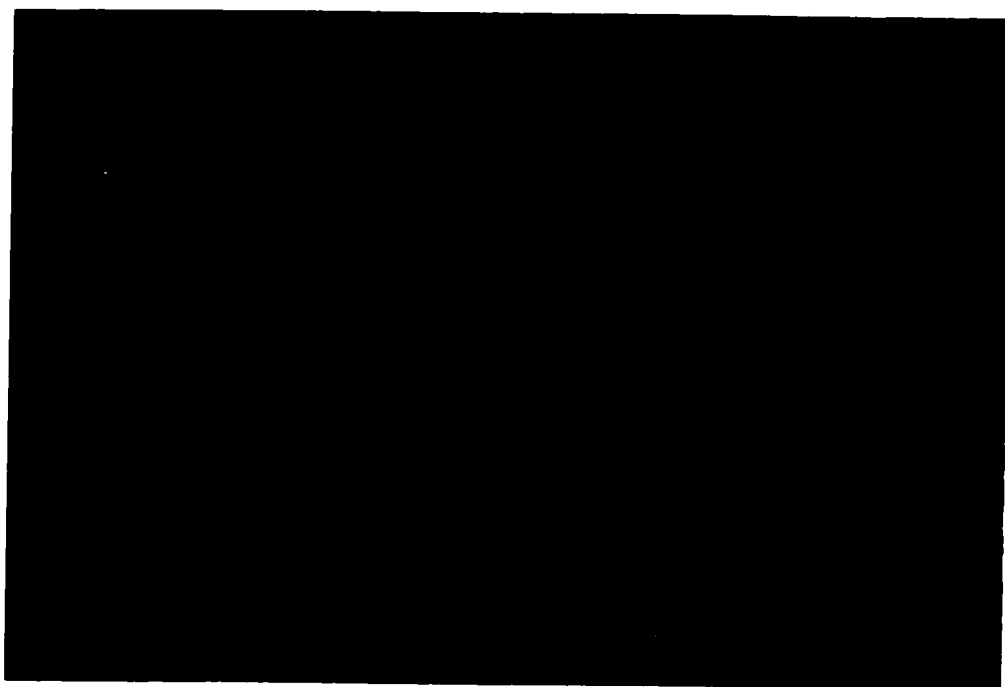
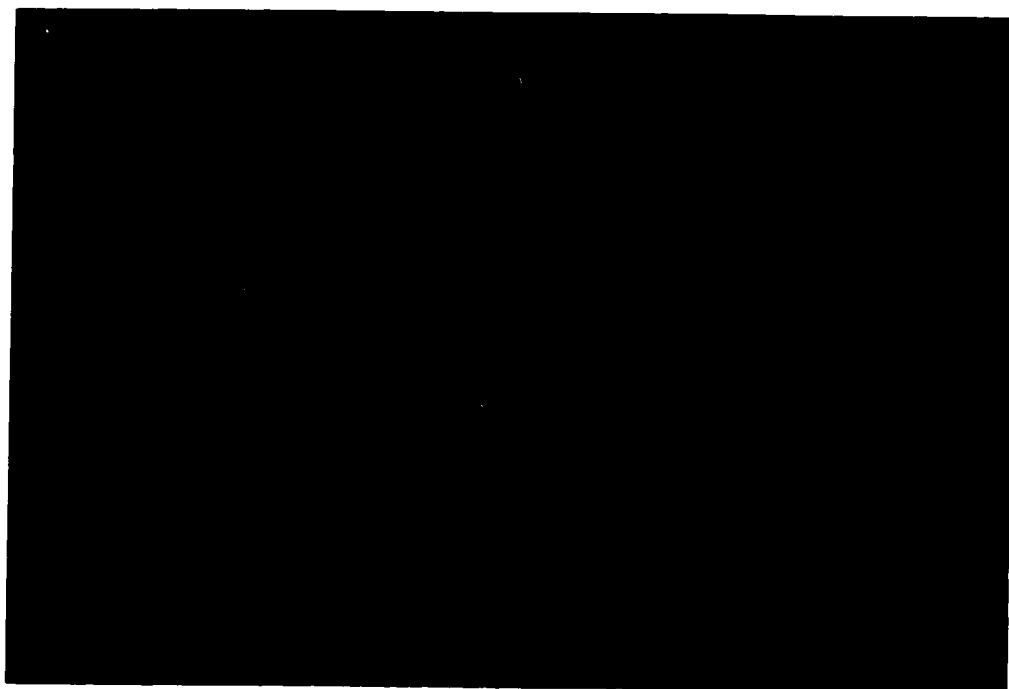
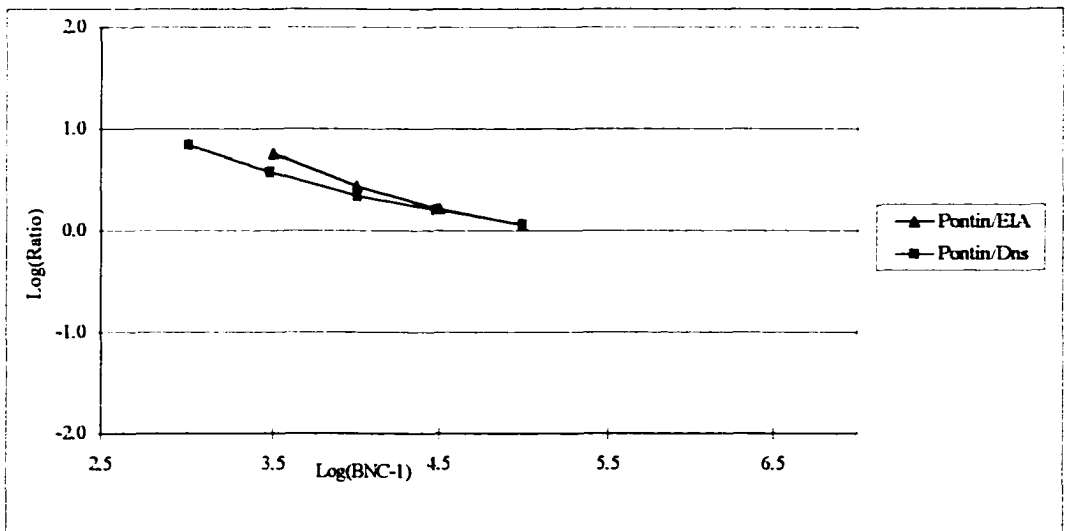
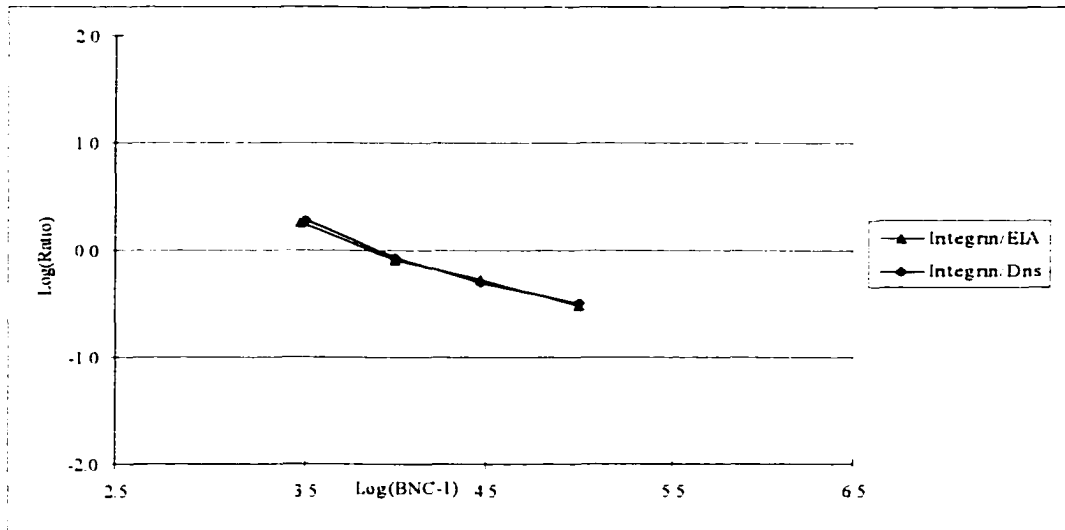
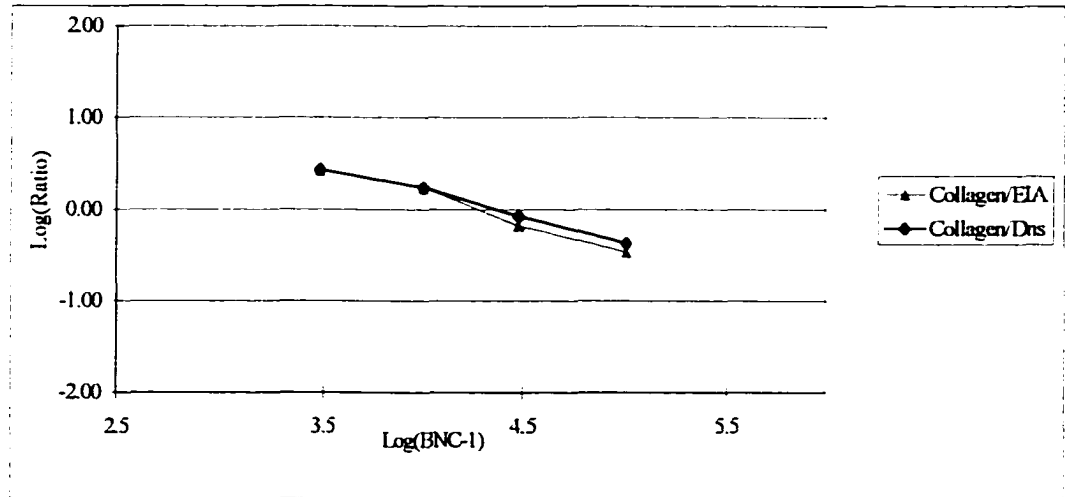
A**B**

Fig. 15. Comparison of densitometry and EIA methodology. These 3 graphs depict direct comparisons between titration curves of the agarose gel and the EIA methodology. The calculated endpoints from each analysis methodology are essentially identical.



Data from quantitative RT-PCR. In order to control for variations in cell number, all quantitative RT-PCR data was normalized to 100,000 copies of HPRT. HPRT, a common housekeeping enzyme has been described by numerous investigators as an especially suitable internal standard (101, 102). Table 3 contains the raw data for mRNA copy number of each target gene normalized to 100,000 copies of HPRT. These data from the quantitative RT-PCR experiments were compared by 2-way ANOVA. Load and time were the two main effects that were analyzed. The Student-Newman-Keuls pairwise multiple means comparison test was used for post-hoc analysis. Interactions of load and time were only examined when ANOVA indicated a significant interaction effect and then only pre-planned comparisons were made (Table 4 and Fig. 16, Table 5 and Fig. 17, and Table 6 and Fig. 18).

Copy number for collagen was elevated with 3000 $\mu\epsilon$ of load and at 24 and 48 hr after loading. β -1 integrin values displayed an increase in copy number at 24 and 48 hr and showed a significant interaction between time and load. A significant increase in copy number was observed for osteopontin 48 hr after loading, but no changes due to load were observed.

Table 3. Quantitative RT-PCR data. This table contains both raw data and data normalized to 100,000 copies of HPRT. The normalized data was used to perform the statistical analysis.

Timepoint	Exp #	Raw Data				Normalized to HPRT (100,000)		
		Collagen	Osteopontin	B1- Integrin	HPRT	Collagen	Osteopontin	B1- Integrin
1 Hr Control I	DR 19	63,583	2,148,769	123,813	258,905	24,558	829,945	47,822
1 Hr Control II	DR 20	128,354	4,366,561	277,670	500,244	25,658	872,886	55,507
1 Hr 3,000 I	DR 19	299,658	8,435,891	239,293	355,338	84,330	2,374,047	67,342
1 Hr 3,000 II	DR 21	304,616	19,062,873	469,266	547,587	55,629	3,481,250	85,697
1 Hr 6,000 I	DR 20	102,213	17,290,219	153,306	573,235	17,831	3,016,253	26,744
1 Hr 6,000 II	DR 21	66,609	3,170,752	115,134	256,641	25,954	1,235,481	44,862
4 Hr Control I	DR 22	387,475	21,991,691	566,054	1,577,522	24,562	1,394,066	35,882
4 Hr Control II	DR 23	161,232	36,327,980	396,801	1,101,491	14,638	3,298,073	36,024
4 Hr 3,000 I	DR 22	81,829	14,191,715	112,113	318,473	25,694	4,456,175	35,203
4 Hr 3,000 II	DR 24	181,031	32,568,419	224,637	375,879	48,162	8,664,602	59,763
4 Hr 6,000 I	DR 23	100,958	18,533,556	854,566	1,041,751	9,691	1,779,077	82,032
4 Hr 6,000 II	DR 24	417,389	35,658,316	403,645	692,997	60,230	5,145,522	58,246
24 Hr Control I	DR 25	365,294	33,363,818	755,786	410,581	88,970	8,126,001	184,077
24 Hr Control II	DR 26	178,309	9,474,429	383,795	231,214	77,119	4,097,688	165,991
24 Hr 3,000 I	DR 25	998,267	27,267,480	572,456	850,322	117,399	3,206,724	67,322
24 Hr 3,000 II	DR 27	350,484	8,219,750	203,980	220,661	158,834	3,725,058	92,440
24 Hr 6,000 I	DR 26	418,940	8,689,203	282,763	328,296	127,610	2,646,759	86,131
24 Hr 6,000 II	DR 27	160,285	6,815,522	142,464	217,944	73,544	3,127,190	65,367
48 Hr Control I	DR 28	305,551	46,838,877	69,981	233,053	131,108	20,097,951	30,028
48 Hr Control II	DR 29	316,518	63,500,619	144,106	286,696	110,402	22,149,112	50,264
48 Hr 3,000 I	DR 28	209,167	47,428,374	267,975	212,428	98,465	22,326,800	126,149
48 Hr 3,000 II	DR 30	123,118	20,543,752	119,658	146,564	84,003	14,016,915	81,642
48 Hr 6,000 I	DR 29	182,368	54,623,404	383,552	377,945	48,253	14,452,739	101,484
48 Hr 6,000 II	DR 30	152,909	18,156,132	157,918	187,447	81,575	9,686,008	84,247

Table 4. Two-way balanced design analysis of variance for collagen.

Normality Test: Passed (p = 0.7060)

Source of Variance	DF	SS	MS
Load	2	3560179729.8	1780089864.9
Hours	3	26259094558.5	8753031519.5
Load vs Hours	6	5978622299.9	996437050.0
Residual	12	5288554598.5	440712883.2
Total	23	41086451186.6	1786367442.9

Source of Variance	F	p
Load	4.04	0.0456
Hours	19.86	< 0.0001
Load vs Hours	2.26	0.1080

Power of performed test with alpha = 0.0500: for Load: 0.474
 Power of performed test with alpha = 0.0500: for Hours: 1.000
 Power of performed test with alpha = 0.0500: for Load vs Hours: 0.318

Load	Average	Time	Average
0	62126.9	1	38993.3
3000	84064.5	4	30496.2
6000	55586.0	24	107246.0
		48	92301.0

All Pairwise Multiple Comparison Procedures (Student-Newman-Keuls Method) :

Comparison	Diff of Means	p	q	p < 0.05
3000 vs 6000	28478.5	3	3.837	Yes
3000 vs 0	21937.6	2	2.956	No
0 vs 6000	6540.9	2	0.881	No

Comparison	Diff of Means	p	q	p < 0.05
24 vs 4	76749.8	4	8.955	Yes
24 vs 1	68252.7	3	7.964	Yes
24 vs 48	14945.0	2	1.744	No
48 vs 4	61804.8	3	7.211	Yes
48 vs 1	53307.7	2	6.220	Yes
1 vs 4	8497.2	2	0.991	No

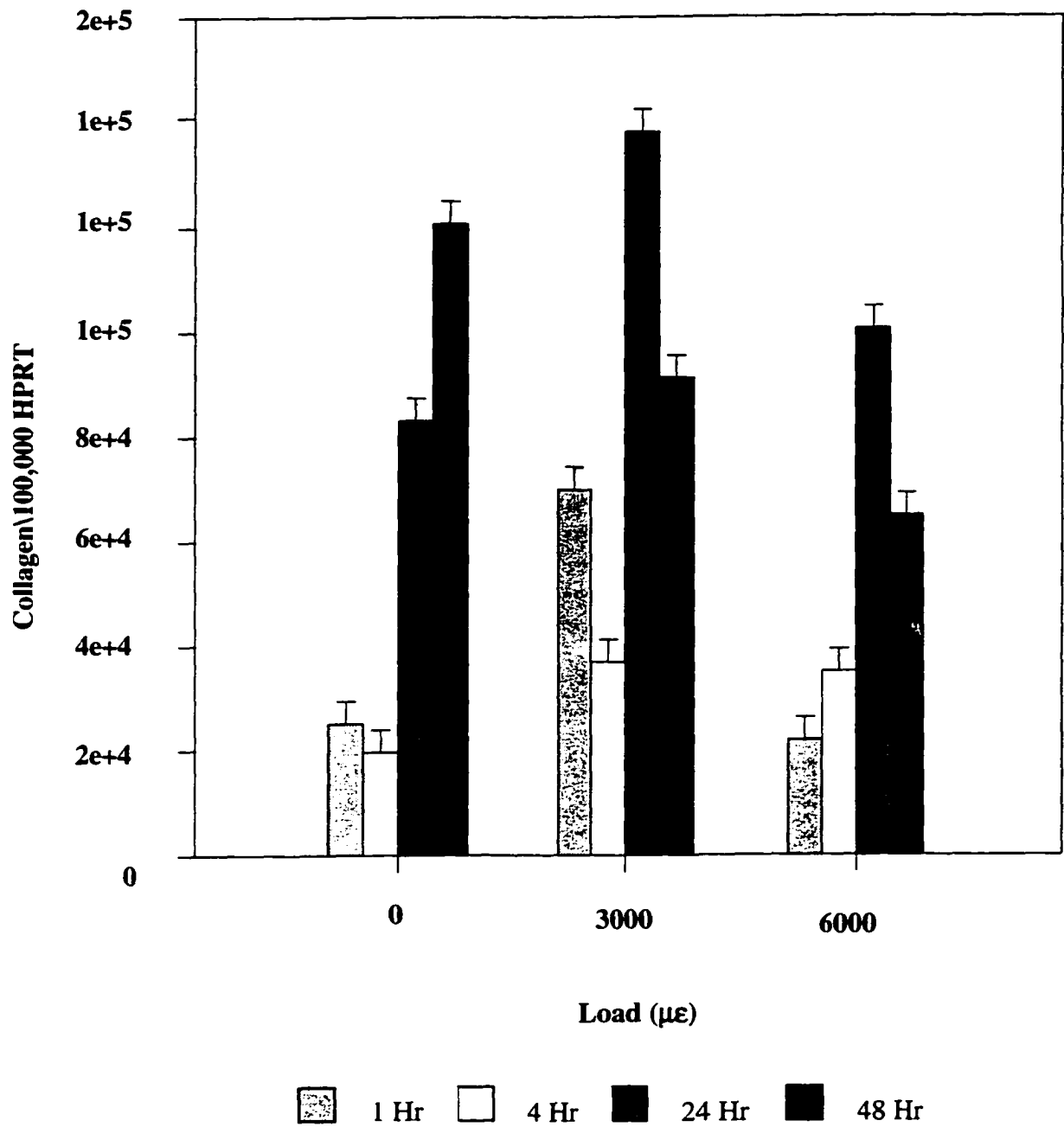


Fig. 16. Graph of collagen expression for 4 timepoints and 3 loads.

Table 5. Two-way balanced design analysis of variance for osteopontin.

Normality Test:

Passed (p = 0.3252)

<u>Source of Variance</u>	<u>DF</u>	<u>SS</u>	<u>MS</u>
Load	2	3.50E+013	1.75E+013
Hours	3	8.64E+014	2.88E+014
Load vs Hours	6	8.55E+013	1.43E+013
Residual	12	7.49E+013	6.24E+012
Total	23	1.06E+015	4.61E+013

<u>Source of Variance</u>	<u>F</u>	<u>p</u>
Load	2.81	0.1000
Hours	46.16	< 0.0001
Load vs Hours	2.28	0.1053

Power of performed test with alpha = 0.0500: for Load: 0.296

Power of performed test with alpha = 0.0500: for Hours: 1.000

Power of performed test with alpha = 0.0500: for Load vs Hours: 0.324

<u>Load</u>	<u>Average</u>	<u>Hours</u>	<u>Average</u>
0	7608215.3	1	1968310.3
3000	7781446.4	4	4122919.2
6000	5136128.6	24	4154903.3
		48	17121587.5

All Pairwise Multiple Comparison Procedures (Student-Newman-Keuls Method) :

<u>Comparison</u>	<u>Diff of Means</u>	<u>p</u>	<u>q</u>	<u>p < 0.05</u>
48 vs 1	15153277.2	4	14.8581	Yes
48 vs 4	12998668.3	3	12.7455	Yes
48 vs 24	12966684.2	2	12.7141	Yes
24 vs 1	2186593.0	3	2.1440	No
24 vs 4	31984.2	2	0.0314	No
4 vs 1	2154608.8	2	2.1126	No

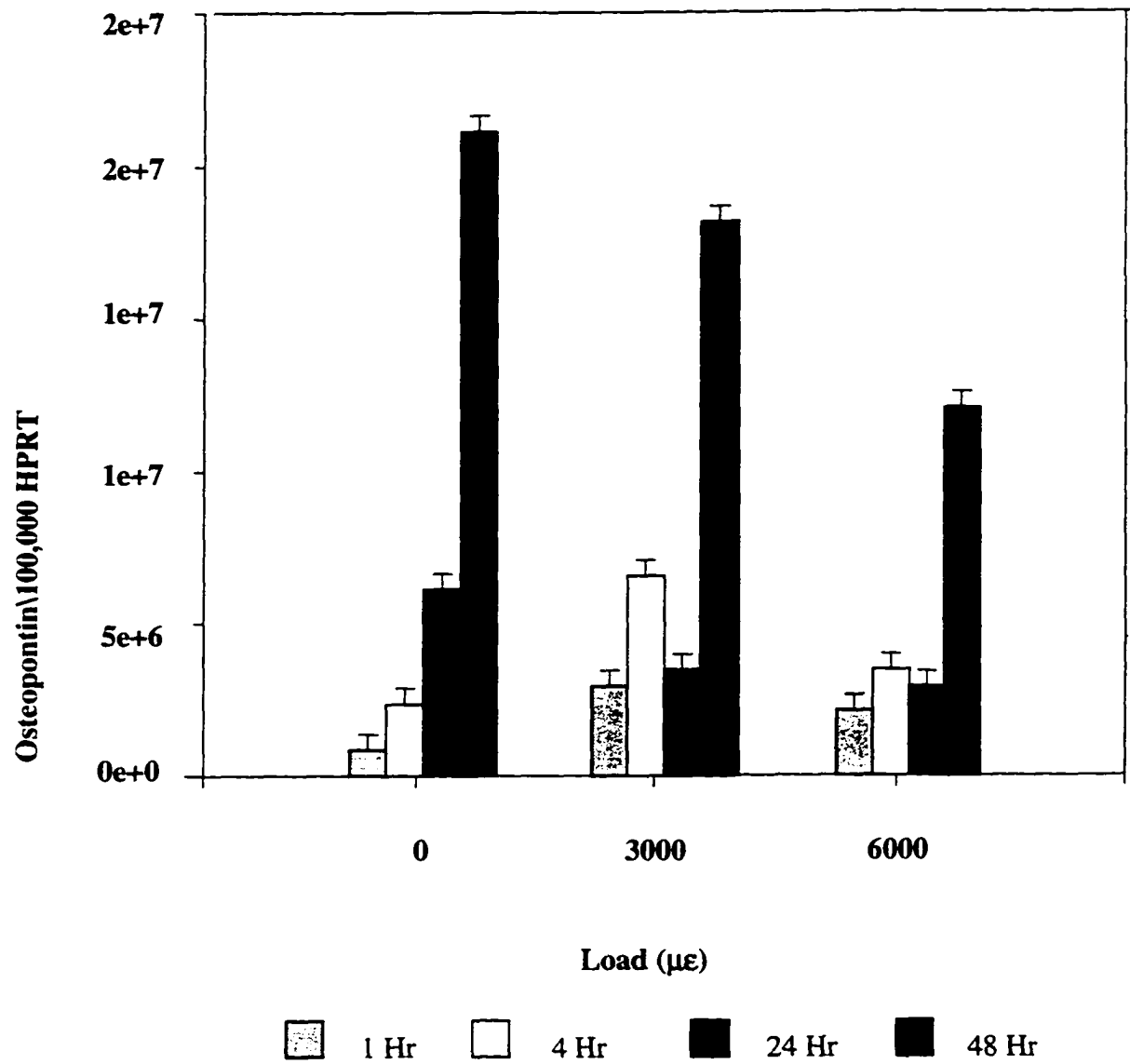


Fig. 17. Graph of osteopontin expression for 4 timepoints and 3 loads.

Table 6. Two-way balanced design analysis of variance for β -1 integrin.

Normality Test:

Passed (p = 0.0671)

<u>Source of Variance</u>	<u>DF</u>	<u>SS</u>	<u>MS</u>
Load	2	320444936.6	160222468.3
Hours	3	13387741785.3	4462580595.1
Load vs Hours	6	19837420523.4	3306236753.9
Residual	12	2982722982.0	248560248.5
Total	23	36528330227.3	1588188270.8

<u>Source of Variance</u>	<u>F</u>	<u>p</u>
Load	0.645	0.5421
Hours	17.954	< 0.0001
Load vs hours	13.302	0.0001

Power of performed test with alpha = 0.0500: for Load: 0.0500

Power of performed test with alpha = 0.0500: for Hours: 1.000

Power of performed test with alpha = 0.0500: for Load vs Hours: 1.000

<u>Load</u>	<u>Average</u>	<u>Hours</u>	<u>Average</u>
0	75699.4	1	54662.3
3000	76933.5	4	51176.7
6000	68639.1	24	110221.3
		48	78969.0

All Pairwise Multiple Comparison Procedures (Student-Newman-Keuls Method) :

<u>Comparison</u>	<u>Diff of Means</u>	<u>p</u>	<u>q</u>	<u>p < 0.05</u>
24 vs 4	59044.7	4	9.174	Yes
24 vs 1	55559.0	3	8.632	Yes
24 vs 48	31252.3	2	4.856	Yes
48 vs 4	27792.3	3	4.318	Yes
48 vs 1	24306.7	2	3.776	Yes
1 vs 4	3485.7	2	0.542	No

<u>Pre-planned Comparisons</u>	<u>p < 0.05</u>
0-24 vs 0-4	Yes
0-24 vs 0-48	Yes
0-24 vs 0-1	Yes
0-24 vs 6000-24	Yes
0-24 vs 3000-24	Yes
3000-48 vs 0-48	Yes
3000-48 vs 3000-4	No

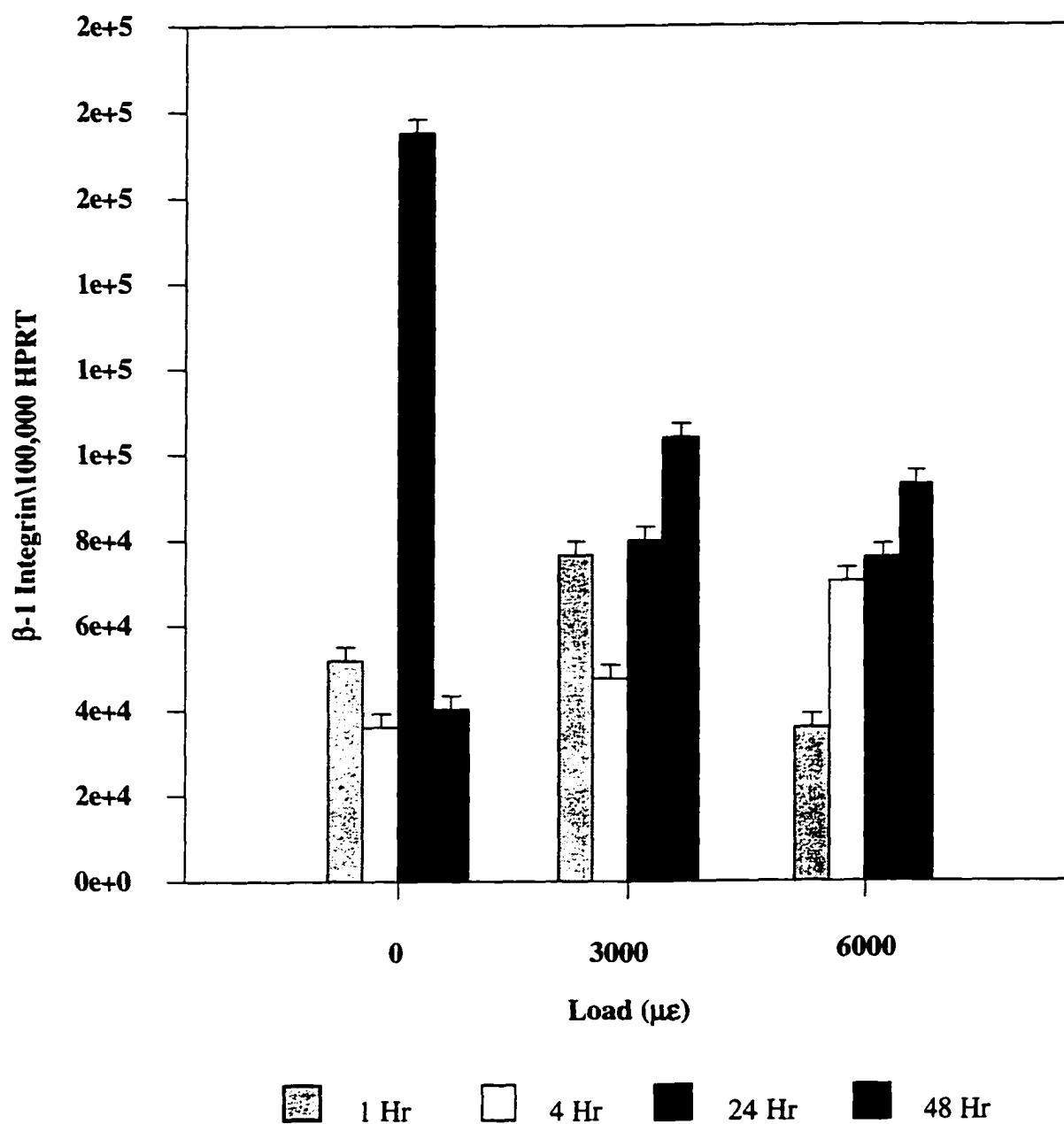


Fig. 18. Graph of β-1 integrin expression for 4 timepoints and 3 loads.

DISCUSSION

One of the major factors influencing the design of dental and orthopedic implants today is the desire to anchor the implant biomechanically to the bone. Characterization of the interface between dental and orthopedic implants and living bone is currently under intense investigation. A cell culture model that utilizes bone cells grown on an actual implant material can provide a means for investigating the cellular response to mechanical strain in more of a physiological situation than that seen with flexible membranes or tissue culture plastic. Ti-6Al-4V is an implant material that is commonly used for osseointegrated implants in both the orthopedic and dental arena. This extremely biocompatible alloy was the substrate of choice for this investigation.

The choice of material on which the cells are grown is not the only issue that must be addressed. Many of the experimental techniques that have been used to evaluate the effects of mechanical deformation on living bone, organ cultures, and cell culture can give us illuminating data, but all of the techniques have drawbacks and sources of error.

Several studies have utilized strain gages attached to living bone as a means of quantifying the applied loads (81, 82). Strain gages are very technique sensitive and are difficult to use with biological tissues due to moisture, heat, irregularity of surface and sometimes poor access to the application site. Their application to animal models can introduce further complications due to the unpredictability of the behavior of the animal.

Movements and loads artificially created when the animal is anesthetized may not give accurate data concerning physiologic loads, but the animal may pull wires loose when awake.

Organ culture analysis may retain some of the spatial accuracy needed to test strain in the matrix, but perfusion is necessary to maintain the organ tissue and there is not much working time before the organ culture dies.

Isolated cell culture models can give very useful information related to the release of certain biological mediators in response to the cellular environment. But again, organization has been lost, and this departure from the *in vivo* situation must be kept in mind when the results of such experiments are analyzed.

All of these experimental techniques are very valuable despite their individual drawbacks. When they are used in combination and their limitations are understood, helpful insight can be obtained and used to further understand functional loading and its biological ramifications.

An attempt was made in this investigation to eliminate some of the sources of error and drawbacks mentioned above. Strain gages were used to monitor the dynamic strain perceived by the cells on the surface of the Ti-6Al-4V sample. The gages; however, were not in contact with any biological tissue or fluid. The symmetrical, rectangular design of the Ti-6Al-4V sample when placed in pure bending, produces strains on both upper and lower surfaces of the sample that are opposite in sign but equal in magnitude. The strain gages were mounted directly beneath the area on which the cells were attached which allowed accurate quantification of the surface strain without any moisture or

contamination problems. Data generated from the axial gage, the transverse gage, and the load cell of the MTS provided a means to characterize and record the exact strain produced on the surface of the substrate that was conveyed to the attached cells.

The actual physiological strain profiles or loading conditions that exist for a osseointegrated implant are admittedly complex, and at this time, not completely characterized. Analysis of the response of osteoblasts attached to a Ti-6Al-4V sample placed in pure bending, the simplest of loading profiles, provides a good starting point for this characterization.

In an attempt to characterize the biological response of osteoblast-like cells to external mechanical loading, many researchers have investigated strain-induced alterations in patterns of osteoblast gene expression (44, 61, 68, 73, 75, 76, 91). Several authors have reported that the initial response to strain is a rapid increase in c-fos mRNA expression, indicative of increased proliferation, paired with a rapid decline in levels of mRNA encoding bone matrix proteins such as type I collagen, osteopontin, and osteocalcin (73, 75). A rebound effect or reversal of this trend is usually seen with time as the proliferation tapers off, accompanied by an increase in expression of the matrix proteins (68, 73, 75, 91).

The term matrix proteins refers to both collagenous and non-collagenous proteins. Type I collagen is the most abundant protein in the organic matrix of bone. Briefly, this molecule consists of 3 chains (two $\alpha 1$ and one $\alpha 2$) synthesized as propeptides assembled into a helical structure intracellularly and fibrils extracellularly. Collagen fibrils

are arranged axially in a staggered array with spaces between aligned fibrils and precise overlap of adjacent fibrils. This arrangement is stabilized by the development of intermolecular crosslinks to produce a porous, repeating structure in three dimensions. This orientation accounts for the typical banded appearance of type I collagen (33). Active osteogenesis involves the expression of genes that result in the production of collagen type I protein. This trait makes the type I collagen molecule a valuable indicator of differentiated osteoblastic activity (91).

The control cells of this investigation expressed increased levels of type I collagen mRNA with increasing time. The 24-hr and 48-hr timepoints increased significantly ($p < 0.05$) from the 1-hr and 4-hr timepoints with the 48-hr timepoint increasing the most. The strained cells (3,000 $\mu\epsilon$ and 6,000 $\mu\epsilon$) also showed a significant difference ($p < 0.05$) between 1 hr, 4 hr and 24 hr, 48 hr, but they appeared to express more collagen at 24 hr with a slight decrease at 48 hr. This suggests, for this experimental model, that strain may induce a trend toward early differentiation.

In the last two decades, the role of the more minor components of the organic bone matrix, noncollagenous proteins, have generated great interest since it has been suggested that they modify and regulate bone function, expression, and turnover.

Osteocalcin (bone gla protein) has been one of the most thoroughly studied noncollagenous proteins in the bone matrix. This calcium-binding protein is present in bone, dentin, and other mineralized tissues and appears to increase in concentration as

bone matures. It is specifically synthesized by differentiated osteoblasts and is an ideal marker for osteoblast phenotypic expression (103).

Osteopontin is a bone sialoprotein synthesized by primary osteoblasts. A repeated sequence of nine aspartic acid residues are present that potentially may lead to mineral binding activity. Osteopontin contains a binding sequence that is recognized by an integrin cell surface receptor related to the vitronectin receptor. In culture, the addition of osteopontin appears to increase cell attachment and spreading (103).

Both osteocalcin and osteopontin are regulated by a number of hormones and growth factors. The predominant promoter of osteocalcin and osteopontin expression and secretion is $1,25-(\text{OH})_2\text{D}_3$, which exerts its influence directly on the genes of both proteins via a vitamin D-responsive element on the gene. In a study by Harter et al. the expression and production of bone matrix proteins in human osteoblast-like osteosarcoma cells, in response to 1-4 days of chronic intermittent mechanical strain, was analyzed. Northern analysis for type I collagen indicated that strain increased collagen message after 48 hr. Immunofluorescent labeling of type I collagen demonstrated that secretion was also enhanced. Osteopontin message levels were increased several fold by the application of mechanical load in the absence of vitamin D, and the two stimuli together produced an additive effect. Osteocalcin secretion was also increased with cyclic strain. Osteocalcin levels were not detectable in vitamin D-untreated control cells; however, after 4 days of induced load, significant levels of osteocalcin were observed in the medium. With vitamin D present, osteocalcin levels were 4 times higher in the medium of strained cells compared to nonstrained controls. This study demonstrated that mechanical strain of osteoblast-

like cells was sufficient to increase the transcription and secretion of matrix proteins via mechano-transduction without hormonal induction (68).

The MC3T3-E1 cells used in this investigation expressed enormous amounts of osteopontin. While the current loading parameters did not statistically alter osteopontin expression, a significant increase in copy number ($p < 0.05$) was observed in all samples at the 48-hr timepoint. More complex loading profiles may be necessary to trigger a load dependent response.

Osteocalcin expression by these MC3T3-E1 cells at the early timepoints was extremely low. The drastic difference in mRNA levels of osteopontin and osteocalcin resulted in the need for an extremely large titration range to analyze both genes. This range proved to be impractical, and only osteopontin expression was investigated in this first round study.

In order for the cells to sense the environmental strain and convert this information into a message that could be understood by the control center of the cell, it would seem that the cellular cytoskeleton which provides a link between the extracellular matrix and the nucleus would be involved. While changes in the distribution of the cytoskeleton in mechanically strained cells have been reported, the exact mechanism for the initial detection and conversion of mechanical force into a biochemical signal has yet to be determined. However, several likely candidates have been proposed. One possible transduction pathway is the extracellular matrix-integrin-cytoskeletal axis (38, 89, 104). To understand how the cells interact with the extracellular matrix, attention must be given to the nature of the attachment.

Integrins are the principal receptors used by animal cells to attach to the extracellular matrix (105). They are heterodimers that function as transmembrane linkers which mediate bi-directional interactions between the extracellular matrix and the actin cytoskeleton. Integrins are composed of two noncovalently associated transmembrane glycoprotein subunits called α and β , both of which contribute to the binding of the matrix protein. Electron micrographs of isolated integrins suggest that the molecule has a globular head projecting more than 20 nm from the lipid bilayer. Following the binding of a typical integrin to its ligand in the matrix, the cytoplasmic tail of the β chain binds to both talin and α -actinin and thereby initiates the assembly of a complex of intracellular attachment proteins that link the integrin to actin filaments in the cell cortex. This process is thought to be how focal contacts form between cells and the extracellular matrix. If the cytoplasmic domain of the β chain is deleted using recombinant DNA techniques, the mutant integrins still bind to their ligands but no longer mediate robust cell adhesion or cluster at focal contacts. The interactions that integrins mediate between the extracellular matrix and the cytoskeleton play an important part in regulating the shape orientation, and movement of the cells (106). Schwartz et al. suggested a direct link between mechanical strain and cellular response (107). Integrins of endothelial cells subjected to shear stress were shown to realign with the direction of flow, indicating that cell adhesion is a dynamic process responding to mechanical strain (108). Furthermore, physical strain applied directly to integrins using a magnetic twisting device was shown to be resisted by the

cytoskeleton (109). These results suggest that the extracellular matrix-integrin-cytoskeletal axis plays an active role with the signal transduction of mechanical strain.

There is also increasing evidence that the clustering of integrins at the sites of contact with the matrix can activate several intracellular signaling pathways. Although the molecular mechanisms are not yet known, it is possible that clustered integrins generate intracellular signals by initiating the assembly of a signaling complex at the cytoplasmic face of the plasma membrane, in much the same way that growth factor receptors operate. Signaling by both integrins and growth factor receptors frequently seems to be required for an optimal cellular response. Many cells in culture will not proliferate in response to growth factors unless the cells are attached via integrins to extracellular matrix molecules (110). The challenge is to determine how these signaling cascades interact to influence complex cell behaviors such as gene expression and cell proliferation.

Many different subunits have been characterized and different combinations of α and β subunits may function as receptors for a variety of extracellular proteins (111, 112). Among this large family, the β_1 -integrin subunit is highly expressed in bone cells *in vitro* and *in vivo* (112). Carvalho et al. (89) demonstrated that changes in the organization of the β_1 subunit were induced by the application of strain as early as 4 hr from its onset. They compared the expression of the β_1 -integrin subunit mRNA from strained cultures with unstrained controls.

Analysis of β -1 integrin expression between strained and unstrained controls for the present study produced significant differences ($p < 0.05$) related to load and time. The

unstrained control cells showed a spike of β -1 integrin expression at the 24-hr timepoint that was very much larger than the 1-hr, 4-hr, or 48-hr timepoints. Loading at both the 3,000 $\mu\epsilon$ and 6,000 $\mu\epsilon$ level effectively reduced this increase in β -1 integrin copy number at 24 hr but showed an increase in copy number at 48 hr for the strained cells (Fig. 18).

When comparing changes in expression of collagen, osteopontin, and β -1 integrin between strained and unstrained control cells, it appears that the loading parameters of this investigation may cause a shift in the timing of expression. A peak of collagen expression occurred at 48 hr with the control cells, but this peak occurred 24 hr earlier in the strained cells. In the case of β -1 integrin, a large increase in mRNA expression occurred at 24 hr but was suppressed in the strained cells at 24 hr. The strained cells, however, expressed increased β -1 integrin message at 48 hr.

The proposed hypotheses concerning alteration in gene expression as a result of changes in the strain environment were tested and proven. Although no statistically significant alignment changes were observed using the baseline, single load application, of this study, it is anticipated that more complex loading parameters may lead to visual alterations in orientation of the cells on the implant material.

The development of this new system for evaluating the effects of quantified, dynamic mechanical load on osteoblasts grown on dental/orthopedic materials sets the stage for numerous follow-up investigations. Studies investigating different loading parameters such as fewer cycles, intermittent cycles, varying waveforms, different magnitudes, to name a few could provide valuable information. This system is also

designed to allow the application of tensile or compressive loads. The 4-point bend fixture can be used to test a variety of other implant materials such as CP-Ti and cobalt chromium, as well as coated versus uncoated samples.

The true goal of this study was to develop a methodology that would provide some answers to a few basic questions regarding the relationship between bone and mechanical load. And as with any good scientific investigation, these answers have led to many more questions.

SUMMARY

The primary objective of this research was the development and testing of a system for evaluating effects of quantified, dynamic mechanical load on osteoblasts cultured on dental and orthopedic implant materials. MC3T3-E1 cells were plated onto Ti-6Al-4V coupons and subjected to uniform, uniaxial stress via a custom 4-point bend apparatus and a model 8581 MTS mini-Bionix, servo-hydraulic testing machine. Peak loads of 3,000 $\mu\epsilon$ or 6,000 $\mu\epsilon$ were established in a cyclic pattern at a rate of 1 Hz. Real-time strain data were obtained by mounting 90° rosette strain gages on the Ti-6Al-4V coupons with subsequent attachment to a DATAQ data acquisition system.

The cells were evaluated for changes in morphology or alignment by digital imaging using CMFDA and rhodamine phalloidin fluorescent stains. Variations in the production of mRNA for HPRT, collagen, osteopontin, and β -1 integrin were evaluated using a customized version of RT-PCR.

No significant, reproducible alterations in morphology or alignment were observed using the current loading parameters. Data from quantitative RT-PCR experiments were compared by 2-way ANOVA of values for mRNA copy number of each target gene normalized to 100,000 copies of the housekeeping gene, HPRT. Main effects examined were load and time. The Student-Newman-Keuls pairwise multiple means comparison test was used for post hoc analysis. Interactions of load and time were only evaluated

when ANOVA indicated a significant interaction effect, and then only pre-planned comparisons were examined. Copy number for collagen was elevated with 3,000 $\mu\epsilon$ of load at 24 and 48 hr after loading. For β -1 integrin, copy number was increased at 24 and 48 hr and significant interactions of time with load were present. A significant increase of osteopontin copy number was observed at the 48-hr timepoints, but no changes due to load were observed.

Measurement of statistically significant changes in gene expression due to loading demonstrates the usefulness of this novel strain application system for evaluating effects of mechanical loading on bone cells in contact with dental and orthopedic implant materials.

CONCLUSIONS

Unique features related to the design of this loading system involve the use of actual dental and orthopedic implant materials as the substrate on which to culture the bone cells. Additionally, this system provides a way to accurately record the dynamic strain induced on the surface of the loaded substrate. Adaptability was also a design feature incorporated into this system, and, as a result, numerous implant materials can be evaluated in both tension and compression.

Dual fluorescent staining methodologies allow the visualization of different cellular characteristics from the same microscopic field of view of osteoblasts cultured on opaque implant materials.

A unique feature of the metabolic analysis used in this investigation involves the development of a custom RNA competitor that allows simultaneous analysis of multiple osteoblast analytes from small populations of cells.

By virtue of the ability to apply quantified, dynamic deformation to osteoblasts attached to implant materials with subsequent metabolic and morphologic analysis, this system will allow exploration of signaling pathways used in mechanosensory force transduction.

LIST OF REFERENCES

1. *Dental implants: emerging technologies, trends and opportunities in oral maxillofacial and periodontal surgery*. 1993. Medical Data International: Irvine, California.
2. Lemons J, Natiella J. Biomaterials, biocompatibility and peri-implant considerations. *Dent Clin North Am* 1986; 30: 4-8.
3. Shulman L. Dental replantation and transplantation. In: Laskin D, ed *Oral and maxillofacial surgery*. CV Mosby: St. Louis. 1985. 132-6.
4. Kent J, Bokrus J. Pyrolytic carbon and carbon-coated metallic dental implants. *Dent Clin North Am* 1980; 24: 465-9.
5. Driskell T, Heller A. Clinical use of aluminum oxide endosseous implants. *J Oral Implant* 1977; 7: 53-62.
6. Monroe EA, Votava W, Bass DB, McMullen J. New calcium phosphate ceramic material for bone and tooth implants. *J Dent Res* 1971; 50: 860-4.
7. Proceedings of the Toronto conferences on osseointegration in clinical dentistry. *J Prosthet Dent* 1983; 49: 50-4.
8. Branemark P, Zarb G, Albrektsson T. Tissue integrated prosthesis: osseointegration in clinical dentistry. *Quintessence Int* 1985; 18: 201-8.
9. Adell R, Lekholm U, Rockler B, Branemark P. A 15 year study of osseointegrated implants in the treatment of the edentulous jaw. *Int J Oral Surg* 1981; 10: 387-92.
10. Dattilo DJ, Misch CM, Arena S. Interface analysis of hydroxyapatite-coated implants in a human vascularized iliac bone graft. *Int J Oral Maxillofac Implants* 1995; 10: 405-9.
11. Ericsson I, Johansson CB, Bystedt H, Norton MR. A histomorphometric evaluation of bone-to-implant contact on machine-prepared and roughened titanium dental implants. A pilot study in the dog. *Clin Oral Implant Res* 1994; 5: 202-6.

12. Cook SD, Salkeld SL, Gaisser DM, Wagner WR. The effect of surface macrotexture on the mechanical and histologic characteristics of hydroxylapatite-coated dental implants. *J Oral Implant* 1993; 19: 288-94.
13. Clift SE, Fisher J, Watson CJ. Stress and strain distribution in the bone surrounding a new design of dental implant: a comparison with a threaded Branemark type implant. *Proceedings of the Institution of Mechanical Engineers Part H - J Engineering in Med* 1993; 207: 133-8.
14. De Lange G, De Putter C. Structure of the bone interface to dental implants *in vivo*. *J Oral Implant* 1993; 19: 123-35; discussion 36-7.
15. Weber HP, Fiorellini JP. The biology and morphology of the implant-tissue interface. *Alpha Omegan* 1992; 85: 61-4.
16. Sisk AL, Steflik DE, Parr GR, Hanes PJ. A light and electron microscopic comparison of osseointegration of six implant types. *J of Oral Maxillofac Surg* 1992; 50: 709-16; discussion 16-7.
17. Pilliar RM, Lee JM, Davies JE. Interface zone - factors influencing its structure for cementless implants. In: Morrey, BF ed. *Biological, material, and mechanical considerations of joint replacement*. Raven Press: New York, 1993. 225 -35.
18. Clemow AJT, Weinstein AM, Klawitter JJ, Koeneman J, Anderson J. Interface mechanics of porous titanium implants. *J Biomed Mat Res* 1981; 15: 73-82.
19. Sadegh AM, Luo GM, Cowin SC. Bone ingrowth: an application of the boundary element method to bone remodeling at the implant interface. *J Biomech* 1992; 26: 167-82.
20. Soballe K, Hansen ES, Rasmussen HB, Jorgensen PH, Bunger C. Tissue ingrowth into titanium and hydroxyapatite-coated implants during stable and unstable mechanical conditions. *J Orthop Res* 1992; 10: 285-9.
21. Schwartz Z, Boyan BD. Underlying mechanisms at the bone-biomaterial interface. *J Cell Biochem* 1994; 56: 340-7.
22. Linder L, Albrektsson T, Branemark PI, Hansson HA, Ivarsson B, Jonsson U, Lundstrom I. Electron microscopic analysis of the bone-titanium interface. *Acta Orthop Scand* 1983; 54: 45-52.
23. Ravaglioli A, Krajewski A, Biansini V, Martinetti R. Interface between hydroxyapatite and mandibular human bone tissue. *J Biomat* 1992; 13: 162-7.

24. Brunski JB, A F Moccia J, Pollack SR, Korostoff E, Trachtenberg DI. The influence of functional use of endosseous dental implants on the tissue-implant interface. II clinical aspects. *J Dent Res* 1979; 58: 1970-80.
25. Brunski JB. The influence of force, motion, and related quantities on the response of bone to implants. In : Fitzgerald, J R, ed. *Non-Cemented Total Hip Arthroplasty*. Raven Press, Ltd: New York, 1988. 7-21.
26. Albrektsson T. Direct bone anchorage of dental implants. *J Prosthet Dent* 1983; 50: 255-61.
27. Boss JH, Shajrawi I, Mendes DG. The nature of the bone-implant interface. *Med Prog through Technology* 1994; 20 : 119-42.
28. Albrektsson T, Branemark PI, Hansson HA, Kasemo B, Larsson K, Lundstrom I, McQueen DH, Skalak R. The interface zone of inorganic implants *in vivo*: titanium implants in bone. *Annals Biomed Eng* 1983; 11: 1-27.
29. Guralnik, DB, ed. *Webster's New World Dictionary*, 2nd ed. NY, NY: Prentice Hall Press, 1986: 734.
30. Davies JE, Lowenberg B, Shiga A. The bone-titanium interface *in vitro*. *J Biomed Mat Res* 1990; 24: 1289-306.
31. Pilliar RM, Lee JM, Maniopoulos C. Observations on the effect of movement on bone ingrowth into porous-surfaced implants. *Clin Orthop Rel Res* 1986; 208: 108-18.
32. Soballe K, Hansen ES, Rasmussen HB, Jorgensen PH, Bunger C. Tissue ingrowth into titanium and hydroxyapatite-coated implants during stable and unstable mechanical conditions. *J Orthop Res* 1992; 10: 285-99.
33. Marks SC, Popoff SN. Bone cell biology: the regulation of development, structure, and function in the skeleton. *Am J Anat* 1988; 183: 1-44.
34. Frost HM. Bone "mass" and the "mechanostat": A proposal. *Anatomical Record* 1987; 219: 1-9.
35. Wolff J. *Das Gesetz der Transformation der Knochen*. Berlin: August Hirschwald, 1892: 183.
36. Clinton T, Lanyon LE. Regulation of bone formation by applied dynamic loads. *J Bone and Joint Surg* 1984; 66-A: 397-402.
37. Cowin SC. Mechanical modeling of the stress adaptation process in bone. *Calcif Tissue Int* 1984; 36: S98-S103.

38. Duncan RL, Turner CH. Mechanotransduction and the functional response of bone to mechanical strain. *Calcif Tissue Int* 1995; 57: 344-58.
39. Pavalko FM, Otey CA, Simon KO, Burrridge K. α -Actinin: a direct link between actin and integrins. *Biochem Soc Trans* 1991; 19: 1065-9.
40. Bockholt SM, Burrridge K. Cell spreading on extracellular matrix proteins induces tyrosine phosphorylation of tensin. *J Biol Chem* 1993; 268: 14565-7.
41. Ingber DE. Cellular tensegrity: defining new rules of biological design that govern the cytoskeleton. *J Cell Sci* 1993; 104: 613-27.
42. McClay DR, Ettensohn CA. Cell adhesion in morphogenesis. *Ann Rev Cell Biol* 1987; 3: 319-45.
43. Ingber DE, Folkman J. Mechanochemical switching between growth and differentiation during fibroblast growth factor-stimulated angiogenesis in vitro: role of extracellular matrix. *J Cell Biol* 1989; 3: 317-30.
44. Hasegawa S, Sata A, Saito S, Suzuki Y, Brunette DM. Mechanical stretching increases the number of cultured bone cells synthesizing DNA and alters their pattern of protein synthesis. *Calcif Tissue Int* 1985; 37: 431-6.
45. Banes AJ, Link GW, Gilbert JW, Tay RTS, Monbureau O. Culturing cells in a mechanically active environment. *Am Bio-technology Lab* 1990; 8: 12-22.
46. Gorfien SF, Winston FK, Thibault LE, Macarak EJ. Effects of biaxial deformation on pulmonary artery endothelial cells. *J Cell Physiol* 1989; 139: 492-500.
47. Yeh CK, Rodan GA. Tensile forces enhance prostaglandin synthesis in osteoblastic cells grown on collagen ribbons. *Calcif Tissue Int* 1984; 36: 67-71.
48. Harell A, Binderman DS. Biochemical effect of mechanical stress on cultured bone cells. *Calcif Tissue Res (Suppl)* 1977; 22: 202-9.
49. Rodan GA, Bourret LA, Harvey A, Mensi T. Cyclic AMP and cGMP mediators of the mechanical effects in bone remodelling. *Science* 1975; 198: 467-9.
50. Reich KM, Frangos JA. Effect of flow on prostaglandin E₂ and inositol triphosphate levels in osteoblasts. *Am J Physiol* 1991; 261: C428-C32.
51. Jones DB, Nolte H, Scholubbers JG, Turner E, Veltel D. Biochemical signal transduction of mechanical strain in osteoblast-like cells. In: *Biointeractions*. Oxford: UK, 1990. 112-23.

52. Brighton CT, Sennett BJ, Farmer JC, Iannotti JP, Hansen CA, Williams JL, Williamson J. The inositol phosphate pathway as a mediator in the proliferative response of rat calvarial bone cells to cyclical biaxial mechanical strain. *J Orthop Res* 1992; 10: 385-93.
53. Alberts B, Bray D, Lewis J, Raff M, Roberts K, Watson JD. Cell Signaling. In: M. Robertson, *et al.*, ed. *Molecular biology of the cell*. Garland Publishing, Inc: New York, 1994. 721-85.
54. Somjen D, Binderman I, Berger E, Harell A. Bone remodeling induced by physical stress is prostaglandin E₂ mediated. *Biochem Biophys Acta* 1980; 627: 91-100.
55. Ozawa H, Imamura K, Abe E, Takahashi N, Hiraide T, Shibasaki Y, Fukuhara T, Suda T. Effect of continuous applied compressive pressure on mouse osteoblast-like-cells (MC3T3-E1) *in vitro*. *J Cell Physiol* 1990; 142: 177-85.
56. Murray DW, Rushton N. The effect of strain on bone cell prostaglandin E₂ release: A new experimental method. *Calcif Tissue Int* 1990; 47: 35-9.
57. Rawlinson SCF, El-Haj AJ, Minter SL, Tavares IA, Bennett A, Lanyon LE. Loading-related increases in prostaglandin production in cores of adult canine cancellous bone *in vitro*: a role for prostacyclin in adaptive bone remodeling? *J Bone Min Res* 1991; 6: 1345-51.
58. Rawlinson SCF, Subburaman M, Baylink DJ, Lanyon LE. Exogenous prostacyclin, but not prostaglandin E₂, produces similar responses in both G6PD activity and RNA production as mechanical loading, and increases IGF-II release, in adult cancellous bone in culture. *Calcif Tissue Int* 1993; 53: 324-9.
59. Chow JWM, Chambers TJ. Indomethacin has distinct early and late actions on bone formation induced by mechanical stimulation. *Am J Physiol* 1994; 267: E287-E92.
60. Butler WT. The nature and significance of osteopontin. *Connect Tissue Res* 1989; 23: 123-36.
61. Sodek J, Chen J, Nagata T, Kasugai S, Todescan R, Li IWS, Kim RH. Regulation of osteopontin expression in osteoblasts. *Annals N Y Acad Sciences* 1995; 760: 223-41.
62. Patterson-Buckendahl P, Globus RK, Bikle DD, Cann CE, Morey-Holton E. Effects of simulated weightlessness on rat osteocalcin and bone calcium. *Am J Physiol* 1989; 257: R1103-R9.

63. Miyajima K, Suzuki S, Iwata T, Tanida K, Iizuka T. Mechanical stress as a stimulant to the production of osteocalcin in osteoblast-like cells. *Aichi-Gakuin Dental Science* 1991; 4: 1-5.
64. Stanford CM, Stevens JW, Brand RA. Cellular deformation reversibly depresses RT-PCR detectable levels of bone-related mRNA. *J Biomech* 1995; 28: 1419-27.
65. Stanford CM, Morcuende JA, Brand RA. Proliferative and phenotypic responses of bone-like cells to mechanical deformation. *J Orthop Res* 1995; 13: 664-70.
66. Towler DA. Use of cultured osteoblastic cells to identify and characterize transcriptional regulatory elements. In: Bilezikian, JP, Rodan, GA and Raisz, LG, ed. *Principles of Bone Biology*. Academic Press: NY. 1996. 1176-92.
67. Nation JL. *Hexamethyldisilazane data sheet #342*. 1985, Polysciences, Inc.: USA.
68. Harter LV, Hruska KA, Duncan RL. Human osteoblast-like cells respond to mechanical strain with increased bone matrix protein production independent of hormonal regulation. *Endocrinology* 1995; 136: 528-35.
69. Schaffer JL, Rizen M, L'Italien GJ, Benbrahim A, Megerman J, Gerstenfeld LC, Gray ML. Device for the application of a dynamic biaxially uniform and isotropic strain to a flexible cell culture membrane. *J Orthop Res* 1994; 12: 709-19.
70. Ochoa JA, Sanders AP, Heck DA, Hillberry BM. Stiffening of the femoral head due to intertrabecular fluid and intraosseous pressure. *J Biomech Eng* 1991; 113: 259-62.
71. Beer FP, Johnston, ER. Pure bending. In: Cerra, FJ and Maisel, JW ed. *Mechanics of materials*. McGraw-Hill: New York. 1981. 616-25.
72. Timoshenko S. *Strength of materials*. Second ed. Lancaster Press: Lancaster, PA. 1941. 510.
73. Buckley MJ, Banes RD, Jordan AJ. The effects of mechanical strain on osteoblasts *in vitro*. *Oral Maxillofac J Surg* 1990; 48: 276-82.
74. Veldhuijzen JP, Bourret GA, Rodan L. In vitro studies of the effects of intermittent compressive forces on cartilage cell proliferation. *J Cell Physiol* 1979; 98: 299-306.
75. Raab-Cullen DM, Thiede MA, Petersen DN, Kimmel DB, Recker RR. Mechanical loading stimulates rapid changes in periosteal gene expression. *Calcif Tissue Int* 1994; 55: 473-8.

76. Sun YQ, McLeod KJ, Rubin CT. Mechanically induced periosteal bone formation is paralleled by the upregulation of collagen type one mRNA in osteocytes as measured by *in situ* reverse transcript-polymerase chain reaction. *Calcif Tissue Int* 1995; 57: 456-62.
77. Brighton CT, Strafford B, Gross SB, Leatherwood DF, Williams JL, Pollack SR. The proliferative and synthetic response of isolated calvarial bone cells of rats to cyclic biaxial mechanical strain. *J Bone Joint Surg* 1991; 73-A: 320-31.
78. Gilbert JA, Weinhold PS, Banes AJ, Link GW, Jones GL. Strain profiles for circular cell culture plates containing flexible surfaces employed to mechanically deform cells *in vitro*. *J Biomech* 1994; 27: 1169-77.
79. DeWitt MT, Handley CJ, Oakes BW, Lowther DA. *In vitro* response of chondrocytes to mechanical loading: the effect of short term mechanical tension. *Connect Tissue Res* 1984; 12: 97-109.
80. Leung DYM, Glagov S, Mathews MB. Cyclic stretching stimulates synthesis of matrix components by arterial smooth muscle cells *in vitro*. *Science* 1976; 191: 475-7.
81. Rubin CT, Lanyon LE. Regulation of bone formation by applied dynamic loads. *J Bone Joint Surg* 1984; 66A: 397-402.
82. Lanyon LE, Rubin CT. Static versus dynamic loads as an influence on bone remodeling. *J Biomech* 1984; 17: 897-906.
83. Flinn RA, Trojan PK. Traditional polymers: fundamentals and high-volume varieties. In: *Engineering Materials and Their Applications*. Houghton Mifflin Company: Boston. 1990. 561-84.
84. Biocompatibility of Clinical Implant Materials, . 1980, CRC Press. p. 92.
85. Ramfjord SP, Ash MM. Functional movements of the mandible. In: *Occlusion*. W B Saunders: Philadelphia, 1968. 71-81.
86. Okeson JP. Etiology of functional disturbances in the masticatory system. In: Reinhardt, RW and Steube, M, ed. *Management of Temporomandibular Disorders and Occlusion*. Mosby: St. Louis, 1993. 149-177.
87. Ives D, Eskin S, McIntire C. Mechanical effects on endothelial cell morphology: *in vitro* assessment. *In Vitro Cell Dev Biol* 1986; 22: 500.

88. Buckley MJ, Banes AJ, Levin LG, Sumpio BE, Sato M, Jordan R, Gilbert J, Link GW, Tay RTS. Osteoblasts increase their rate of division and align in response to cyclic, mechanical tension in vitro. *J Bone and Mineral Res* 1988; 4: 225-36.
89. Carvalho RS, Scott JE, Suga DM, Yen EHK. Stimulation of signal transduction pathways in osteoblasts by mechanical strain potentiated by parathyroid hormone. *J Bone and Mineral Res* 1994; 9: 999-1011.
90. Carvalho RS, Scott JE, Yen EHK. The effects of mechanical stimulation on the distribution of B1 integrin and expression of B1 integrin mRNA in TE-85 human osteosarcoma cells. *Archs Oral Biol* 1995; 40: 257-64.
91. Zaman G, Dallas SL, Lanyon LE. Cultured embryonic bone shafts show osteogenic responses to mechanical loading. *Calcif Tissue Int* 1992; 51: 132-6.
92. Puleo DA, Preston KE, Shaffer JB, Bizios R. Examination of osteoblast-orthopaedic biomaterial interactions using molecular techniques. *J Biomat* 1993; 14: 111-4.
93. Wang AM, Doyle MV, Mark DF. Quantitation of mRNA by the polymerase chain reaction. *Proc Natl Acad Sci* 1989; 86: 9717-21.
94. Piatek M, Saag MS, Yang LC, Clark SJ, Kappes JC, Luk KC, Hahn BH, Shaw GM, Lifson JD. High levels of HIV-1 in plasma during all stages of infection determined by competitive PCR. *Science* 1993; 259: 1749-54.
95. Menzo S, Bagnarelli P, Giacca M, Varal A. Absolute quantitation of viremia in human immunodeficiency virus infection by competitive reverse transcription and polymerase chain reaction. *J Clin Microbiol* 1992; 30: 1752-7.
96. Becker-Andre' M, Hahlbrook K. A novel approach by PCR aided transcript titration assay (PATY). *Nucleic Acids Res* 1989; 17: 9437-46.
97. Gilliland G, Perrin S, Blanchard K, Bunn HF. Analysis of cytokine mRNA and DNA: detection and quantitation by competitive polymerase chain reaction. *Proc Natl Acad Sci* 1990; 87: 2725-9.
98. Scadden DT, Wang Z, Groopman JE. Quantitation of plasma human immunodeficiency virus type 1 RNA by competitive polymerase chain reaction. *J Infect Dis* 1992; 165: 1119-23.
99. Hockett RD, Janowski KM, Bucy RP. Simultaneous quantitation of multiple cytokine mRNA by RT-PCR utilizing plate based EIA methodology. *J Immun Meth* 1995; 187: 273-85.

100. Chomczynski P, Sacchi N. Single step method of RNA isolation by acid guanidinium thiocyanate phenol-chloroform extraction. *Anal Biochem* 1987; 162: 156-9.
101. Murphy E, Hieny S, Sher A, O'Garra A. Detection of in vivo expression of interleukin-10 using a semi-quantitative polymerase chain reaction method in *Schistosoma mansoni* infected mice. *J Immun Meth* 1993; 162: 211-23.
102. Foss RD, Guha-Thakurta N, Conran RM, Gutman P. Effects of fixative and fixation time on the extraction and polymerase chain reaction amplification of RNA from paraffin-embedded tissue. Comparison of two housekeeping gene mRNA controls. *Diagnostic Molec Path* 1994; 3: 148-55.
103. Stanford CM, Keller JC. The concept of osseointegration and bone matrix expression. *Critical Reviews in Oral Biology and Medicine* 1991; 2: 83-101.
104. Ingber D. Integrins as mechanochemical transducers. *Curr Opin Cell Biol* 1991; 3: 841-8.
105. Alberts B, Bray D, Lewis J, Raff M, Roberts K, Watson JD. Extracellular matrix receptors on animal cells: the integrins. In: Robertson, M *et al.*, ed. *Molecular biology of the cell*. Garland Publishing, Inc: New York, 1994. 995-1009.
106. Sastry SK, Horwitz AF. Integrin cytoplasmic domains: mediators of cytoskeletal linkages and extra- and intercellular initiated transmembrane signaling. *Curr Opin Cell Biol* 1993; 5: 831-53.
107. Schwartz MA, Ingber DE. Integrating with integrins. *Mol Biol Cell* 1994; 5: 389-93.
108. Davies PF, Robotewskyj A, Griem ML. Quantitative studies of endothelial cell adhesion: directional remodeling of focal adhesion sites in response to flow forces. *J Clin Invest* 1994; 93: 2031-8.
109. Wang N, Butler JP, Ingber DE. Mechanotransduction across the cell surface and through the cytoskeleton. *Science* 1993; 260: 1124-7.
110. Damsky CH, Werb Z. Signal transduction by integrin receptors for extracellular matrix: cooperative processing of extracellular information. *Curr Opin Cell Biol* 1992; 5: 772-81.
111. Hynes RO. Integrins: versatility, modulation and signalling in cell adhesion. *Cell* 1992; 69: 11-25.
112. Clover J, Dodds RA, Gowen M. Integrin subunit expression by human osteoblasts and osteoclasts *in situ* and in culture. *J Cell Science* 1992; 103: 267-71.

APPENDIX

CALCULATIONS AND GRAPHS OF INDIVIDUAL EIAS

QC-RT-PCR Experiment Calculation

Plate 1	
Controls	
RT+	1.50
PCR+	2.00
EIA+	2.00
EIA-	0.190

Backgrounds	
MCC	0.160
Collage	0.182
Pontin	0.175
Integrin	0.159
mHPRT	0.179

Plate 2	
Controls	
RT+	1.50
PCR+	2.00
EIA+	0.00
EIA-	0.000

Low OD cutoff
0.014

		Error Corrected Average Specific O.D.															
PCR primer		Collagen				Pontin				Integrin				mHPRT			
BNC-I	copies	Collagen	stuffer	Ratio	log R	Pontin	stuffer	Ratio	log R	Integrin	stuffer	Ratio	log R	mHPRT	stuffer	Ratio	log R
1.0	10																
1.5	30																
2.0	100																
2.5	300	3.4125	0.06	56.88	1.75	2.4025	low			1.4475	0.0255	56.76	1.75	3.2085	0.046	69.75	1.84
3.0	1,000	3.455	0.161	21.46	1.33	1.8785	0.0245	76.67	1.88	1.1675	0.0245	47.65	1.68	3.0875	0.2765	11.17	1.05
3.5	3,000	2.742	0.351	7.81	0.89	1.861	0.0495	37.60	1.58	1.415	0.151	9.37	0.97	3.303	0.6285	5.26	0.72
4.0	10,000	2.6325	1.0885	2.42	0.38	2.0455	0.1305	15.67	1.20	1.2945	0.3205	4.04	0.61	2.6225	0.725	3.62	0.56
4.5	30,000	2.1985	1.4745	1.49	0.17	1.9425	0.2235	8.69	0.94	1.364	0.769	1.77	0.25	2.8475	1.6845	1.69	0.23
5.0	100,000	2.1435	2.6645	0.80	-0.09	1.9105	0.3465	5.51	0.74	1.2565	1.229	1.02	0.01	2.602	2.0925	1.24	0.09
5.5	300,000	1.241	3.0425	0.41	-0.39	1.9475	0.6605	2.95	0.47	1.273	1.7295	0.74	-0.13	2.6295	2.3035	1.14	0.06
6.0	1,000,000																
6.5	3,000,000																
7.0	10,000,000																
7.5	30,000,000																

Calculation Template for End Point

Collagen	
BNC-I	R-1
3.5	0.89
4.0	0.38
4.5	0.17
5.0	-0.09
5.5	-0.39

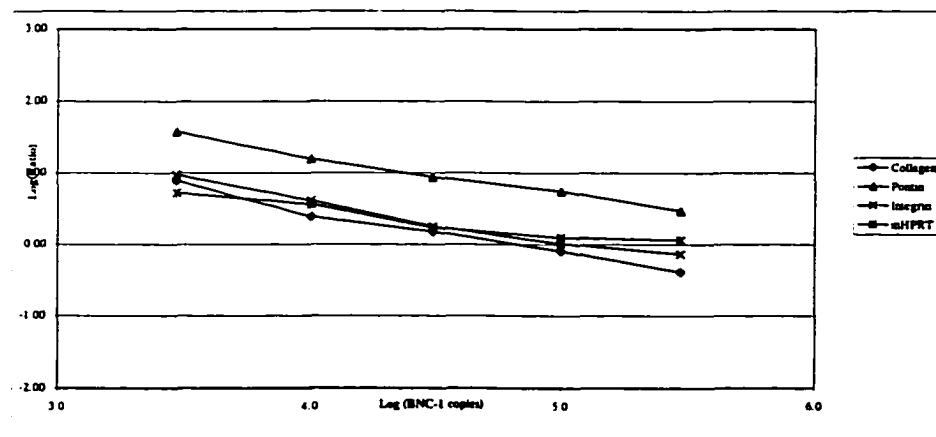
Pontin	
BNC-I	R-2
3.5	1.58
4.0	1.20
4.5	0.94
5.0	0.74
5.5	0.47

Integrin	
BNC-I	R-3
3.5	0.97
4.0	0.61
4.5	0.25
5.0	0.01
5.5	-0.13

mHPRT	
BNC-I	R-4
3.5	0.72
4.0	0.56
4.5	0.23
5.0	0.09
5.5	0.057

1 Hr Control I
DR 19

	Collagen	Pontin	Integrin	mHPRT
End Pt/Reaction	63,583	2,148,769	123,813	258,905
Slope	-0.61	-0.53	-0.56	-0.36
Corr Coeff	-0.99	-0.99	-0.99	-0.96



QC-RT-PCR Experiment Calculation

Plate 1
Controls
RT+ 1.50
PCR+ 2.00
EIA+ 2.00
EIA- 0.190

Backgrounds
MCC 0.144
Collag 0.182
Pontin 0.163
Integri 0.153
mHPRT 0.152

Plate 2
Controls
RT+ 1.50
PCR+ 2.00
EIA+ 0.00
EIA- 0.000

Low OD cutoff
0.014

Error Corrected Average Specific O.D.																	
PCR primer		Collagen		20 min		Pontin		20 min		Integrin		30 min		mHPRT		30 min	
BNC-1 copies	Colla	stuffer	Ratio	log R	Pontin	stuffer	Ratio	log R	Integrin	stuffer	Ratio	log R	mHPRT	stuffer	Ratio	log R	
1.0	10																
1.5	30																
2.0	100																
2.5	300	1.895	0.0465	40.75	1.61	3.488	0.021	170.15	2.23	2.6495	0.016	165.59	2.22	1.576	0.0215	73.30	1.87
3.0	1,000	1.393	0.047	29.63	1.47	2.842	0.016	177.63	2.25	1.8385	0.045	41.31	1.62	1.74	0.126	13.81	1.14
3.5	3,000	1.327	0.153	8.67	0.94	2.848	0.062	46.30	1.67	2.274	0.248	9.19	0.96	1.3455	0.1355	9.93	1.00
4.0	10,000	1.304	0.355	3.67	0.56	2.634	0.156	16.94	1.23	1.7875	0.431	4.15	0.62	1.412	0.464	3.04	0.48
4.5	30,000	0.923	0.253	3.65	0.56	2.498	0.146	17.17	1.23	1.3845	0.464	2.99	0.48	1.063	0.29	3.67	0.56
5.0	100,000	0.991	0.484	2.05	0.31	2.23	0.218	10.25	1.01	1.094	0.765	1.43	0.16	0.9465	0.4275	2.21	0.35
5.5	300,000	1.038	1.166	0.89	-0.05	3.173	0.798	3.98	0.60	1.716	1.828	0.94	-0.03	1.3365	1.455	0.92	-0.04
6.0	1,000,000																
6.5	3,000,000																
7.0	10,000,000																
7.5	30,000,000																

Calculation Template for End Point

Collagen	
BNC-1	R-1
3.5	0.94
4.0	0.56
5.0	0.31
5.5	-0.05

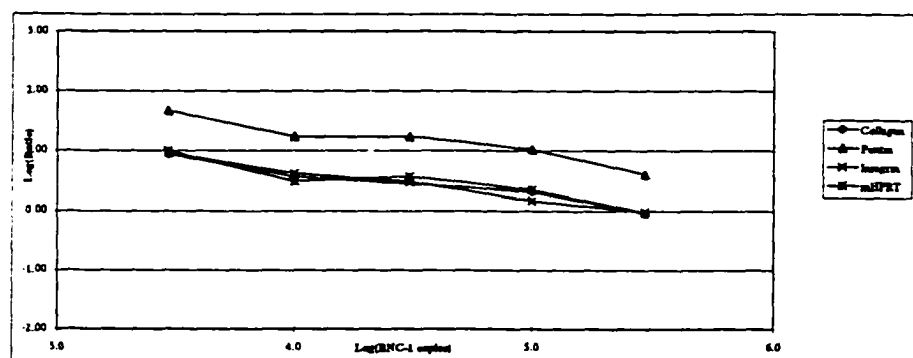
Pontin	
BNC-1	R-2
3.5	1.67
4.0	1.22
4.5	1.23
5	1.01
5.5	0.60

Integrin	
BNC-1	R-3
3.5	0.96
4.0	0.62
4.5	0.48
5.0	0.16
5.5	-0.03

mHPRT	
MCC-4	R-4
3.5	1.00
4.0	0.48
4.5	0.56
5	0.35
5.5	-0.04

1 Hr 3,000 Microstrain I
DR 19

	Collagen	Pontin	Integrin	mHPRT
End Pt/Reaction	299,658	8,435,891	239,293	355,338
Slope	-0.45	-0.47	-0.49	-0.44
Corr Coeff	-0.98	-0.96	-0.99	-0.93



QC-RT-PCR Experiment Calculation

Plate 1	
Controls	
RT+	1.50
PCR+	2.00
EIA+	2.00
EIA-	0.190

Backgrounds	
BNC	0.202
Collagen	0.222
Pontin	0.173
Integrin	0.195
mHPRT	0.219

Plate 2	
Controls	
RT+	1.50
PCR+	2.00
EIA+	0.00
EIA-	0.000

Low OD cutoff
0.014

		Error Corrected Average Specific O.D.											
PCR primer	Collagen	30 min	Pontin		15 min	Integrin		15 min	mHPRT		15 min		
BNC-I copies	Collagen	stuffer	Ratio	log R	Ratio	log R	Ratio	log R	Ratio	log R	Ratio	log R	Ratio
1.0	10												
1.5	30												
2.0	100												
2.5	300												
3.0	1,000												
3.5	3,000												
4.0	10,000	2.0415	0.2745	7.44	0.87	1.2815	0.0445	28.80	1.46	2.1715	0.712	3.05	0.48
4.5	30,000	1.3165	0.3735	3.52	0.55	1.0505	0.081	12.97	1.11	1.17	0.432	2.71	0.43
5.0	100,000	1.292	1.575	0.82	-0.09	1.1565	0.2865	4.04	0.61	0.6975	0.9305	0.75	-0.13
5.5	300,000	1.3715	2.12	0.65	-0.19	1.056	0.3705	2.85	0.45	1.6225	2.034	0.80	-0.10
6.0	1,000,000	1.11	2.4515	0.45	-0.34	1.1685	0.516	2.26	0.35	1.875	2.532	0.74	-0.13
6.5	3,000,000	0.2395	2.6265	0.09	-1.04	1.0055	0.6255	1.61	0.21	0.717	2.204	0.33	-0.49
7.0	10,000,000	0.0225	2.9415	0.01	-2.12	1.0225	0.8635	1.18	0.07	1.389	3.0075	0.46	-0.34
7.5	30,000,000												

Calculation Template for End Point

Collagen	
BNC-I	R-1
4.0	0.87
4.5	0.55
5.0	-0.09
5.5	-0.19

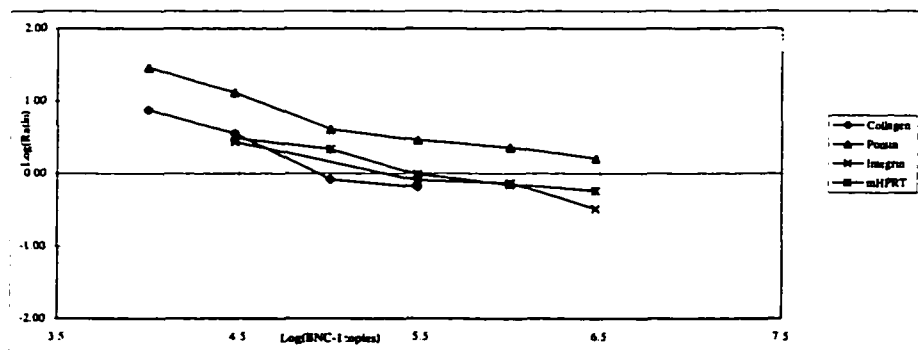
Pontin	
BNC-I	R-2
4.0	1.46
4.5	1.11
5.0	0.61
5.5	0.45
6.0	0.35
6.5	0.21

Integrin	
BNC-I	R-3
4.5	0.43
5.5	-0.10
6.0	-0.13
6.5	-0.49

mHPRT	
BNC-I	R-4
4.5	0.49
5.0	0.33
5.5	-0.02
6.0	-0.15
6.5	-0.23

I HR CONTROL II
DR

	Collagen	Pontin	Integrin	mHPRT
End Pt/Reaction	128,354	4,366,561	277,670	500,244
Slope	-0.77	-0.50	-0.43	-0.38
Corr Coeff	-0.97	-0.96	-0.98	-0.97



QC-RT-PCR Experiment Calculation

Plate 1	
Controls	
RT+	1.50
PCR+	2.00
EIA+	2.00
EIA-	0.190

Backgrounds	
BNC	0.180
Collagen	0.194
Pontin	0.193
Integrin	0.204
mHPRT	0.182

Plate 2	
Controls	
RT+	1.50
PCR+	2.00
EIA+	0.00
EIA-	0.000

Low OD cutoff
0.014

		Error Corrected Average Specific O.D.															
PCR primer	Collagen	30 min		Pontin		15 min		Integrin		15 min		mHPRT		15 min			
BNC-I copies	Collagen stuffer	Ratio	log R	Pontin stuffer	Ratio	log R	Integrin stuffer	Ratio	log R	mHPRT stuffer	Ratio	log R	mHPRT stuffer	Ratio	log R		
1.0	10																
1.5	30																
2.0	100																
2.5	300																
3.0	1,000																
3.5	3,000																
4.0	10,000	2.363	0.586	4.03	0.61	2.5135	0.2285	11.00	1.04	0.488	0.0835	5.84	0.77	2.682	0.59	4.55	0.66
4.5	30,000	1.461	0.5205	2.81	0.45	1.692	0.216	7.83	0.89	0.948	0.4775	1.99	0.30	1.758	0.6955	2.53	0.40
5.0	100,000	1.037	1.3245	0.78	-0.11	1.5265	0.4265	3.58	0.55	1.0355	0.9665	1.07	0.03	2.052	1.245	1.65	0.22
5.5	300,000	0.762	1.579	0.48	-0.32	1.363	0.4205	3.24	0.51	0.808	1.106	0.73	-0.14	1.5935	1.3005	1.23	0.09
6.0	1,000,000	0.367	1.754	0.21	-0.68	1.4855	0.662	2.24	0.35	0.9	1.676	0.54	-0.27	1.4995	1.399	1.07	0.03
6.5	3,000,000	low	1.9045			1.3135	0.8075	1.63	0.21	2.8505	3.5515	0.80	-0.10	0.5795	1.1665	0.50	-0.30
7.0	10,000,000	0.936	2.426	0.39	-0.41	1.7435	1.238	1.41	0.15					1.5975	2.6945	0.59	-0.23
7.5	30,000,000																

Calculation Template for End Point

Collagen	
BNC-I	R-1
4.5	0.45
5.0	-0.11
5.5	-0.32
6.0	-0.68

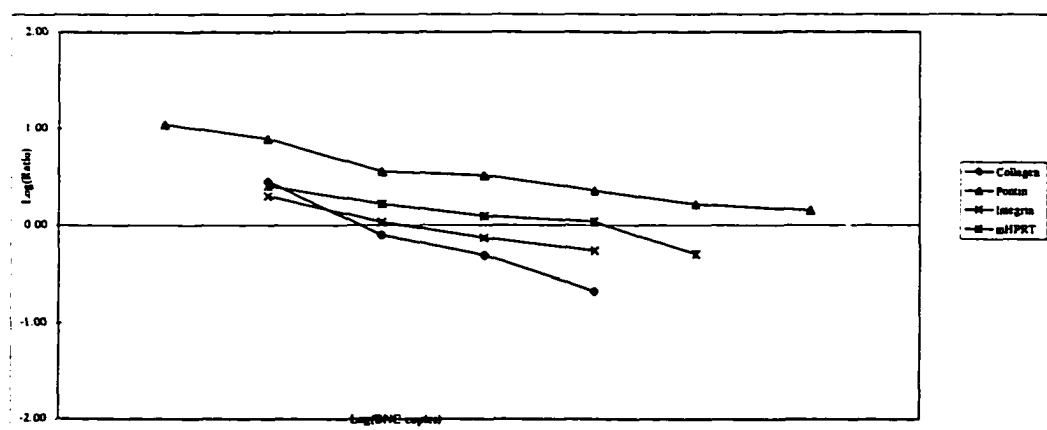
Pontin	
BNC-I	R-2
4.0	1.04
4.5	0.89
5.0	0.55
5.5	0.51
6.0	0.35
6.5	0.21
7.0	0.149

Integrin	
BNC-I	R-3
4.5	0.30
5.0	0.03
5.5	-0.14
6.0	-0.27

mHPRT	
BNC-I	R-4
4.5	0.40
5.0	0.22
5.5	0.09
6.0	0.03
6.5	-0.30

1 HR 6,000 I
DR

	Collagen	Pontin	Integrin	mHPRT
End Pt/Reaction	102,213	17,290,219	153,306	573,235
Slope	-0.71	-0.30	-0.37	-0.32
Corr Coeff	-0.99	-0.98	-0.99	-0.97



QC-RT-PCR Experiment Calculation

Plate 1	
Controls	
RT+	1.50
PCR+	2.00
EIA+	2.00
EIA-	0.190

Backgrounds	
BNC	0.135
Collage	0.164
Pontin	0.151
Integrin	0.168
mHPRT	0.190

Plate 2	
Controls	
RT+	1.50
PCR+	2.00
EIA+	0.00
EIA-	0.000

Low OD cutoff
0.014

		Error Corrected Average Specific O.D.															
PCR primer		Collagen				Pontin				Integrin				mHPRT			
BNC-1 copies	Collagen	10 min	Ratio	log R	Pontin	15 min	Ratio	log R	Integrin	15 min	Ratio	log R	mHPRT	15 min	Ratio	log R	
1.0	10																
1.5	30																
2.0	100																
2.5	300																
3.0	1,000																
3.5	3,000																
4.0	10,000	1.3375	0.251	5.34	0.73	1.46	0.1285	11.36	1.06	3.1565	0.605	5.22	0.72	3.567	0.8465	4.21	0.62
4.5	30,000	1.109	0.544	2.04	0.31	1.317	0.2425	5.43	0.73	2.658	1.326	2.00	0.30	1.9305	0.2195	8.79	0.94
5.0	100,000	0.9955	0.732	1.36	0.13	1.0225	0.3955	2.59	0.41	2.215	1.8435	1.20	0.08	2.355	1.653	1.42	0.15
5.5	300,000	0.6075	0.719	0.84	-0.07	1.222	0.4345	2.81	0.45	1.8905	1.73	1.09	0.04	1.9155	1.4815	1.29	0.11
6.0	1,000,000	0.7305	1.35	0.54	-0.27	1.1535	0.768	1.50	0.18	2.5905	2.853	0.91	-0.04	2.134	2.5685	0.83	-0.08
6.5	3,000,000	0.657	1.544	0.43	-0.37	1.4045	0.803	1.75	0.24	1.909	2.5045	0.76	-0.12	1.672	2.5595	0.65	-0.18
7.0	10,000,000	0.558	1.674	0.33	-0.48	0.9695	0.958	1.01	0.01	2.1935	3.202	0.69	-0.16	1.729	2.9475	0.59	-0.23
7.5	30,000,000																

Calculation Template for End Point

Collagen	
BNC	R-1
4.0	0.73
4.5	0.31
5.0	0.13
5.5	-0.07
6.0	-0.27
6.5	-0.37
7.0	-0.48

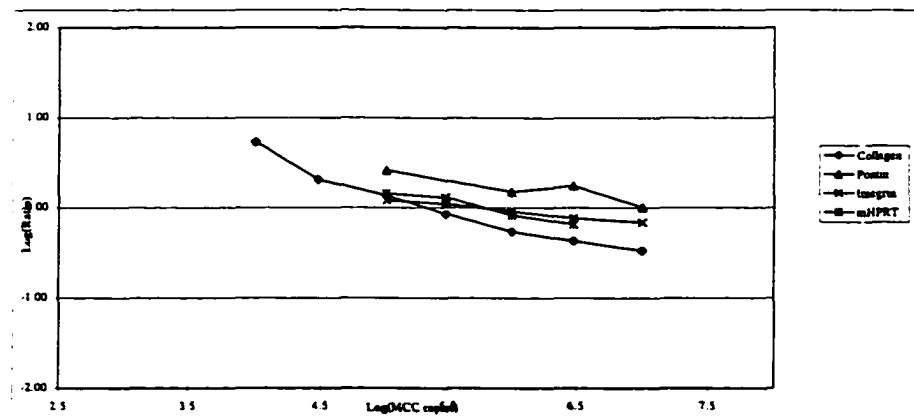
Pontin	
BNC	R-2
5.0	0.41
6.0	0.177
6.5	0.243
7.0	0.005

Integrin	
BNC	R-3
5.0	0.08
5.5	0.04
6.0	-0.04
6.5	-0.12
7.0	-0.16

mHPRT	
BNC	R-4
5.0	0.15
5.5	0.11
6.0	-0.08
6.5	-0.18

I HR 3,000 II
DR 21

	Collagen	Pontin	Integrin	mHPRT
End Pt/Reaction	304,616	19,062,873	469,266	547,587
Slope	-0.38	-0.18	-0.13	-0.24
Corr Coeff	-0.97	-0.91	-0.99	-0.98



QC-RT-PCR Experiment Calculation

Plate 1	
Controls	
RT+	1.50
PCR+	2.00
EIA+	2.00
EIA-	0.190

Backgrounds	
BNC	0.132
Collage	0.163
Pontin	0.198
Integrin	0.172
mHPRT	0.261

Plate 2	
Controls	
RT+	1.50
PCR+	2.00
EIA+	0.00
EIA-	0.000

Low OD cutoff
0.014

		Error Corrected Average Specific O.D.															
PCR primer		Collagen				Pontin				Integrin				mHPRT			
BNC-I copies	Collagen	stuffer	Ratio	log R	Pontin	stuffer	Ratio	log R	Integrin	stuffer	Ratio	log R	mHPRT	stuffer	Ratio	log R	15 min
1.0	10																
1.5	30																
2.0	100																
2.5	300																
3.0	1,000																
3.5	3,000																
4.0	10,000	2.2905	0.769	2.98	0.47	2.9695	0.814	3.65	0.56	1.909	0.7925	2.41	0.38	1.9415	0.3025	6.42	0.81
4.5	30,000	2.043	1.409	1.45	0.16	1.068	0.039	27.74	1.44	1.3125	0.8935	1.47	0.17	1.9985	0.667	3.00	0.48
5.0	100,000	0.789	1.019	0.77	-0.11	2.1455	0.974	2.20	0.34	0.918	0.971	0.95	-0.02	0.531	0.454	1.17	0.07
5.5	300,000	0.8995	1.963	0.46	-0.34	2.559	1.442	1.77	0.25	1.3165	1.767	0.75	-0.13	1.3615	1.566	0.87	-0.06
6.0	1,000,000	1.061	2.513	0.42	-0.37	2.5705	2.211	1.16	0.07	1.4095	2.701	0.52	-0.28	1.034	1.809	0.57	-0.24
6.5	3,000,000	0.8805	3.299	0.27	-0.57	2.262	2.463	0.92	-0.04	1.738	3.0455	0.57	-0.24	1.073	2.696	0.40	-0.40
7.0	10,000,000	0.773	3.517	0.22	-0.66	2.835	3.27	0.87	-0.06	1.606	3.325	0.48	-0.32	0.7895	2.6075	0.30	-0.52
7.5	30,000,000																

Calculation Template for End Point

Collagen	
BNC	R-1
4.0	0.47
4.5	0.16
5.0	-0.11
5.5	-0.34

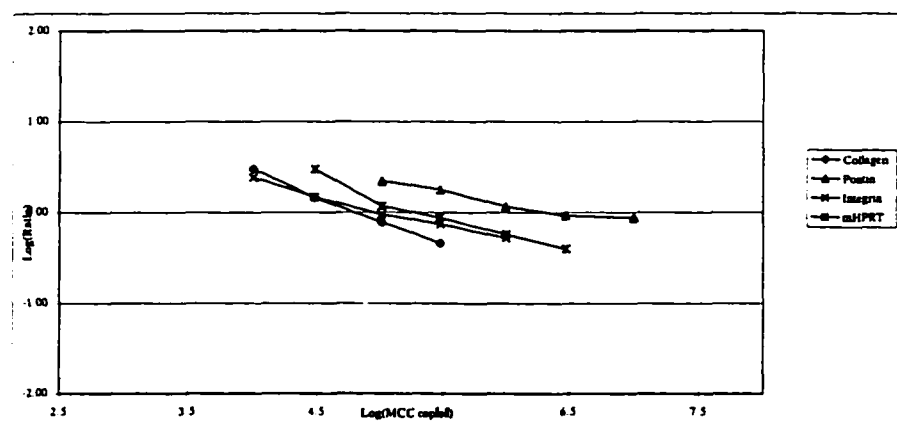
Pontin	
BNC	R-2
5.0	0.34
5.5	0.249
6.0	0.066
6.5	-0.04
7.0	-0.06

Integrin	
BNC	R-3
4.0	0.38
4.5	0.17
5.0	-0.02
5.5	-0.13
6.0	-0.28

mHPRT	
BNC	R-4
4.5	0.48
5.0	0.07
5.5	-0.06
6.0	-0.24
6.5	-0.4

I HR 6,000 II
DR 21

	Collagen	Pontin	Integrin	mHPRT
End Pt/Reaction	66,609	3,170,752	115,134	256,641
Slope	-0.55	-0.22	-0.32	-0.41
Corr Coeff	-1.00	-0.97	-0.99	-0.98



QC-RT-PCR Experiment Calculation

Plate 1	
Controls	
RT+	1.50
PCR+	2.00
EIA+	2.00
EIA-	0.190

Backgrounds	
BNC	0.154
Collage	0.177
Pontin	0.161
Integrin	0.169
mHPR	0.174

Plate 2	
Controls	
RT+	1.50
PCR+	2.00
EIA+	0.00
EIA-	0.000

Low OD cutoff
0.014

Error Corrected Average Specific O.D.									
PCR primer	Collagen	30 min	Pontin	15 min	Integrin	15 min	mHPRT	15 min	
BNC-1 copies	Collagen stuffer	Ratio log R	Pontin stuffer	Ratio log R	Integrin stuffer	Ratio log R	mHPRT stuffer	Ratio log R	
1.0	10								
1.5	30								
2.0	100								
2.5	300								
3.0	1,000								
3.5	3,000								
4.0	10,000	3.1355 0.697	4.50 0.65	3.6975 0.3035	12.18 1.09	2.804 0.571	4.91 0.69	2.8945 0.688	4.21 0.62
4.5	30,000	2.4315 0.8695	2.80 0.45	3.4135 0.5095	6.70 0.83	1.6765 0.4405	3.81 0.58	2.4345 0.74	3.29 0.52
5.0	100,000	2.017 1.442	1.40 0.15	3.4355 0.846	4.06 0.61	1.82 1.2185	1.49 0.17	2.26 1.0865	2.08 0.32
5.5	300,000	1.2585 1.1435	1.10 0.04	3.046 0.7795	3.91 0.59	0.5725 0.5145	1.11 0.05	1.7015 1.154	1.47 0.17
6.0	1,000,000	1.943 2.5065	0.78 -0.11	2.8915 1.401	2.06 0.31	1.67 2.187	0.76 -0.12	1.802 1.49	1.21 0.08
6.5	3,000,000	1.8105 2.2165	0.82 -0.09	2.8635 1.6255	1.76 0.25	1.2685 2.3025	0.55 -0.26	1.7665 2.278	0.78 -0.11
7.0	10,000,000	0.766 2.7775	0.28 -0.56	2.923 1.9195	1.52 0.18	1.0575 2.7785	0.38 -0.42	1.101 1.7415	0.63 -0.20
7.5	30,000,000								

Calculation Template for End Point

Collagen	
BNC	R-1
4.0	0.65
4.5	0.45
5.0	0.15
5.5	0.04
6.0	-0.11
7.0	-0.56

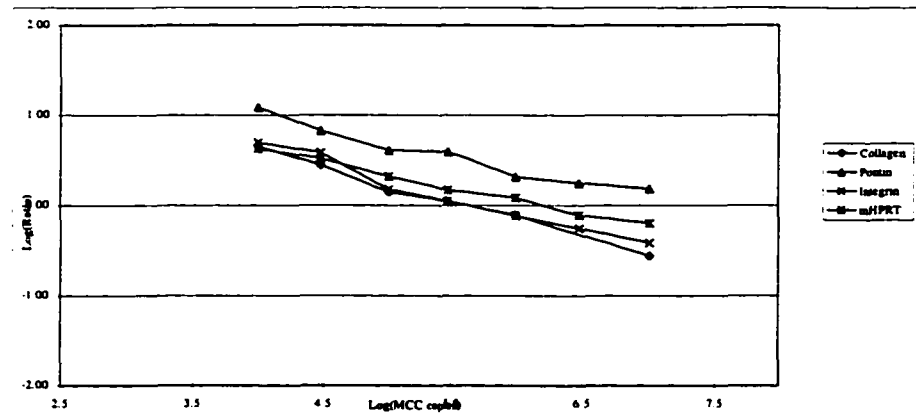
Pontin	
BNC	R-2
4.0	1.09
4.5	0.83
5.0	0.61
5.5	0.592
6.0	0.315
6.5	0.246
7.0	0.18

Integrin	
BNC	R-3
4.0	0.69
4.5	0.58
5.0	0.17
5.5	0.05
6.0	-0.12
6.5	-0.26
7.0	-0.42

mHPRT	
BNC	R-4
4.0	0.62
4.5	0.52
5.0	0.32
5.5	0.17
6.0	0.08
6.5	-0.11
7.0	-0.2

4 HR CONTROL I
DR 22

	Collagen	Pontin	Integrin	mHPRT
End Pt/Reaction	387.475	21,991.691	566.054	1,577.522
Slope	-0.39	-0.30	-0.38	-0.28
Corr Coeff	-0.99	-0.98	-0.99	-1.00



QC-RT-PCR Experiment Calculation

Plate 1	
Controls	
RT+	1.50
PCR+	2.00
EIA+	2.00
EIA-	0.190

Backgrounds	
BNC	0.354
Collagen	0.296
Pontin	0.155
Integrin	0.166
mHPRT	0.278

Plate 2	
Controls	
RT+	1.50
PCR+	2.00
EIA+	0.00
EIA-	0.000

Low OD cutoff
0.014

		Error Corrected Average Specific O.D.															
PCR primer	Collagen	30 min	Pontin		15 min	Integrin		15 min	mHPRT		15 min						
BNC-1 copies	Collagen	Ratio log R	Pontin	stuffer	Ratio log R	Integrin	stuffer	Ratio log R	mHPRT	stuffer	Ratio log R	mHPRT	stuffer	Ratio log R	mHPRT	stuffer	Ratio log R
1.0	10																
1.5	30																
2.0	100																
2.5	300																
3.0	1,000																
3.5	3,000																
4.0	10,000	2.5055 0.8665	2.89 0.46	0.872 0.0985	8.85 0.95	3.834 1.2705	3.02 0.48	0.942 0.069	13.65 1.14								
4.5	30,000	1.2175 0.9385	1.30 0.11	0.6105 0.1065	5.73 0.76	2.7075 1.5345	1.76 0.25	1.376 0.916	1.50 0.18								
5.0	100,000	1.508 1.5875	0.95 -0.02	0.7085 0.2565	2.76 0.44	2.2415 2.076	1.08 0.03	1.7865 1.2135	1.47 0.17								
5.5	300,000	0.6635 1.4465	0.46 -0.34	0.536 0.2825	1.97 0.29	1.2535 2.479	0.51 -0.30	0.886 0.8445	1.00 0.00								
6.0	1,000,000	1.1775 2.8175	0.42 -0.38	0.687 0.4315	1.59 0.20	1.3965 3.0265	0.46 -0.34	1.423 1.7275	0.82 -0.08								
6.5	3,000,000	1.053 2.2695	0.46 -0.33	0.61 0.5085	1.20 0.08	2.1425 3.0545	0.70 -0.15	1.208 2.1135	0.57 -0.24								
7.0	10,000,000	0.8485 2.9515	0.29 -0.54	0.699 0.586	1.19 0.08	1.8225 3.325	0.55 -0.26	0.6715 2.763	0.24 -0.61								
7.5	30,000,000																

Calculation Template for End Point

Collagen	
BNC	R-1
4.0	0.46
4.5	0.11
5.0	-0.02
5.5	-0.34
6.0	-0.38

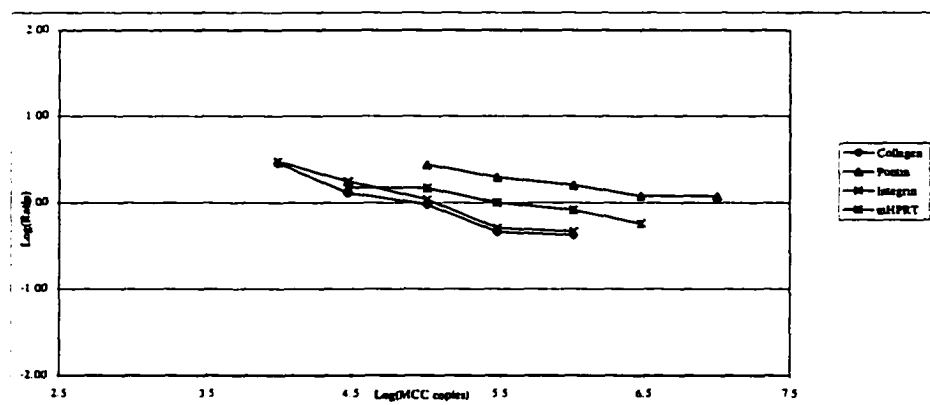
Pontin	
BNC	R-2
5.0	0.44
5.5	0.294
6.0	0.202
6.5	0.079
7.0	0.08

Integrin	
BNC	R-3
4.0	0.48
4.5	0.25
5.0	0.03
5.5	-0.3
6.0	-0.34

mHPRT	
BNC	R-4
4.5	0.18
5.0	0.17
5.5	0.00
6.0	-0.08
6.5	-0.24

4 HR 3,000 I
DR 22

	Collagen	Pontin	Integrin	mHPRT
End Pt/Reaction	81,829	14,191,715	112,113	318,473
Slope	-0.42	-0.19	-0.43	-0.22
Corr Coeff	-0.97	-0.96	-0.98	-0.97



QC-RT-PCR Experiment Calculation

Plate 1	
Controls	
RT+	1.50
PCR+	2.00
EIA+	2.00
EIA-	0.190

Backgrounds	
BNC	0.162
Collage	0.181
Pontin	0.168
Integrin	0.186
mHPRT	0.175

Plate 2	
Controls	
RT+	1.50
PCR+	2.00
EIA+	0.00
EIA-	0.000

Low OD cutoff
0.014

Error Corrected Average Specific O.D.									
PCR primer	Collagen	20 min	Pontin	15 min	Integrin	15 min	mHPRT	15 min	
BNC-1 copies	Collagen stuffer	Ratio log R	Pontin stuffer	Ratio log R	Integrin stuffer	Ratio log R	mHPRT stuffer	Ratio log R	
1.0	10								
1.5	30								
2.0	100								
2.5	300								
3.0	1,000								
3.5	3,000								
4.0	10,000	0.8155 0.1095	7.45 0.87	1.0295 low		2.0805 0.335	6.21 0.79	1.5865 0.194	8.18 0.91
4.5	30,000	0.995 0.587	1.70 0.23	0.7605 0.067	11.35 1.06	1.813 0.618	2.93 0.47	1.501 0.297	5.05 0.70
5.0	100,000	1.995 1.9625	1.02 0.01	0.8575 0.177	4.84 0.69	1.518 0.6365	2.38 0.38	1.185 0.4035	2.94 0.47
5.5	300,000	1.9345 2.374	0.81 -0.09	0.879 0.2455	3.58 0.55	1.744 1.592	1.10 0.04	1.887 1.6255	1.16 0.06
6.0	1,000,000	0.9855 2.5855	0.38 -0.42	0.796 0.283	2.81 0.45	1.2765 2.051	0.62 -0.21	1.6605 1.908	0.87 -0.06
6.5	3,000,000	1.3745 2.836	0.48 -0.31	0.8545 0.384	2.23 0.35	1.7805 2.719	0.65 -0.18	1.5545 2.1915	0.71 -0.15
7.0	10,000,000	0.8775 2.335	0.38 -0.43	0.653 0.3965	1.65 0.22	1.5135 2.4555	0.62 -0.21	1.1895 2.436	0.49 -0.31
7.5	30,000,000								

Calculation Template for End Point

Collagen	
BNC	R-1
4.5	0.23
5.0	0.01
5.5	-0.09
6.5	-0.31
7.0	-0.43

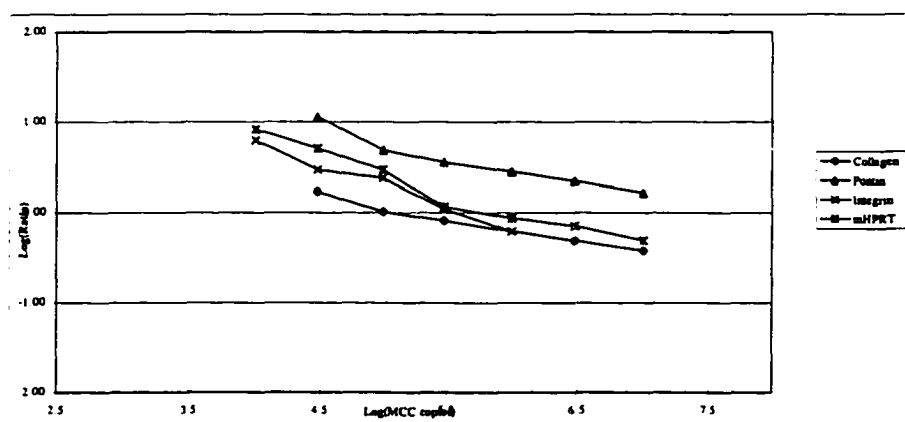
Pontin	
BNC	R-2
4.5	1.06
5.0	0.69
5.5	0.554
6.0	0.449
6.4771	0.347
7.0	0.22

Integrin	
BNC	R-3
4.0	0.79
4.5	0.47
5.0	0.38
5.5	0.04
6.0	-0.21

mHPRT	
BNC	R-4
4.0	0.91
4.5	0.70
5.0	0.47
5.5	0.06
6.0	-0.06
6.4771	-0.15
7.0	-0.31

4 Hr Control II
DR 23

	Collagen	Pontin	Integrin	mHPRT
End Pt/Reaction	161,232	36,327,980	396,801	1,101,491
Slope	-0.25	-0.30	-0.48	-0.42
Corr Coeff	-0.99	-0.96	-0.99	-0.98



QC-RT-PCR Experiment Calculation

Plate 1	
Controls	
RT+	1.50
PCR+	2.00
EIA+	2.00
EIA-	0.190

Backgrounds	
BNC	0.172
Collage	0.179
Pontin	0.162
Integrin	0.180
mHPRT	0.172

Plate 2	
Controls	
RT+	1.50
PCR+	2.00
EIA+	0.00
EIA-	0.000

Low OD cutoff
0.014

Error Corrected Average Specific O.D.											
PCR primer	Collagen	20 min	Pontin	15 min	Integrin	15 min	mHPRT	15 min			
BNC-1 copies	Collagen stuffer	Ratio log R	Pontin stuffer	Ratio log R	Integrin stuffer	Ratio log R	mHPRT stuffer	Ratio log R			
1.0	10										
1.5	30										
2.0	100										
2.5	300										
3.0	1,000										
3.5	3,000										
4.0	10,000	1.842 0.756	2.44 0.39	0.988 0.05	19.76 1.30	3.82 0.4325	8.83 0.95	3.458 0.591	5.85 0.77		
4.5	30,000	0.812 0.742	1.10 0.04	0.616 0.041	15.02 1.18	1.2555 0.092	13.65 1.14	2.0625 0.612	3.37 0.53		
5.0	100,000	0.793 0.846	0.94 -0.03	0.6755 0.108	6.25 0.80	2.9325 1.709	1.72 0.23	2.107 1.0655	1.98 0.30		
5.5	300,000	0.92 1.566	0.59 -0.23	0.651 0.189	3.44 0.54	1.204 0.939	1.28 0.11	2.365 1.89	1.25 0.10		
6.0	1,000,000	0.8495 1.66	0.51 -0.29	0.6305 0.279	2.26 0.35	2.4395 3.097	0.79 -0.10	2.1025 2.3725	0.89 -0.05		
6.5	3,000,000	0.8155 2.38	0.34 -0.47	0.802 0.3735	2.15 0.33	2.8405 3.135	0.91 -0.04	2.1265 3	0.71 -0.15		
7.0	10,000,000	0.7195 1.917	0.38 -0.43	0.583 0.487	1.20 0.08	2.639 3.3255	0.79 -0.10	1.734 2.8825	0.60 -0.22		
7.5	30,000,000										

Calculation Template for End Point

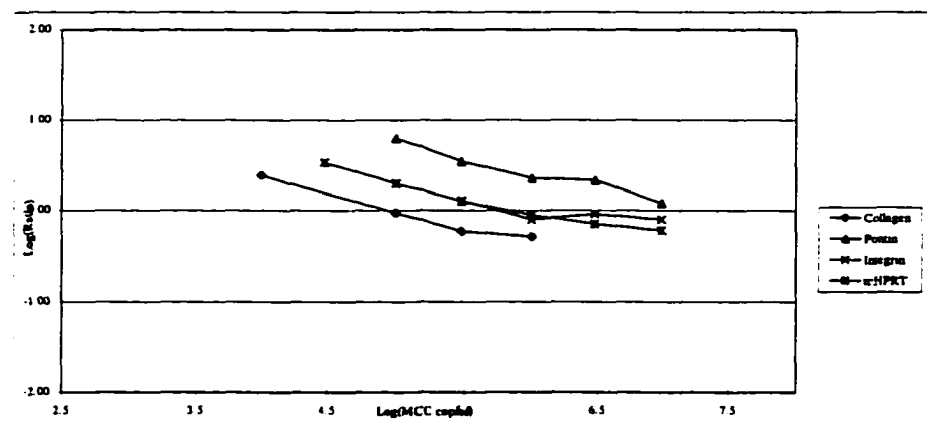
Collagen	
BNC	R-1
4.0	0.39
5.0	-0.03
5.5	-0.23
6.0	-0.29

Pontin	
BNC	R-2
5.0	0.80
5.5	0.54
6.0	0.35
6.5	0.33
7.0	0.078

Integrin	
BNC	R-3
5.5	0.108
6.0	-0.1
6.5	-0.04
7.0	-0.1

mHPRT	
BNC	R-4
4.5	0.53
5.0	0.30
5.5	0.1
6.0	-0.05
6.5	-0.15
7.0	-0.22

4 Hr 6,000 I DR 23				
	Collagen	Pontin	Integrin	mHPRT
End Pt/Reaction	100,958	18,533,556	854,566	1,041,751
Slope	-0.35	-0.33	-0.11	-0.30
Corr Coeff	-0.98	-0.97	-0.74	-0.98



QC-RT-PCR Experiment Calculation

Plate 1	
Controls	
RT+	1.50
PCR+	2.00
EIA+	2.00
EIA-	0.190

Backgrounds	
BNC	0.156
Collagen	0.167
Pontin	0.172
Integrin	0.172
mHPRT	0.180

Plate 2	
Controls	
RT+	1.50
PCR+	2.00
EIA+	0.00
EIA-	0.000

Low OD cutoff
0.014

Error Corrected Average Specific O.D.

PCR primer	Collagen				Pontin				Integrin				mHPRT				
	BNC-1 copies	Collagen	stuffer	Ratio	log R	Pontin	stuffer	Ratio	log R	Integrin	stuffer	Ratio	log R	mHPRT	stuffer	Ratio	log R
1.0	10																
1.5	30																
2.0	100																
2.5	300																
3.0	1,000																
3.5	3,000																
4.0	10,000	1.62	0.232	6.98	0.84	2.7625	0.093	29.70	1.47	2.721	0.2165	12.57	1.10	2.6405	0.444	5.95	0.77
4.5	30,000	1.433	0.617	2.32	0.37	3.433	0.3105	11.06	1.04	3.2735	1.0055	3.26	0.51	2.378	1.062	2.24	0.35
5.0	100,000	1.0585	0.7815	1.35	0.13	2.3015	0.32	7.19	0.86	2.1815	1.068	2.04	0.31	0.7835	0.536	1.46	0.16
5.5	300,000	1.506	2.2115	0.68	-0.17	3.061	1.0305	2.97	0.47	2.76	2.832	0.97	-0.01	1.3555	1.5925	0.85	-0.07
6.0	1,000,000	1.0195	2.5225	0.40	-0.39	2.5325	1.4285	1.77	0.25	2.0025	2.9405	0.68	-0.17	1.6605	2.9045	0.57	-0.24
6.5	3,000,000	1.1655	3.0365	0.38	-0.42	2.6025	1.644	1.58	0.20	2.525	3.065	0.82	-0.08	1.866	2.7215	0.69	-0.16
7.0	10,000,000	0.6215	3.105	0.20	-0.70	2.2915	1.997	1.15	0.06	2.02	3.2875	0.61	-0.21	0.7435	3.3685	0.22	-0.66
7.5	30,000,000																

Calculation Template for End Point

Collagen	
BNC	R-1
4.0	0.84
4.5	0.37
5.0	0.13
5.5	-0.17
6.0	-0.39

Pontin	
BNC	R-2
5.0	0.86
5.5	0.4728
6.0	0.2487
6.5	0.1995
7.0	0.06

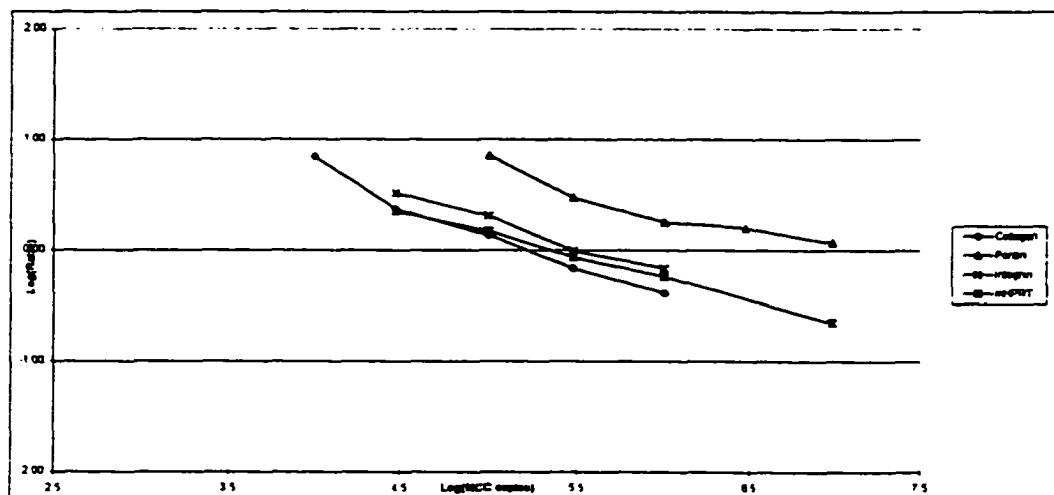
Integrin	
BNC	R-3
4.5	0.51
5.0	0.3102
5.5	-0.0112
6.0	-0.1668

mHPRT	
BNC	R-4
4.5	0.35
5.0	0.16
5.5	-0.07
6.0	-0.243
7	-0.656

24 HR CONTROL II

DR 26

	Collagen	Pontin	Integrin	mHPRT
End Pt/Reaction	178,309	9,474,429	383,795	231,214
Slope	-0.60	-0.37	-0.47	-0.40
Corr Coeff	-0.99	-0.95	-0.99	-1.00



QC-RT-PCR Experiment Calculation

Plate 1	
Controls	
RT+	1.50
PCR+	2.00
EIA+	2.00
EIA-	0.190

Backgrounds	
BNC	0.1e8
Collagen	0.1e8
Pontin	0.150
Integrin	0.170
mHPRT	0.140

Plate 2	
Controls	
RT+	1.50
PCR+	2.00
EIA+	0.00
EIA-	0.000

Low OD cutoff
0.014

		Collagen				Pontin				Integrin				mHPRT			
PCR primer		Collagen		15 min		Pontin		15 min		Integrin		15 min		mHPRT		15 min	
BNC-1 copies		Collagen	stuffer	Ratio	log R	Pontin	stuffer	Ratio	log R	Integrin	stuffer	Ratio	log R	mHPRT	stuffer	Ratio	log R
1.0	10																
1.5	30																
2.0	100																
2.5	300																
3.0	1,000																
3.5	3,000																
4.0	10,000	3.193	0.395	8.08	0.91	1.8775	0.0245	76.63	1.88	1.784	0.0855	20.87	1.32	0.9625	0.0985	9.77	0.99
4.5	30,000	2.3705	0.422	5.62	0.75	1.3535	0.0415	32.61	1.51	0.2255	low			0.539	0.071	7.59	0.88
5.0	100,000	2.1905	1.1305	1.94	0.29	1.232	0.1355	9.09	0.96	1.187	0.489	2.43	0.39	1.2075	0.5325	2.27	0.36
5.5	300,000	1.055	0.7595	1.39	0.14	1.1845	0.151	7.84	0.89	1.9355	1.904	1.02	0.01	1.284	0.9845	1.30	0.12
6.0	1,000,000	1.184	1.047	1.13	0.05	1.1995	0.417	2.88	0.46	1.5455	2.457	0.63	-0.20	0.908	1.084	0.84	-0.08
6.5	3,000,000	1.3375	1.9985	0.67	-0.17	1.315	0.666	1.97	0.30	1.967	2.858	0.69	-0.16	1.019	1.6405	0.62	-0.21
7.0	10,000,000	1.3125	2.598	0.51	-0.30	1.3875	0.754	1.84	0.26	0.8495	3.1145	0.27	-0.56	1.1145	2.1495	0.52	-0.29
7.5	30,000,000																

Calculation Template for End Point

Collagen	
BNC	R-1
5.0	0.29
5.5	0.14
6.0	0.05
6.5	-0.17
7.0	-0.30

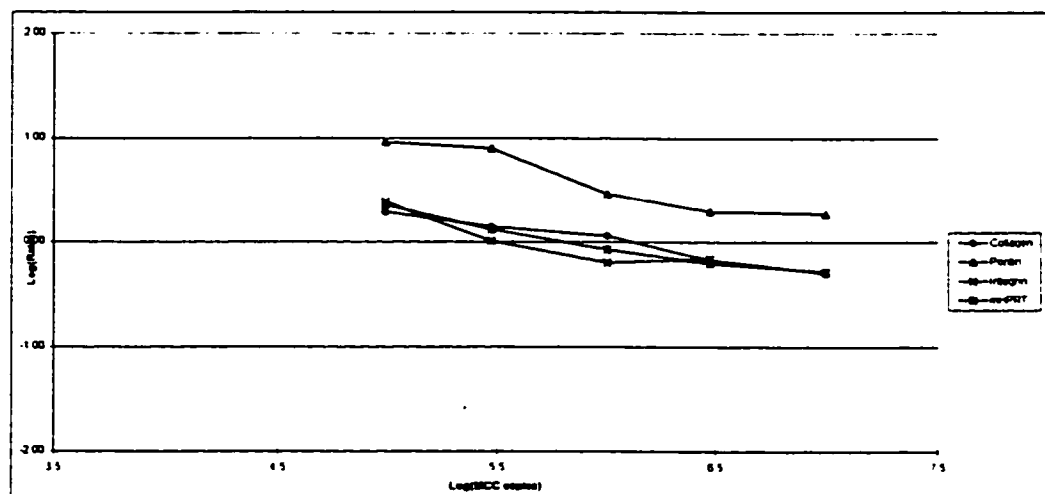
Pontin	
BNC	R-2
5.0	0.96
5.5	0.89
6.0	0.46
6.5	0.30
7.0	0.26

Integrin	
BNC	R-3
5.0	0.39
5.5	0.01
6.0	-0.20
6.5	-0.16

mHPRT	
BNC	R-4
5.0	0.36
5.5	0.12
6.0	-0.08
6.5	-0.21
7.0	-0.29

24 HR 3,000 I
DR 25

	Collagen	Pontin	Integrin	mHPRT
End Pt/Reaction	998,267	27,267,480	572,456	850,322
Slope	-0.30	-0.40	-0.37	-0.32
Corr Coeff	-0.99	-0.95	-0.89	-0.98



QC-RT-PCR Experiment Calculation

Plate 1	
Controls	
RT+	1.50
PCR+	2.00
EIA+	2.00
EIA-	0.190

Backgrounds	
BNC	0.159
Collagen	0.150
Pontin	0.142
Integrin	0.172
mHPRT	0.443

Plate 2	
Controls	
RT+	1.50
PCR+	2.00
EIA+	0.00
EIA-	0.000

Low OD cutoff
0.014

Error Corrected Average Specific O.D													
PCR primer	Collagen	15 min		Pontin	15 min		Integrin	15 min		mHPRT	15 min		
BNC-1 copies	Collagen	stuffer	Ratio	log R	Pontin	stuffer	Ratio	log R	Integrin	stuffer	Ratio	log R	
1.0	10												
1.5	30												
2.0	100												
2.5	300												
3.0	1,000												
3.5	3,000												
4.0	10,000	2.851	0.125	22.81	1.36	3.2515	0.107	30.39	1.48	1.8365	0.0765	24.01	1.38
4.5	30,000	0.053	0.043	1.23	0.09	0.7495	0.065	11.53	1.06	low	low		
5.0	100,000	2.716	2.233	1.22	0.09	2.546	0.558	4.56	0.66	0.6875	0.571	1.20	0.08
5.5	300,000	2.032	2.14	1.23	0.09	2.459	0.538	4.57	0.66	0.361	0.345	1.05	0.02
6.0	1,000,000	2.491	2.9325	0.85	-0.07	2.5115	1.042	2.41	0.38	1.697	2.901	0.58	-0.23
6.5	3,000,000	2.3645	3.046	0.78	-0.11	2.4005	1.174	2.04	0.31	1.006	2.824	0.36	-0.45
7.0	10,000,000	1.9435	3.26	0.60	-0.22	2.4025	1.5775	1.52	0.18	1.163	3.2025	0.36	-0.44
7.5	30,000,000												

Calculation Template for End Point

Collagen	
BNC	R-1
4.5	0.09
5.0	0.09
5.5	0.09
6.0	-0.07
6.5	-0.11
7.0	-0.22

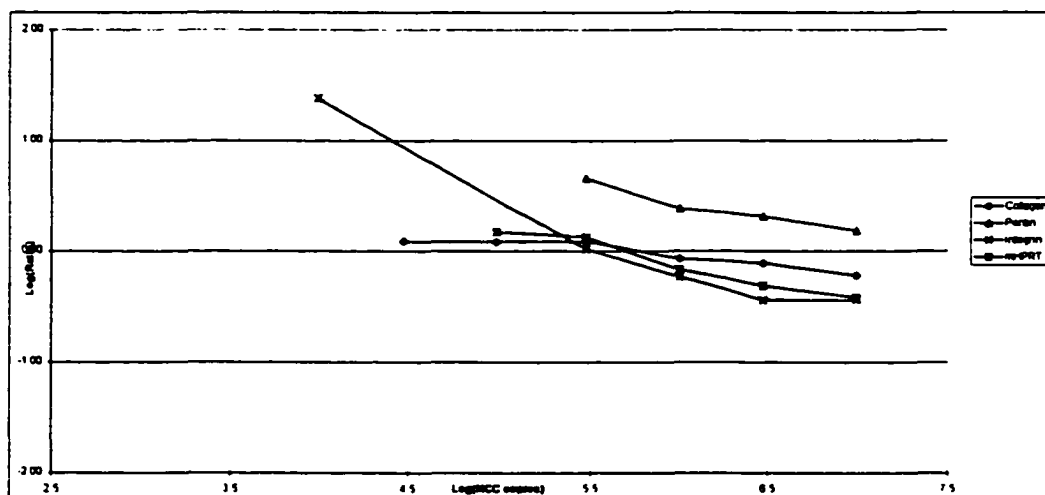
Pontin	
BNC	R-2
5.5	0.66
6.0	0.3821
6.5	0.3106
7.0	0.18

Integrin	
BNC	R-3
4.0	1.3803
5.5	0.0197
6.0	-0.2329
6.5	-0.4483
7.0	-0.4399

mHPRT	
BNC	R-4
5.0	0.17
5.5	0.1254
6.0	-0.171
6.5	-0.315
7.0	-0.424

24 HR CONTROL I
DR 25

	Collagen	Pontin	Integrin	mHPRT
End Pt/Respon	365,294	33,363,818	755,786	410,581
Slope	-0.13	-0.30	-0.64	-0.33
Corr Coeff	-0.94	-0.96	-0.96	-0.98



QC-RT-PCR Experiment Calculation

Plate 1	
Controls	
RT+	1.50
PCR+	2.00
EIA+	2.00
EIA-	0.190

Backgrounds	
BNC	0.158
Collagen	0.168
Pontin	0.178
Integrin	0.195
mHPRT	0.167

Plate 2	
Controls	
RT+	1.50
PCR+	2.00
EIA+	0.00
EIA-	0.000

Low OD cutoff
0.014

Error Corrected Average Specific O D																	
PCR primer	Collagen		15 min		Pontin		15 min		Integrin		15 min		mHPRT		15 min		
BNC-1 copies	Collagen	stuffer	Ratio	log R	Pontin	stuffer	Ratio	log R	Integrin	stuffer	Ratio	log R	mHPRT	stuffer	Ratio	log R	
1.0	10																
1.5	30																
2.0	100																
2.5	300																
3.0	1,000																
3.5	3,000																
4.0	10,000	2.095	0.25	8.38	0.92	3.165	0.229	13.82	1.14	0.3975	low		2.4805	0.438	5.66	0.75	
4.5	30,000	1.1725	0.2335	5.02	0.70	2.78	0.416	6.68	0.82	1.227	0.316	3.88	0.59	0.2545	0.029	8.78	0.94
5.0	100,000	1.3515	0.5375	2.51	0.40	2.646	0.445	5.95	0.77	1.772	0.965	1.84	0.26	1.6935	0.787	2.15	0.33
5.5	300,000	0.9745	0.9355	1.04	0.02	2.346	0.6755	3.47	0.54	1.5015	1.9445	0.77	-0.11	2.2095	1.8165	1.22	0.09
6.0	1,000,000	1.148	1.79	0.64	-0.19	2.219	0.8555	2.59	0.41	1.6685	2.768	0.60	-0.22	1.5525	2.0135	0.77	-0.11
6.5	3,000,000	0.939	2.3285	0.40	-0.39	2.2755	1.084	2.10	0.32	1.6305	2.964	0.55	-0.26	1.6365	2.453	0.67	-0.18
7.0	10,000,000	1.2465	2.538	0.49	-0.31	2.502	1.687	1.48	0.17	1.1545	3.233	0.36	-0.45	0.6055	2.8015	0.22	-0.67
7.5	30,000,000																

Calculation Template for End Point

Collagen	
BNC	R-1
4.5	0.70
5.0	0.40
5.5	0.02
6.0	-0.19

Pontin	
BNC	R-2
5.0	0.77
5.5	0.54
6.0	0.41
6.5	0.32
7.0	0.17

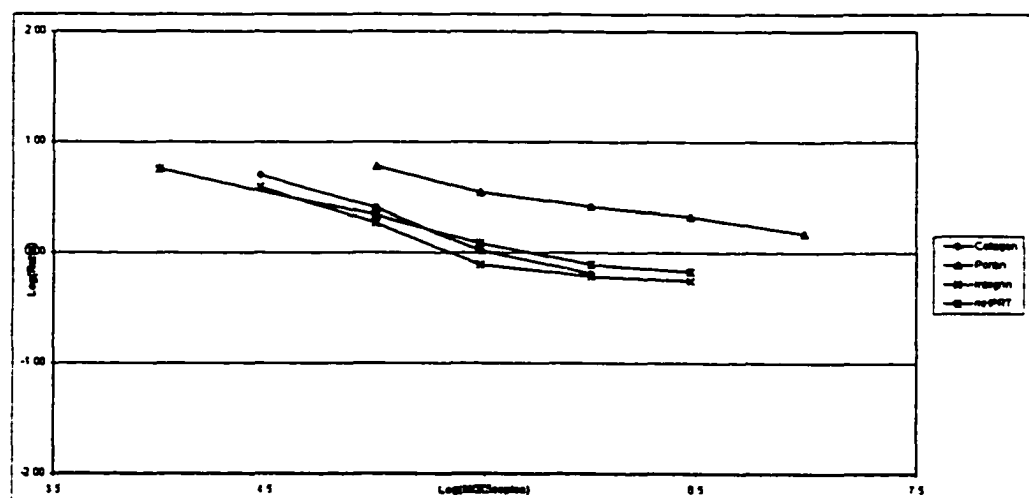
Integrin	
BNC	R-3
4.5	0.59
5.0	0.26
5.5	-0.11
6.0	-0.22
6.5	-0.26

mHPRT	
BNC	R-4
4.0	0.75
5.0	0.33
5.5	0.09
6.0	-0.11
6.5	-0.18

4 Hr 6,000 II

DR 24

	Collagen	Pontin	Integrin	mHPRT
End Pt/Reaction	417,389	35,658,316	403,645	692,997
Slope	-0.61	-0.28	-0.44	-0.39
Corr Coeff	-0.99	-0.99	-0.95	-0.99



QC-RT-PCR Experiment Calculation

Plate 1	
Controls	
RT+	1.50
PCR+	2.00
ELA+	2.00
ELA-	0.190

Backgrounds	
BNC	0.167
Collagen	0.175
Pontin	0.188
Integrin	0.181
mHPRT	0.203

Plate 2	
Controls	
RT+	1.50
PCR+	2.00
ELA+	0.00
ELA-	0.000

Low OD cutoff
0.014

Error Corrected Average Specific O.D.																	
	PCR primer BNC-1 copies	Collagen		15 min		Pontin		15 min		Integrin		15 min		mHPRT		15 min	
		Collagen	stuffer	Ratio	log R	Pontin	stuffer	Ratio	log R	Integrin	stuffer	Ratio	log R	mHPRT	stuffer	Ratio	log R
1.0	10																
1.5	30																
2.0	100																
2.5	300																
3.0	1,000																
3.5	3,000																
4.0	10,000	1.469	0.111	13.23	1.12	1.6615	low			1.14	0.058	19.66	1.29	1.287	0.1305	9.86	0.99
4.5	30,000	1.5935	0.5195	3.07	0.49	1.791	0.215	8.33	0.92	0.8215	0.1225	6.71	0.83	1.144	0.3135	3.65	0.56
5.0	100,000	1.4125	1.264	1.12	0.05	1.6005	0.361	4.43	0.65	0.609	0.452	1.35	0.13	1.6865	1.272	1.33	0.12
5.5	300,000	0.8575	1.332	0.64	-0.19	1.927	0.443	4.35	0.64	0.9305	1.465	0.64	-0.20	2.056	1.884	1.09	0.04
6.0	1,000,000	1.2785	2.5745	0.50	-0.30	1.3835	0.58	2.39	0.38	0.948	2.381	0.40	-0.40	1.1815	2.069	0.57	-0.24
6.5	3,000,000	low	low			0.229	0.109	2.10	0.32	low	0.032			low	0.2695		
7.0	10,000,000	0.5805	2.9755	0.20	-0.71	1.5205	1.056	1.44	0.16	1.2925	3.3295	0.39	-0.41	1.167	3.788	0.31	-0.51
7.5	30,000,000																

Calculation Template for End Point

Collagen	
BNC	R-1
4.5	0.49
5.0	0.05
5.5	-0.19
6.0	-0.30

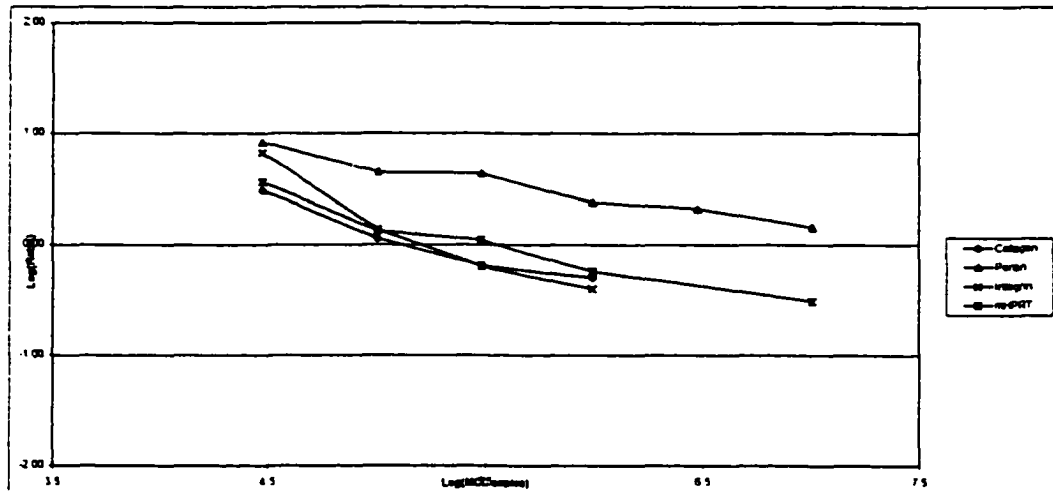
Pontin	
BNC	R-2
4.5	0.92
5.0	0.65
5.5	0.6385
6.0	0.3776
6.477121	0.3224
7.0	0.16

Integrin	
BNC	R-3
4.5	0.83
5.0	0.12948
5.5	-0.1971
6.0	-0.4

mHPRT	
BNC	R-4
4.5	0.56
5.0	0.12
5.5	0.0379
6.0	-0.243
7	-0.511

4 Hr 3,000 II
DR 24

	Collagen	Pontin	Integrin	mHPRT
End Pt/Reaction	181.031	32,568,419	224,637	375,879
Slope	-0.52	-0.29	-0.79	-0.41
Corr Coeff	-0.96	-0.98	-0.96	-0.97



QC-RT-PCR Experiment Calculation

Plate 1	
Controls	
RT+	1.50
PCR+	2.00
ELA+	2.00
ELA-	0.190

Backgrounds	
BNC	0.172
Collagen	0.179
Pontin	0.162
Integrin	0.180
mHPRT	0.172

Plate 2	
Controls	
RT+	1.50
PCR+	2.00
ELA+	0.00
ELA-	0.000

Low OD cutoff
0.014

Error Corrected Average Specific O.D.																	
PCR primer		Collagen		20 min		Pontin		15 min		Integrin		15 min		mHPRT		15 min	
BNC-I copies		Collagen	stuffer	Ratio	log R	Pontin	stuffer	Ratio	log R	Integrin	stuffer	Ratio	log R	mHPRT	stuffer	Ratio	log R
1.0	10																
1.5	30																
2.0	100																
2.5	300																
3.0	1,000																
3.5	3,000																
4.0	10,000	1.842	0.756	2.44	0.39	0.988	0.05	19.76	1.30	3.82	0.4325	8.83	0.95	3.458	0.591	5.85	0.77
4.5	30,000	0.812	0.7415	1.10	0.04	0.616	0.041	15.02	1.18	1.2555	0.092	13.65	1.14	2.0625	0.612	3.37	0.53
5.0	100,000	0.793	0.846	0.94	-0.03	0.6755	0.108	6.25	0.80	2.9325	1.709	1.72	0.23	2.107	1.0655	1.98	0.30
5.5	300,000	0.92	1.3655	0.59	-0.23	0.651	0.189	3.44	0.54	1.204	0.939	1.28	0.11	2.365	1.89	1.25	0.10
6.0	1,000,000	0.8495	1.6595	0.51	-0.29	0.6305	0.279	2.26	0.35	2.4395	3.097	0.79	-0.10	2.1025	2.3725	0.89	-0.05
6.5	3,000,000	0.8155	2.38	0.34	-0.47	0.802	0.3735	2.15	0.33	2.8405	3.135	0.91	-0.04	2.1265	3	0.71	-0.15
7.0	10,000,000	0.7195	1.917	0.38	-0.43	0.583	0.487	1.20	0.08	2.639	3.3255	0.79	-0.10	1.734	2.8825	0.60	-0.22
7.5	30,000,000																

Calculation Template for End Point

Collagen	
BNC	R-1
4.0	0.39
5.0	-0.03
5.5	-0.23
6.0	-0.29

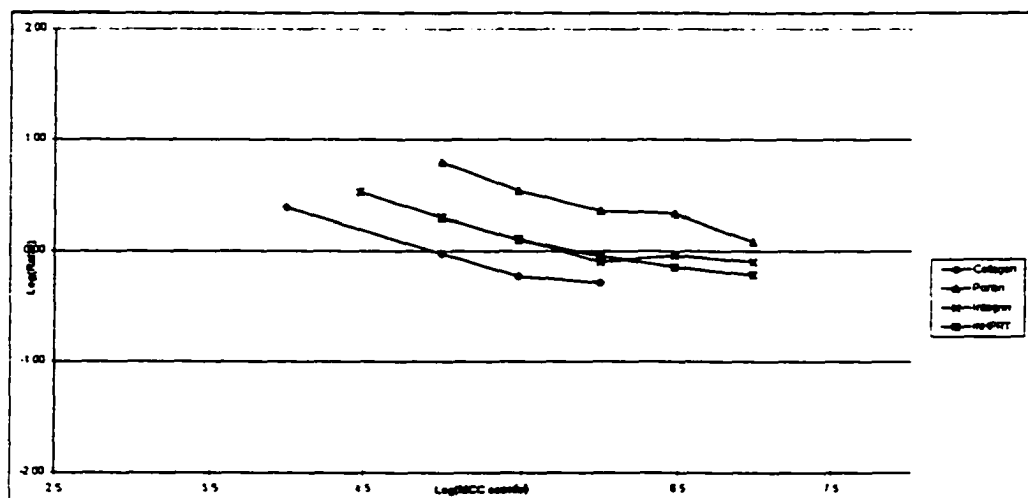
Pontin	
BNC	R-2
5.0	0.80
5.5	0.54
6.0	0.35
6.5	0.33
7.0	0.0781

Integrin	
BNC	R-3
5.5	0.108
6.0	-0.1036
6.5	-0.0428
7.0	-0.1004

mHPRT	
BNC	R-4
4.5	0.53
5.0	0.30
5.5	0.0974
6.0	-0.052
6.5	-0.149
7.0	-0.221

4 Hr 6,000 l
DR 23

	Collagen	Pontin	Integrin	mHPRT
End Pt/Reaction	100,958	18,533,556	854,566	1,041,751
Slope	-0.35	-0.33	-0.11	-0.30
Corr Coeff	-0.98	-0.97	-0.74	-0.98



QC-RT-PCR Experiment Calculation

Plate 1	
Controls	
RT+	1.50
PCR+	2.00
ELA+	2.00
ELA-	0.190

Backgrounds	
BNC	0.162
Collagen	0.181
Pontin	0.168
Integrin	0.186
mHPRT	0.175

Plate 2	
Controls	
RT+	1.50
PCR+	2.00
ELA+	0.00
ELA-	0.000

Low OD cutoff
0.014

Error Corrected Average Specific O.D																	
	PCR primer	Collagen			Pontin			Integrin			mHPRT						
	BNC-I copies	Collagen	stuffer	Ratio	log R	Pontin	stuffer	Ratio	log R	Integrin	stuffer	Ratio	log R	mHPRT	stuffer	Ratio	log R
1.0	10																
1.5	30																
2.0	100																
2.5	300																
3.0	1,000																
3.5	3,000																
4.0	10,000	0.8155	0.1095	7.45	0.87	1.0295	low			2.0805	0.335	6.21	0.79	1.5865	0.194	8.18	0.91
4.5	30,000	0.995	0.587	1.70	0.23	0.7605	0.067	11.35	1.06	1.813	0.618	2.93	0.47	1.501	0.297	5.05	0.70
5.0	100,000	1.995	1.9625	1.02	0.01	0.8575	0.177	4.84	0.69	1.518	0.6365	2.38	0.38	1.185	0.4035	2.94	0.47
5.5	300,000	1.9345	2.374	0.81	-0.09	0.879	0.2455	3.58	0.55	1.744	1.592	1.10	0.04	1.887	1.6255	1.16	0.06
6.0	1,000,000	0.9855	2.5855	0.38	-0.42	0.796	0.283	2.81	0.45	1.2765	2.051	0.62	-0.21	1.6605	1.908	0.87	-0.06
6.5	3,000,000	1.3745	2.836	0.48	-0.31	0.8545	0.384	2.23	0.35	1.7805	2.719	0.65	-0.18	1.5545	2.1915	0.71	-0.15
7.0	10,000,000	0.8775	2.335	0.38	-0.43	0.653	0.3965	1.65	0.22	1.5135	2.4555	0.62	-0.21	1.1895	2.436	0.49	-0.31
7.5	30,000,000																

Calculation Template for End Point

Collagen	
BNC	R-1
4.5	0.23
5.0	0.01
5.5	-0.09
6.5	-0.31
7.0	-0.43

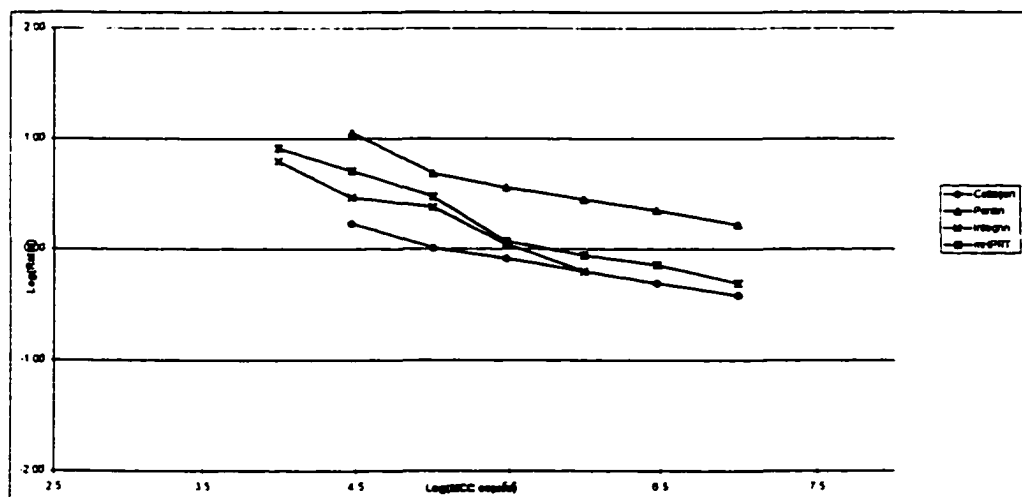
Pontin	
BNC	R-2
4.5	1.06
5.0	0.69
5.5	0.5539
6.0	0.4491
6.477121	0.3474
7.0	0.22

Integrin	
BNC	R-3
4.0	0.79
4.5	0.47
5.0	0.3775
5.5	0.0396
6.0	-0.206

mHPRT	
BNC	R-4
4.0	0.91
4.5	0.70
5.0	0.47
5.5	0.0648
6.0	-0.06
6.47712	-0.149
7.0	-0.311

4 Hr Control II
DR 23

	Collagen	Pontin	Integrin	mHPRT
End Pt/Reaction	161,232	36,327,980	396,801	1,101,491
Slope	-0.25	-0.30	-0.48	-0.42
Corr Coeff	-0.99	-0.96	-0.99	-0.98



QC-RT-PCR Experiment Calculation

Plate 1		
Controls		
RT+	1.50	
PCR+	2.00	
ELA+	2.00	
ELA-	0.190	

Backgrounds	
BNC	0.354
Collagen	0.296
Pontin	0.155
Integrin	0.166
mHPRT	0.278

Plate 2		
Controls		
RT+	1.50	
PCR+	2.00	
ELA+	0.00	
ELA-	0.000	

Low OD cutoff
0.014

Error Corrected Average Specific O.D													
PCR primer		Collagen		30 min		Pontin		15 min		Integrin		15 min	
BNC-I copies		Collagen	stuffer	Ratio	log R	Pontin	stuffer	Ratio	log R	Integrin	stuffer	Ratio	log R
1.0	10												
1.5	30												
2.0	100												
2.5	300												
3.0	1,000												
3.5	3,000												
4.0	10,000	2.5055	0.8665	2.89	0.46	0.872	0.0985	8.85	0.95	3.834	1.2705	3.02	0.48
4.5	30,000	1.2175	0.9385	1.30	0.11	0.6105	0.1065	5.73	0.76	2.7075	1.5345	1.76	0.25
5.0	100,000	1.508	1.5875	0.95	-0.02	0.7085	0.2565	2.76	0.44	2.2415	2.076	1.08	0.03
5.5	300,000	0.0035	1.4405	0.46	-0.34	0.556	0.2825	1.97	0.29	1.2535	2.479	0.51	-0.30
6.0	1,000,000	1.1775	2.8175	0.42	-0.38	0.687	0.4315	1.59	0.20	1.3965	3.0265	0.46	-0.34
6.5	3,000,000	1.053	2.2695	0.46	-0.33	0.61	0.5085	1.20	0.08	2.1425	3.0545	0.70	-0.15
7.0	10,000,000	0.8485	2.9515	0.29	-0.54	0.699	0.586	1.19	0.08	1.8225	3.325	0.55	-0.26
7.5	30,000,000												

Calculation Template for End Point

Collagen	
BNC	R-1
4.0	0.46
4.5	0.11
5.0	-0.02
5.5	-0.34
6.0	-0.38

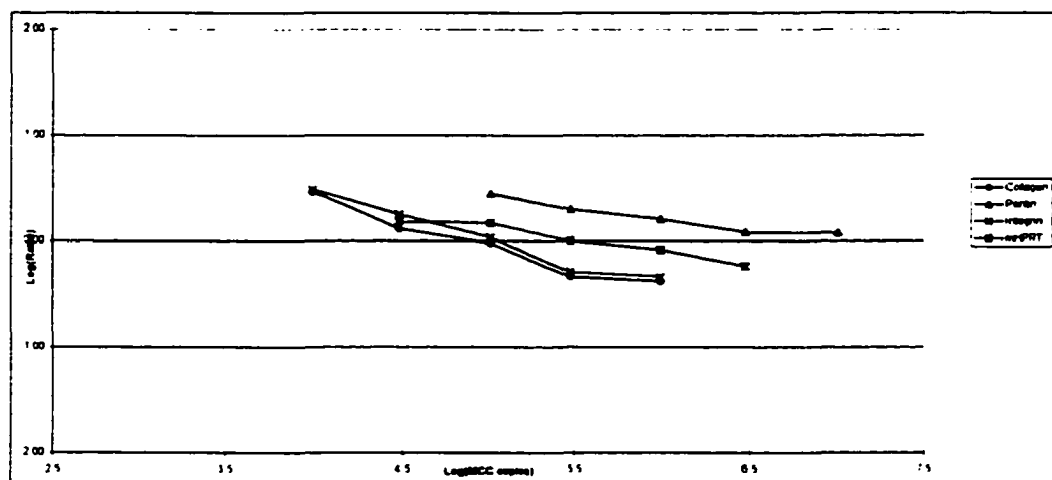
Pontin	
BNC	R-2
5.0	0.44
5.5	0.2941
6.0	0.202
6.5	0.079
7.0	0.08

Integrin	
BNC	R-3
4.0	0.48
4.5	0.25
5.0	0.0333
5.5	-0.296
6.0	-0.336

mHPRT	
BNC	R-4
4.5	0.18
5.0	0.17
5.5	0.00
6.0	-0.0842
6.5	-0.2429

4 HR 3,000 I
DR 22

	Collagen	Pontin	Integrin	mHPRT
End Pt/Reaction	81.829	14,191,715	112,113	318,473
Slope	-0.42	-0.19	-0.43	-0.22
Corr Coeff	-0.97	-0.96	-0.98	-0.97



QC-RT-PCR Experiment Calculation

Plate 1	
Controls	
RT+	1.50
PCR+	2.00
EIA+	2.00
EIA-	0.190

Backgrounds	
BNC	0.154
Collagen	0.177
Pontin	0.161
Integrin	0.109
mHPRT	0.174

Plate 2	
Controls	
RT+	1.50
PCR+	2.00
EIA+	0.00
EIA-	0.000

Low OD cutoff
0.014

Error Corrected Average Specific O.D.																		
	PCR primer	Collagen		30 min		Pontin		15 min		Integrin		15 min		mHPRT		15 min		
	BNC-1 copies	Collagen	stuffer	Ratio	log R	Pontin	stuffer	Ratio	log R	Integrin	stuffer	Ratio	log R	mHPRT	stuffer	Ratio	log R	
1.0	10																	
1.5	30																	
2.0	100																	
2.5	300																	
3.0	1,000																	
3.5	3,000																	
4.0	10,000		3.1355	0.697	4.50	0.65	3.6975	0.3035	12.18	1.09	2.804	0.571	4.91	0.69	2.8945	0.688	4.21	0.62
4.5	30,000		2.4315	0.8695	2.80	0.45	3.4135	0.5095	6.70	0.83	1.6765	0.4405	3.81	0.58	2.4345	0.74	3.29	0.52
5.0	100,000		2.017	1.442	1.40	0.15	3.4355	0.846	4.06	0.61	1.82	1.2185	1.49	0.17	2.26	1.0865	2.08	0.32
5.5	300,000		1.2585	1.1435	1.10	0.04	3.046	0.7795	3.91	0.59	0.5725	0.5145	1.11	0.05	1.7015	1.154	1.47	0.17
6.0	1,000,000		1.943	2.5065	0.78	-0.11	2.8915	1.401	2.06	0.31	1.67	2.187	0.76	-0.12	1.802	1.49	1.21	0.08
6.5	3,000,000		1.8105	2.2165	0.82	-0.09	2.8635	1.6255	1.76	0.25	1.2685	2.3025	0.55	-0.16	1.7665	2.278	0.78	-0.11
7.0	10,000,000		0.766	2.7775	0.28	-0.56	2.923	1.9195	1.52	0.18	1.0575	2.7785	0.38	-0.42	1.101	1.7415	0.63	-0.20
7.5	30,000,000																	

Calculation Template for End Point

Collagen	
BNC	R-1
4.0	0.65
4.5	0.45
5.0	0.15
5.5	0.04
6.0	-0.11
7.0	-0.56

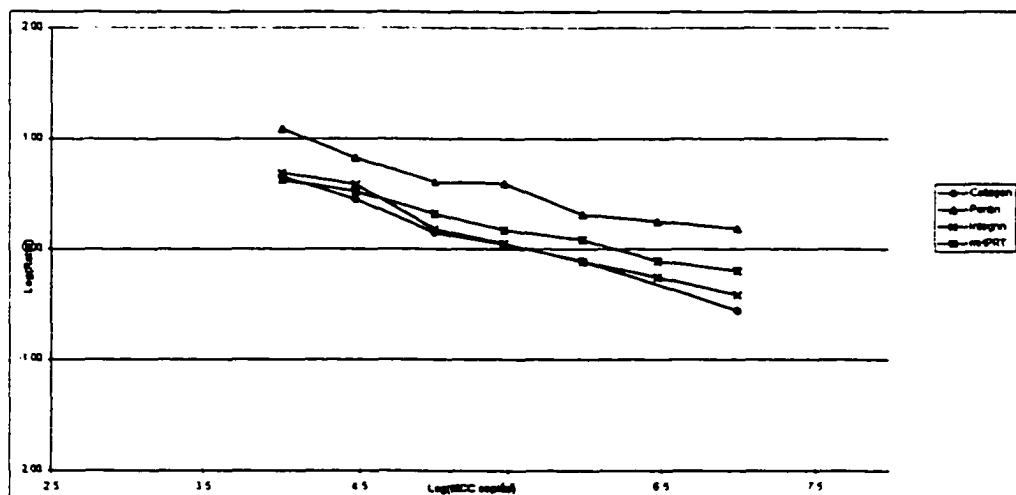
Pontin	
BNC	R-2
4.0	1.09
4.5	0.83
5.0	0.61
5.5	0.9919
6.0	0.3147
6.5	0.2459
7.0	0.18

Integrin	
BNC	R-3
4.0	0.69
4.5	0.58
5.0	0.1742
5.5	0.0464
6.0	-0.117
6.5	-0.259
7.0	-0.42

mHPRT	
BNC	R-4
4.0	0.62
4.5	0.52
5.0	0.32
5.5	0.1686
6.0	0.0826
6.5	-0.11
7.0	-0.199

4 HR CONTROL I
DR 22

	Collagen	Pontin	Integrin	mHPRT
End Pt/Reaction	387,475	21,991,691	566,054	1,577,522
Slope	-0.39	-0.30	-0.38	-0.28
Corr Coeff	-0.99	-0.98	-0.99	-1.00



QC-RT-PCR Experiment Calculation

Plate 1	
Controls	
RT+	1.50
PCR+	2.00
ELA+	2.00
ELA-	0.190

Backgrounds	
BNC	0.132
Collagen	0.163
Pontin	0.198
Integrin	0.172
mHPRT	0.261

Plate 2	
Controls	
RT+	1.50
PCR+	2.00
ELA+	0.00
ELA-	0.000

Low OD cutoff
0.014

Error Corrected Average Specific O.D.																	
	PCR primer BNC-1 copies	Collagen		20 min		Pontin		20 min		Integrin		20 min		mHPRT		15 min	
		Collagen	stuffer	Ratio	log R	Pontin	stuffer	Ratio	log R	Integrin	stuffer	Ratio	log R	mHPRT	stuffer	Ratio	log R
1.0	10																
1.5	30																
2.0	100																
2.5	300																
3.0	1,000																
3.5	3,000																
4.0	10,000	2.2905	0.7685	2.98	0.47	2.9695	0.814	3.65	0.56	1.909	0.7925	2.41	0.38	1.9415	0.3025	6.42	0.81
4.5	30,000	2.043	1.4085	1.45	0.16	1.068	0.0385	27.74	1.44	1.3125	0.8935	1.47	0.17	1.9985	0.667	3.00	0.48
5.0	100,000	0.789	1.0185	0.77	-0.11	2.1455	0.974	2.20	0.34	0.918	0.971	0.95	-0.02	0.531	0.454	1.17	0.07
5.5	300,000	0.8995	1.963	0.46	-0.34	2.559	1.442	1.77	0.25	1.3165	1.767	0.75	-0.13	1.3615	1.566	0.87	-0.06
6.0	1,000,000	1.061	2.513	0.42	-0.37	2.5705	2.2105	1.16	0.07	1.4095	2.701	0.52	-0.28	1.034	1.809	0.57	-0.24
6.5	3,000,000	0.8805	3.2985	0.27	-0.57	2.262	2.4625	0.92	-0.04	1.738	3.0455	0.57	-0.24	1.073	2.696	0.40	-0.40
7.0	10,000,000	0.773	3.517	0.22	-0.66	2.835	3.2695	0.87	-0.06	1.606	3.325	0.48	-0.32	0.7895	2.6075	0.30	-0.52
7.5	30,000,000																

Calculation Template for End Point

Collagen	
BNC	R-1
4.0	0.47
4.5	0.16
5.0	-0.11
5.5	-0.34

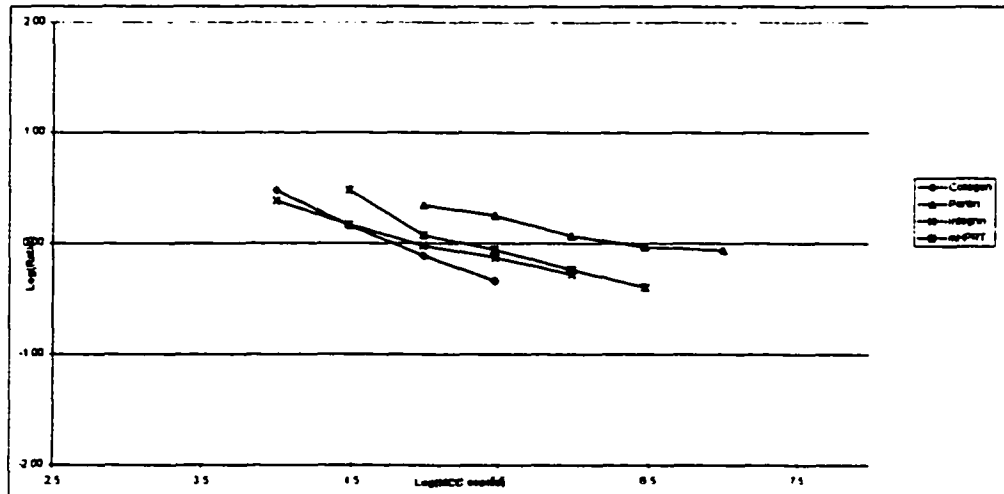
Pontin	
BNC	R-2
5.0	0.34
5.5	0.2491
6.0	0.0655
6.5	-0.037
7.0	-0.06

Integrin	
BNC	R-3
4.0	0.38
4.5	0.17
5.0	-0.024
5.5	-0.128
6.0	-0.282

mHPRT	
BNC	R-4
4.5	0.48
5.0	0.07
5.5	-0.061
6.0	-0.243
6.5	-0.4

1 HR 6,000 fl
DR 21

	Collagen	Pontin	Integrin	mHPRT
End Pt/Reaction	66,609	3,170,752	115,134	256,641
Slope	-0.55	-0.22	-0.32	-0.41
Corr Coeff	-1.00	-0.97	-0.99	-0.98



QC-RT-PCR Experiment Calculation

Plate 1	
Controls	
RT+	1.50
PCR+	2.00
EIA+	2.00
EIA-	0.190

Backgrounds	
BNC	0.135
Collagen	0.164
Pontin	0.151
Integrin	0.168
mHPRT	0.190

Plate 2	
Controls	
RT+	1.50
PCR+	2.00
EIA+	0.00
EIA-	0.000

Low OD cutoff
0.014

Error Corrected Average Specific O.D.													
PCR primer	Collagen	10 min		Pontin	15 min		Integrin	15 min		mHPRT	15 min		
BNC-1 copies	Collagen	stuffer	Ratio log R	Pontin	stuffer	Ratio log R	Integrin	stuffer	Ratio log R	mHPRT	stuffer	Ratio log R	
1.0	10												
1.5	30												
2.0	100												
2.5	300												
3.0	1,000												
3.5	3,000												
4.0	10,000	1.3375	0.2505	5.34	0.73	1.46	0.1285	11.36	1.06	3.1565	0.605	5.22	0.72
4.5	30,000	1.109	0.544	2.04	0.31	1.317	0.2425	5.43	0.73	2.658	1.326	2.00	0.30
5.0	100,000	0.9955	0.7315	1.36	0.13	1.0225	0.3955	2.59	0.41	2.215	1.8435	1.20	0.08
5.5	300,000	0.6075	0.719	0.84	-0.07	1.222	0.4345	2.81	0.45	1.8905	1.73	1.09	0.04
6.0	1,000,000	0.7305	1.3495	0.54	-0.27	1.1535	0.768	1.50	0.18	2.5905	2.853	0.91	-0.04
6.5	3,000,000	0.657	1.544	0.43	-0.37	1.4045	0.803	1.75	0.24	1.909	2.5045	0.76	-0.12
7.0	10,000,000	0.558	1.674	0.33	-0.48	0.9695	0.958	1.01	0.01	2.1935	3.202	0.69	-0.16
7.5	30,000,000												

Calculation Template for End Point

Collagen	
BNC	R-1
4.0	0.73
4.5	0.31
5.0	0.13
5.5	-0.07
6.0	-0.27
6.5	-0.37
7.0	-0.48

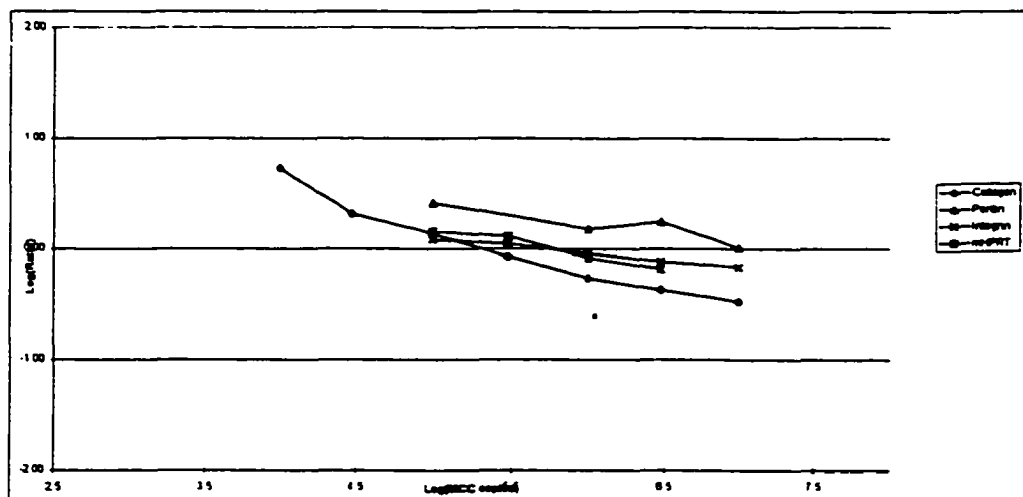
Pontin	
BNC	R-2
5.0	0.41
6.0	0.1767
6.5	0.2428
7.0	0.0052

Integrin	
BNC	R-3
5.0	0.0797
5.5	0.0385
6.0	-0.042
6.5	-0.118
7.0	-0.164

mHPRT	
BNC	R-4
5.0	0.15
5.5	0.1116
6.0	-0.08
6.5	-0.185

1 HR 3,000 II
DR 21

	Collagen	Pontin	Integrin	mHPRT
End PV/Reaction	304,616	19,062,873	469,266	547,587
Slope	-0.38	-0.18	-0.13	-0.24
Corr Coeff	-0.97	-0.91	-0.99	-0.98



QC-RT-PCR Experiment Calculation

Plate 1	
Controls	
RT+	1.50
PCR+	2.00
EIA+	2.00
EIA-	0.190

Backgrounds	
BNC	0.180
Collagen	0.194
Pontin	0.193
Integrin	0.204
mHPRT	0.182

Plate 2	
Controls	
RT+	1.50
PCR+	2.00
EIA+	0.00
EIA-	0.000

Low OD cutoff
0.014

Error Corrected Average Specific O.D.																	
PCR primer	Collagen		30 min		Pontin		15 min		Integrin		15 min		mHPRT		15 min		
BNC-1 copies	Collagen	stuffer	Ratio	log R	Pontin	stuffer	Ratio	log R	Integrin	stuffer	Ratio	log R	mHPRT	stuffer	Ratio	log R	
1.0	10																
1.5	30																
2.0	100																
2.5	300																
3.0	1,000																
3.5	3,000																
4.0	10,000	2.363	0.586	-4.03	0.61	2.5135	0.2285	11.00	1.04	0.488	0.0835	5.84	0.77	2.682	0.59	4.55	0.66
4.5	30,000	1.461	0.5205	2.81	0.45	1.692	0.216	7.83	0.89	0.948	0.4775	1.99	0.30	1.738	0.6955	2.53	0.40
5.0	100,000	1.037	1.3245	0.78	-0.11	1.5265	0.4265	3.58	0.55	1.0355	0.9665	1.07	0.03	2.052	1.245	1.65	0.22
5.5	300,000	0.762	1.579	0.48	-0.32	1.363	0.4205	3.24	0.51	0.808	1.106	0.73	-0.14	1.5935	1.3005	1.23	0.09
6.0	1,000,000	0.367	1.754	0.21	-0.68	1.4855	0.662	2.24	0.35	0.9	1.676	0.54	-0.27	1.4995	1.399	1.07	0.03
6.5	3,000,000	low	1.9045			1.3135	0.8075	1.63	0.21	2.8505	3.5515	0.80	-0.10	0.5795	1.1665	0.50	-0.30
7.0	10,000,000	0.936	2.426	0.39	-0.41	1.7435	1.238	1.41	0.15					1.5975	2.6945	0.59	-0.23
7.5	30,000,000																

Calculation Template for End Point

Collagen	
BNC-1	R-1
4.5	0.45
5.0	-0.11
5.5	-0.32
6.0	-0.68

Pontin	
BNC-1	R-2
4.0	1.04
4.5	0.89
5.0	0.55
5.5	0.51
6.0	0.35
6.5	0.21
7.0	0.1487

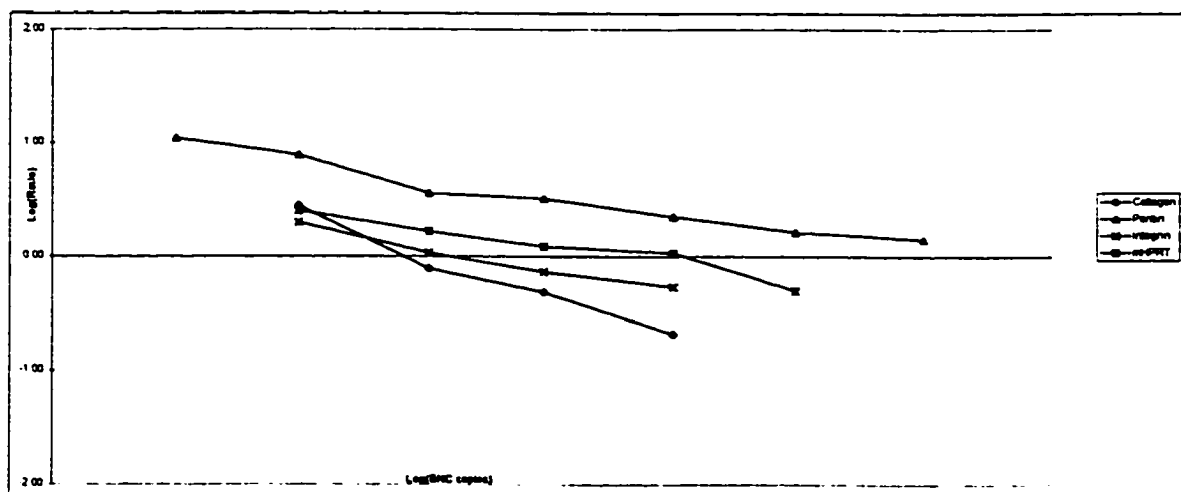
Integrin	
BNC-1	R-3
4.5	0.30
5.0	0.0299
5.5	-0.14
6.0	-0.27

mHPRT	
BNC-1	R-4
4.5	0.40
5.0	0.22
5.5	0.09
6.0	0.03
6.5	-0.30

1 HR 6,000 I

DR

	Collagen	Pontin	Integrin	mHPRT
End Pt/Reaction	102,213	17,290,219	153,306	573,235
Slope	-0.71	-0.30	-0.37	-0.32
Corr Coeff	-0.99	-0.98	-0.99	-0.97



QC-RT-PCR Experiment Calculation

Plate 1	
Controls	
RT+	1.50
PCR+	2.00
EIA+	2.00
EIA-	0.190

Backgrounds	
BNC	0.202
Collagen	0.222
Pontin	0.173
Integrin	0.195
mHPRT	0.219

Plate 2	
Controls	
RT+	1.50
PCR+	2.00
EIA+	0.00
EIA-	0.000

Low OD cutoff
0.014

Error Corrected Average Specific O.D													
PCR primer		Collagen		30 min		Pontin		15 min		Integrin		15 min	
BNC-1 copies		Collagen	stuffer	Ratio	log R	Pontin	stuffer	Ratio	log R	Integrin	stuffer	Ratio	log R
1.0	10												
1.5	30												
2.0	100												
2.5	300												
3.0	1,000												
3.5	3,000												
4.0	10,000	2.0415	0.2745	7.44	0.87	1.2815	0.0445	28.80	1.46	2.1715	0.712	3.05	0.48
4.5	30,000	1.3165	0.3735	3.52	0.55	1.0505	0.081	12.97	1.11	1.17	0.432	2.71	0.43
5.0	100,000	1.292	1.575	0.82	-0.09	1.1565	0.2865	4.04	0.61	0.6975	0.9305	0.75	-0.13
5.5	300,000	1.3715	2.12	0.65	-0.19	1.056	0.3705	2.85	0.45	1.6225	2.034	0.80	-0.10
6.0	1,000,000	1.11	2.4515	0.45	-0.34	1.1685	0.516	2.26	0.35	1.875	2.532	0.74	-0.13
6.5	3,000,000	0.2395	2.6265	0.09	-1.04	1.0055	0.6255	1.61	0.21	0.717	2.204	0.33	-0.49
7.0	10,000,000	0.0225	2.9415	0.01	-2.12	1.0225	0.8635	1.18	0.07	1.389	3.0075	0.46	-0.34
7.5	30,000,000												

Calculation Template for End Point

Collagen	
BNC-1	R-1
4.0	0.87
4.5	0.55
5.0	-0.09
5.5	-0.19

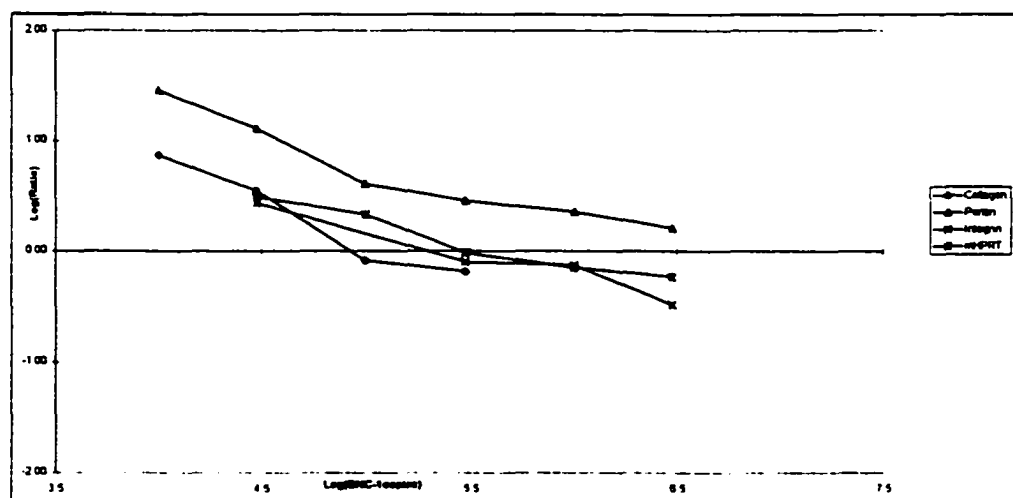
Pontin	
BNC-1	R-2
4.0	1.46
4.5	1.11
5.0	0.61
5.5	0.45
6.0	0.35
6.5	0.21

Integrin	
BNC-1	R-3
4.5	0.4327
5.5	-0.10
6.0	-0.13
6.5	-0.49

mHPRT	
BNC-1	R-4
4.5	0.49
5.0	0.33
5.5	-0.02
6.0	-0.15
6.5	-0.23

I HR CONTROL II
DR

	Collagen	Pontin	Integrin	mHPRT
End Pt/Reaction	128,354	4,366,561	277,670	500,244
Slope	-0.77	-0.50	-0.43	-0.38
Corr Coeff	-0.97	-0.96	-0.98	-0.97



QC-RT-PCR Experiment Calculation

Plate 1	
Controls	
RT+	1.50
PCR+	2.00
EIA+	2.00
EIA-	0.190

Backgrounds	
MCC	0.144
Collagen	0.182
Pontin	0.163
Integrin	0.153
mHPRT	0.152

Plate 2	
Controls	
RT+	1.50
PCR+	2.00
EIA+	0.00
EIA-	0.000

Low OD cutoff
0.014

Error Corrected Average Specific O.D.													
PCR primer	Collagen	20 min		Pontin	20 min		Integrin	30 min		mHPRT	30 min		
BNC-1 copies	Collagen stuffer	Ratio	log R	Pontin stuffer	Ratio	log R	Integrin stuffer	Ratio	log R	mHPRT stuffer	Ratio	log R	
1.0	10												
1.5	30												
2.0	100												
2.5	300	1.895	0.0465	40.75	1.61	3.488	0.0205	170.15	2.23	2.6495	0.016	165.59	2.22
3.0	1,000	1.3925	0.047	29.63	1.47	2.842	0.016	177.63	2.25	1.8385	0.0445	41.31	1.62
3.5	3,000	1.3265	0.153	8.67	0.94	2.8475	0.0615	46.30	1.67	2.274	0.2475	9.19	0.96
4.0	10,000	1.3035	0.355	3.67	0.56	2.634	0.1555	16.94	1.23	1.7875	0.431	4.15	0.62
4.5	30,000	0.923	0.253	3.65	0.56	2.498	0.1455	17.17	1.23	1.3845	0.4635	2.99	0.48
5.0	100,000	0.991	0.484	2.05	0.31	2.2295	0.2175	10.25	1.01	1.094	0.7645	1.43	0.16
5.5	300,000	1.0375	1.166	0.89	-0.05	3.173	0.798	3.98	0.60	1.716	1.8275	0.94	-0.03
6.0	1,000,000												
6.5	3,000,000												
7.0	10,000,000												
7.5	30,000,000												

Calculation Template for End Point

Collagen	
BNC-1	R-1
3.5	0.94
4.0	0.56
5.0	0.31
5.5	-0.05

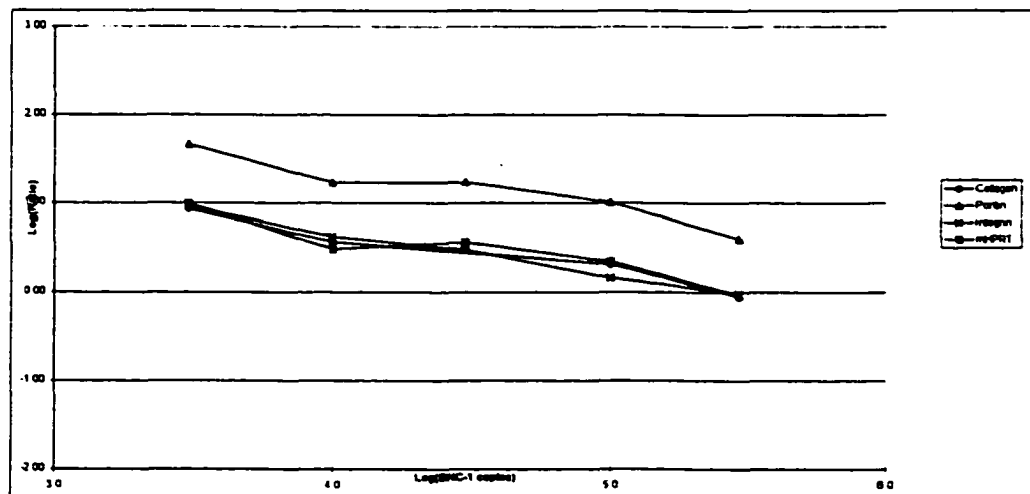
Pontin	
BNC-1	R-2
3.5	1.67
4.0	1.23
4.5	1.23
5	1.01
5.5	0.60

Integrin	
BNC-1	R-3
3.5	0.96
4.0	0.62
4.5	0.48
5.0	0.16
5.5	-0.03

mHPRT	
MCC-4	R-4
3.5	1.00
4.0	0.48
4.5	0.56
5	0.35
5.5	-0.0369

1 Hr 3,000 Microgram I
DR 19

	Collagen	Pontin	Integrin	mHPRT
End Pt/Reaction	299.658	8,435.891	239.293	355.338
Slope	-0.45	-0.47	-0.49	-0.44
Corr Coeff	-0.98	-0.96	-0.99	-0.93



QC-RT-PCR Experiment Calculation

Plate 1	
Controls	
RT+	1.50
PCR+	2.00
EIA+	2.00
EIA-	0.190

Backgrounds	
MCC	0.100
Collagen	0.182
Pontin	0.175
Integrin	0.159
mHPRT	0.179

Plate 2	
Controls	
RT+	1.50
PCR+	2.00
EIA+	0.00
EIA-	0.000

Low OD cutoff
0.014

Error Corrected Average Specific O.D																	
PCR primer		Collagen		20 min		Pontin		20 min		Integrin		20 min		mHPRT		30 min	
	BNC-1 copies	Collagen	stuffer	Ratio	log R	Pontin	stuffer	Ratio	log R	Integrin	stuffer	Ratio	log R	mHPRT	stuffer	Ratio	log R
1.0	10																
1.5	30																
2.0	100																
2.5	300	3.4125	0.06	56.88	1.75	2.4025	low			1.4475	0.0255	56.76	1.75	3.2085	0.046	69.75	1.84
3.0	1,000	3.455	0.161	21.46	1.33	1.8785	0.0245	76.67	1.88	1.1675	0.0245	47.65	1.68	3.0875	0.2765	11.17	1.05
3.5	3,000	2.742	0.351	7.81	0.89	1.861	0.0495	37.60	1.58	1.415	0.151	9.37	0.97	3.303	0.6285	5.26	0.72
4.0	10,000	2.6325	1.0885	2.42	0.38	2.0455	0.1305	15.67	1.20	1.2945	0.3205	4.04	0.61	2.6225	0.725	3.62	0.56
4.5	30,000	2.1985	1.4745	1.49	0.17	1.9425	0.2235	8.69	0.94	1.364	0.769	1.77	0.25	2.8475	1.6845	1.69	0.23
5.0	100,000	2.1435	2.6645	0.80	-0.09	1.9105	0.3465	5.51	0.74	1.2565	1.229	1.02	0.01	2.602	2.0925	1.24	0.09
5.5	300,000	1.241	3.0425	0.41	-0.39	1.9475	0.6605	2.95	0.47	1.273	1.7295	0.74	-0.13	2.6295	2.3035	1.14	0.06
6.0	1,000,000																
6.5	3,000,000																
7.0	10,000,000																
7.5	30,000,000																

Calculation Template for End Point

Collagen	
BNC-1	R-1
3.5	0.89
4.0	0.38
4.5	0.17
5.0	-0.09
5.5	-0.39

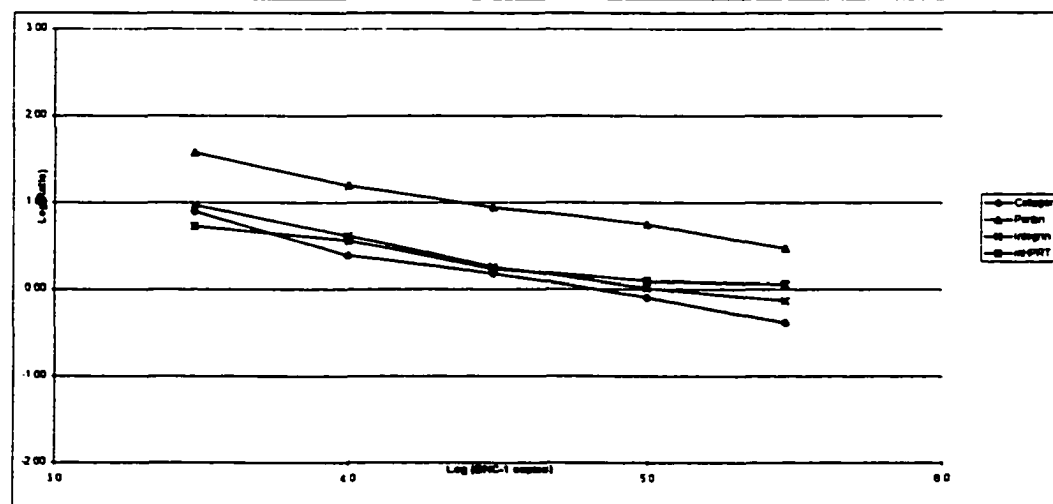
Pontin	
BNC-1	R-2
3.5	1.58
4.0	1.20
4.5	0.94
5.0	0.74
5.5	0.47

Integrin	
BNC-1	R-3
3.5	0.97
4.0	0.61
4.5	0.25
5.0	0.01
5.5	-0.1331

mHPRT	
BNC-1	R-4
3.5	0.72
4.0	0.56
4.5	0.23
5.0	0.09
5.5	0.05748

1 Hr Control
DR 19

	Collagen	Pontin	Integrin	mHPRT
End Pt/Reaction	63,583	2,148,769	123,813	258,905
Slope	-0.61	-0.53	-0.56	-0.36
Corr Coeff	-0.99	-0.99	-0.99	-0.96



**GRADUATE SCHOOL
UNIVERSITY OF ALABAMA AT BIRMINGHAM
DISSERTATION APPROVAL FORM
DOCTOR OF PHILOSOPHY**

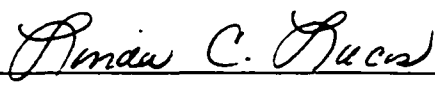
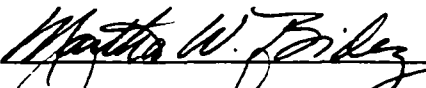
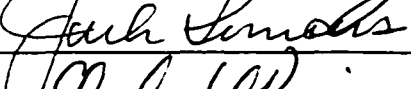
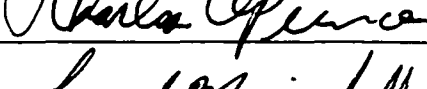

Name of Candidate Deborah F. Rigsby

Major Subject Biomedical Engineering

Title of Dissertation Analysis and Characterization of the Metabolic and
Morphologic Responses to Uniaxial Deformation of Osteoblasts Cultured
on TI-6AL-4V

I certify that I have read this document and examined the student regarding its content. In my opinion, this dissertation conforms to acceptable standards of scholarly presentation and is adequate in scope and quality, and the attainments of this students are such that she may be recommended for the degree of Doctor of Philosophy.

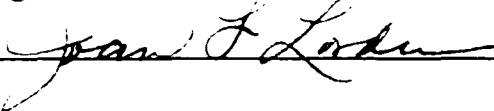
Dissertation Committee:

Name	Signature
<u>Linda C. Lucas, Ph.D.</u> , Chair	<u></u>
<u>Martha W. Bidez, Ph.D.</u>	<u></u>
<u>Jack E. Lemons, Ph.D.</u>	<u></u>
<u>Charles W. Prince, Ph.D.</u>	<u></u>
<u>Leonard Mueninghoff, DDS</u>	<u></u>

Director of Graduate Program



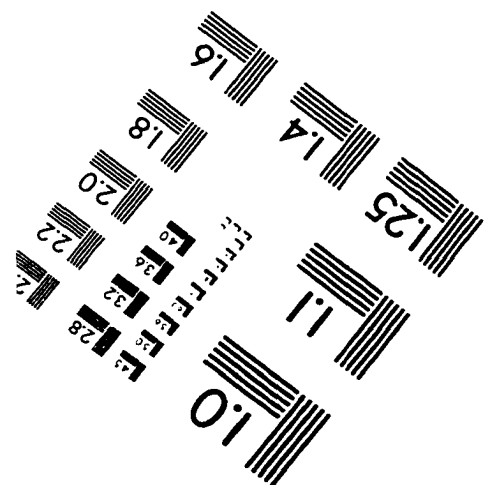
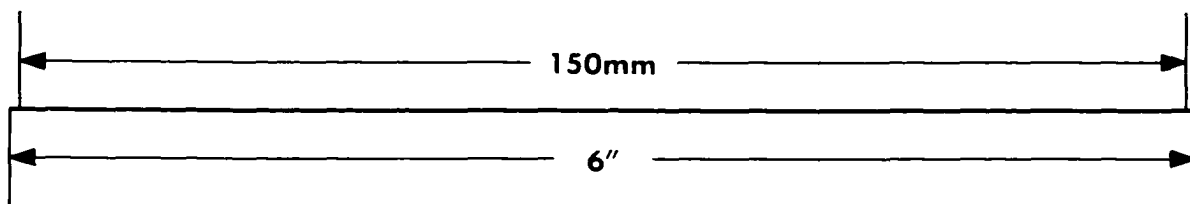
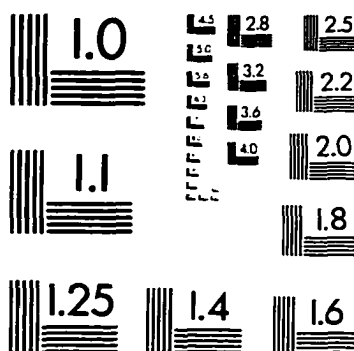
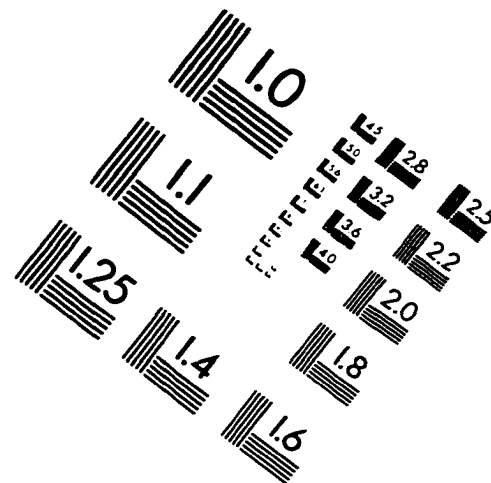
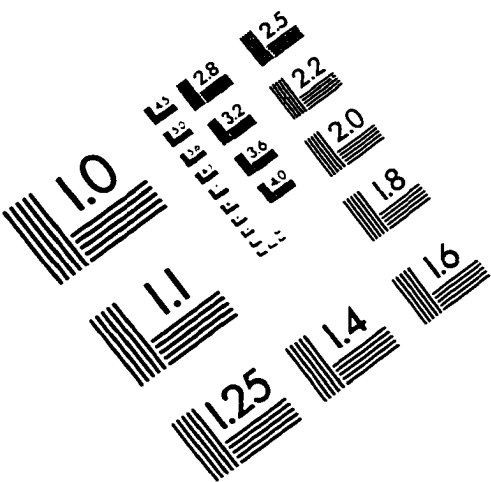
Dean, UAB Graduate School



Date

7/8/98

IMAGE EVALUATION TEST TARGET (QA-3)



APPLIED IMAGE, Inc.
1653 East Main Street
Rochester, NY 14609 USA
Phone: 716/482-0300
Fax: 716/288-5989

© 1993, Applied Image, Inc.. All Rights Reserved

